SHEAR ALFVÉN WAVES IN TOKAMAKS

by

CYNTHIA ELIZABETH KIERAS

A thesis submitted in partial fulfillment of the

requirements for the degree of

Doctor of Philosophy

(Physics)

at the

UNIVERSITY OF WISCONSIN--MADISON

1982

This thesis is dedicated to my parents,

Henry and Elizabeth Kieras.

ACKNOWLEDGEMENTS

I wish to express my sincerest thanks to my advisors, Keith Symon and John Tataronis, for their invaluable contributions to this thesis and for the support, advice, and time they have given to me during my graduate studies. I thank Stuart Prager for suggesting this are of research to me. Also, I have benefitted from numerous discussions with Stuart Prager and Doug Witherspoon on the experimental aspects of shear Alfvén wave heating of tokamaks. I thank Jim Callen for his continuing interest in my work and for his enlightening explainations of tokamak physics. Special thanks are due my husband, Michael Phillips, for his expert advice on numerical procedures, numerous informal discussions of physics, and for helping me to survive life as a graduate student.

This work was supported in part by an award from the Research Committee of the University of Wisconsin Graduate School and in part by the National Science Foundation under Contract ECS-8110038.

SHEAR ALFVÉN WAVES IN TOKAMAKS

Cynthia Elizabeth Kieras

Under the supervision of Associate Professor John Andrew Tataronis

and Professor Keith Randolph Symon

Shear Alfvén waves in an axisymmetric tokamak are examined within the framework of the linearized ideal MHD equations. Properties of the shear Alfvén continuous spectrum are studied both analytically and numerically. Implications of these results in regards to low frequency RF heating of toroidally confined plasmas are discussed. The structure of the spatial singularities associated with these waves is determined. A reduced set of ideal MHD equations is derived to describe these waves in a very low beta plasma.

Analytic expressions for the continuum are obtained by solving a set of coupled differential equations on each flux surface in an expansion scheme in powers of the small inverse aspect ratio, $\varepsilon = a/R_o$, where a and R_o are the minor and major radii, respectively, of the toroid. To lowest order in ε, the continuum is given by an appropriate generalization of its counterpart in an infinitely long, axially periodic, cylindrically symmetric screw pinch. First order corrections due to toroidicity induce a coupling of particular poloidal harmonics about rational q surfaces, where q is the safety factor. The coupling leads to the formation of gaps in the continuum. Depending on the structure of the continuum near the gaps, it may not be possible to heat the plasma with certain oscillator frequencies and helicities.

Numerical solutions for the shear Alfvén continuum of the Tokapole II device at the University of Wisconsin - Madison are in qualitative agreement with the predictions of the analytic model. Additional effects due to finite aspect ratio, noncircular flux surfaces and regions of high shear in the equilibrium magnetic field are evident in the numerical results.

The singular nature of the wavestructure is analyzed using a generalized method of Frobenius. The perturbed velocity and magnetic field components, along with the equilibrium quantities, are expanded in power series about the flux surface on which the wave frequency is equal to the local shear Alfvén resonance frequency. The wavestructure is shown to be always non-square-integrable about these surfaces, thereby lending support to the ideal MHD model for low frequency RF heating of tokamaks.

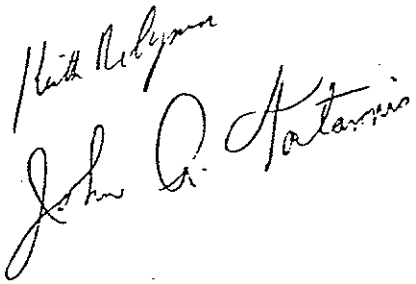

TABLE OF CONTENTS

CHAPTER 1

INTRODUCTION

For nearly thirty years, scientists have been attempting to develop a viable means to produce controlled thermonuclear fusion reactions in a deuterium-tritium plasma and to harness the released energy for commercial power production. Such a scheme is particularly attractive because the fuel source is virtually inexhaustible. Progress towards this goal has been hindered by the lack of an economic, technically feasible means of heating the plasma to the high temperature range necessary for the onset of the fusion reactions. Some success has been attained with RF heating methods which attempt to supply energy to the plasma via resonant wave-particle interactions at the ion cyclotron, electron cyclotron or lower hybrid wave frequencies[1,2]. A relatively unexplored yet promising scheme for providing supplementary heating to a magnetically confined plasma involves the resonant excitation of modes which lie within the shear Alfvén continuum of ideal MHD theory. Tataronis and Grossmann[3,4] and Hasegawa and Chen[46,47] originally demonstrated that because these modes exhibit spatial, non-square-integrable singularities at particular locations in an inhomogeneous plasma, it may be possible to transfer energy efficiently to the plasma via these modes. Any small non-ideal plasma effects may then result in the thermalization of the wave energy.

Experiments designed to test the feasibility of this heating scheme have been conducted on the Proto-Cleo stellarator at the University of Wisconsin-Madison[5], the RO-2 stellarator in Sukhumi in the U.S.S.R.[6], on the Heliotron-D device in Kyoto, Japan[7], and on the linear theta pinch in Lausanne, Switzerland[8]. Evidence of plasma heating was observed in each experiment. Some indication of localized energy absorption was observed in the Proto-Cleo data, while the plasma impedances measured on the Lausanne theta pinch agree excellently with the theoretical predictions of Tataronis and Grossmann[9]. More recently, the technique is being tested in tokamak devices. Initial results from the TCA tokamak in Lausanne[10], the Tokapole II device at the University of Wisconsin-Madison[11], and the Pretext tokamak at the University of Texas-Austin[12] have been very encouraging.

The physical basis for the heating mechanism may be understood within the context of ideal MHD theory[13,14]. Shear Alfvén waves in a homogeneous equilibrium can propagate only at a single frequency, $\omega_A = k_\parallel V_A$, where ω_A is the shear Alfvén resonance frequency, $k_\parallel$ is the magnitude of the component of the wavevector $\vec{k}$ along the equilibrium magnetic field and the Alfvén speed, V_A, is equal to $B/\sqrt{\mu_o \rho}$, where B is the magnitude of $\vec{B}$, μ_o is the vacuum permeability and ρ is the equilibrium mass density. However, realistic plasma equilibria are spatially inhomogeneous due to variations in the equilibrium magnetic field and plasma density. As a result, the frequencies at which shear Alfvén waves may be excited consist of a continuous

spectrum, the range of which is determined by the equilibrium. The characteristic feature of a wave belonging to the continuous spectrum is that its Laplace transform is non-square-integrable at locations in the plasma where the wave frequency is equal to the local shear Alfvén resonance frequency. As a consequence, the corresponding physical perturbations experience a localized non-zero, time-averaged growth. This, in turn, implies a localized temporal growth of the plasma energy. Non-ideal and/or nonlinear plasma effects presumably will limit the growth of the perturbations and thermalize the wave energy.

A correspondence may be established between the energy absorption which can occur in an inhomogeneous plasma due to the singular nature of the localized Alfvén waves and the wave absorption which can occur at the shear Alfvén resonance in an infinite homogeneous plasma imbedded in a unidirectional equilibrium magnetic field, $\vec{B}$. The dispersion relation for waves in the ideal MHD model[15] is given by

$$(\omega^2-k^2V_A^2\cos^2\theta)[\omega^4-(V_A^2+V_S^2)k^2\omega^2+V_A^2V_S^2k^4\cos^2\theta] = 0 \qquad (1.1)$$

where $\sqrt{\gamma P_o/\rho}$ is the sound speed, V_S, the magnitude of the wave vector is equal to k, the equilibrium fluid pressure is denoted by P_o, and θ is the angle between $\vec{k}$ and $\vec{B}$. Three types of waves may propagate according to Eq. (1.1). Shear Alfvén waves satisfy the dispersion relation

$$\omega^2 - k^2V_A^2\cos^2\theta = \omega^2 - k_\parallel^2V_A^2 = 0 \quad . \qquad (1.2)$$

The fast and slow magnetoacoustic waves satisfy the dispersion relation

$$\omega^4 - (V_A^2+V_S^2)k^2\omega^2 + V_A^2V_S^2k^4\cos^2\theta = 0 \quad . \qquad (1.3)$$

Propagation of the shear Alfvén and slow waves is strongly localized about the field line on which the disturbance is initiated. This localization occurs because these two waves do not propagate in the direction perpendicular to $\vec{B}$, as can be seen by setting θ=0 in Eq. (1.2) and in the low frequency solution of Eq. (1.3). The slow wave is often referred to as the cusp wave, since its propagation is localized to a cone, the vertex of which trails behind the wavefront. Cumberbatch[16] has shown that the cusp origin is a point which moves along only on a particular field line, and that the cusp wave propagates unidirectionally at the cusp speed , which is equal to $V_A\sqrt{\gamma P_o/(B^2+\gamma P_o)}$. Propagation of the fast wave is isotropic, as can be seen by inspection of the higher frequency solution of Eq. (1.3). The structure of the wavefronts of the three MHD waves at some instant in time after a point disturbance is excited at the origin of the x-z Cartesian coordinate system is displayed in Fig. 1.1. Localization of the shear Alfvén and cusp waves results in the existence of resonances of these two waves. Wave absorption

is possible at a resonance, which occurs when the wave vector $\vec{k}$ becomes infinite. The dispersion diagram for the three MHD waves is displayed in Fig. 1.2. In this diagram, ω is plotted versus $k_\perp$, the component of the wavevector perpendicular to $\vec{B}$, for a fixed value of $k_\parallel$. Two resonances are evident in Fig. 1.2: the shear Alfvén resonance at $\omega=\omega_A$ and the cusp resonance at $\omega=\omega_c$. These resonances are broadened into continuous spectra by variations of the equilibrium magnetic field and/or plasma density in an inhomogeneous equilibrium. The spatial structure of a wave excited at a frequency which lies within either of these two continuous spectra is non-square-integrable about the regions where the wave frequency is equal to the local shear Alfvén or cusp resonance frequency. Hence, the spatial singularities present in the inhomogeneous plasma occur at locations corresponding to the resonances present in a homogeneous equilibrium. This suggests[14] that energy absorption is possible in the inhomogeneous medium at the local shear Alfvén and cusp resonances.

As was mentioned in the preceding paragraphs, there exists a definite connection between the continuous spectrum of the ideal MHD operator and the possibility of plasma heating. To make this connection more explicit, consider a linear differential operator, $L(x,\omega)$, where ω is a parameter and x is the independent variable on which L depends. Let S denote the particular space consisting of all functions upon which L may operate. The domain of L consists of those functions, u_i in the space S, for which $Lu_i=f_i$ belongs to S,

satisfies specified boundary conditions, and has a continuous derivative of the same order as those contained in L. The set of all such functions, f_i, form the range of the operator, L. Let the inner product of any two functions in S be defined as

$$\langle v_i | v_j \rangle = \oint dx\ v_i^*\ v_j \tag{1.4}$$

where the integration is over the allowed range of the independent variable, x. The norm of a vector is defined in turns of its inner product with its complex conjugate as

$$||v|| \equiv \sqrt{\langle v|v\rangle} \quad . \tag{1.5}$$

An operator, L, is a bounded operator if its domain is equal to the space, S, and if for every function, u_i, in its domain, there exists a finite constant, c, such that

$$||Lu_i|| < c||u_i|| \quad . \tag{1.6}$$

Otherwise, the operator, L, is unbounded. To define the spectrum of the operator, L, one considers its inverse, i.e., L^{-1}, for all values of ω. Consider the equation

$$L(x,\omega)u = a \quad . \tag{1.7}$$

A necessary and sufficient condition that L^{-1} does not exist is that

a nontrivial solution, g, of the corresponding homogeneous equation, $Lg=0$, exists in the domain of L. The function satisfying $Lg=0$ is an eigenfunction of L corresponding to the eigenvalue ω. The set of all such ω's forms the discrete spectrum of L. If a nontrivial solution to the homogeneous equation for a given ω does not exist, then L^{-1} does exist and the corresponding ω belongs to either the resolvent spectrum of L or else to the continuous spectrum of L. If the inverse of the operator, L, is bounded, i.e., if

$$\frac{\langle u|u\rangle}{\langle a|a\rangle} = \frac{\langle L^{-1}a|L^{-1}a\rangle}{\langle a|a\rangle} < c \qquad (1.8)$$

where c is some finite constant, then ω belongs to the resolvent spectrum of L. If the inverse is an unbounded operator, i.e., $\langle L^{-1}a|L^{-1}a\rangle=\langle u_i|u_i\rangle$ is unbounded, then the corresponding ω belongs to the continuous spectrum of L. The functions, u_i, corresponding to the solutions, ω, in the continuous spectrum of L are non-square-integrable and therefore are spatially singular.

The spatial singularities associated with the continuous spectrum may readily be connected with energy absorption in ideal MHD theory. The Laplace transform of the system of linearized ideal MHD equations may be written in the form (1.7), where ω represents the mode frequency, u represents the macroscopic fluid and magnetic field perturbations, a contains the initial conditions, and x represents physical position in the equilibrium. Tataronis and

Grossmann[3,4] and Hasegawa and Chen[46,47] originally demonstrated that the linearized ideal MHD equations admit solutions corresponding to a continuous spectrum in certain inhomogeneous equilibria. The singularities inherent in the Laplace transform of certain components of the perturbed macroscopic quantities lead to a nonzero time-averaged growth of these perturbations in localized regions in the equilibrium. Since the fluid energy is proportional to the square of the perturbed fluid velocity, it likewise grows in time when the fluid is driven by an oscillator at a frequency belonging to the continuous spectrum. Any small non-ideal plasma effects may then provide a mechanism for the thermalization of the absorbed energy.

The introduction of inhomogeneities into the plasma equilibrium causes the shear Alfvén and cusp frequency spectra to spread out into continuous spectra. This can best be illustrated by considering a relatively simple inhomogeneous equilibrium, i.e. an incompressible, cylindrically symmetric linear theta pinch with equilibrium variations allowed in the radial direction only. The ideal MHD equations describing perturbations of this plasma with a frequency ω and a longitudinal wave vector k reduce to a single, second-order ordinary differential equation for the Laplace transform of the perturbed radial velocity, $\hat{v}_r$, of the form[18]:

$$\frac{d}{dr}\left[\frac{A}{r}\frac{d}{dr}(r\hat{v}_r)\right] - \frac{k^2}{r}(r\hat{v}_r) = 0 \qquad (1.9)$$

In this equation, the coefficient A is defined as follows,

$$A = \rho(r)[\omega_A^2(r)-\omega^2)] \quad , \tag{1.10}$$

where $\rho(r)$ is the equilibrium mass density, ω_A is the local shear Alfvén wave frequency,

$$\omega_A^2 = \frac{k^2 B_z^2(r)}{\mu_o \rho(r)} \quad , \tag{1.11}$$

and B_z is the equilibrium magnetic field strength. The singular point of Eq. (1.9), i.e., A=0, identifies the shear Alfvén continuous spectrum. Based on the method of Frobenius[19,14], the general solution to Eq. (1.9) may be written as

$$r\hat{v}_r = c(\omega,k)[g(r,\omega)ln(r-r_o) + (r-r_o)h(r,\omega) + p(\omega,k)g(r,\omega)] \tag{1.12}$$

where $g(r,\omega)$ and $h(r,\omega)$ are analytic functions of r in some region about the radius, r_o, where $\omega^2=\omega_A^2(r_o)$, and $c(\omega,k)$, $p(\omega,k)$ are functions determined by the source and the boundary conditions. For azimuthally symmetric perturbations, the corresponding solution for the Laplace transform of the perturbed axial velocity, $\hat{v}_z$, is proportional to

$$\hat{v}_z \sim \frac{c(\omega,k)}{r-r_o} \quad . \tag{1.13}$$

This behavior follows from the condition of incompressibility, i.e., $\nabla\cdot\hat{\mathbf{v}}=0$. Comparison of Eq. (1.13) to (1.12) reveals that, while the perturbed radial velocity is square-integrable, the perturbed axial velocity is non-square-integrable. These modes therefore belong to the continuous spectrum of the ideal MHD equations. The constant, $c(\omega,k)$, is determined by the source of the perturbations, i.e., by the external oscillator which is driving the plasma boundary sinusoidally at a frequency, ω_o. It is thus proportional to the Laplace transform of the source, i.e.,

$$c(\omega,k) \sim \frac{\omega_o}{\omega^2-\omega_o^2} \quad . \tag{1.14}$$

The physical components of the perturbed velocity are obtained by taking the inverse Laplace transform of Eqs. (1.12)-(1.13), using Eq. (1.14). Because the inverse Laplace transform involves an integration over modes of the form Eqs. (1.12)-(1.13), the physical perturbations are, in general, not singular for finite time intervals. When the source frequency lies in the continuous spectrum of the equilibrium, then, about the surface where $\omega_o^2=\omega_A^2(r_o)$, the perturbed axial velocity, v_z, behaves as

$$v_z(r=r_o,t) \sim t \sin \omega_o t \quad . \tag{1.15}$$

Away from the resonant surface, $r \neq r_o$, the behavior of v_z is instead given as

$$v_z(r \neq r_o,t) \sim \sin \omega_o t \quad . \tag{1.16}$$

The implication of Eqs. (1.15) and (1.16) is that the energy input to the fluid from the external oscillator accumulates about the surfaces, r_o, where the oscillator frequency equals the local shear Alfvén resonant frequency.

In the ideal MHD model, the possibility of heating a plasma via the resonant excitation of shear Alfvén waves is therefore based on the premise that these waves belong to the continuous spectrum of the linearized ideal MHD operator and hence are characterized by non-square-integrable singularities. The presence of these singularities leads to a localized growth in the wave energy. Non-ideal effects will presumably thermalize the absorbed energy.

For equilibria which are inhomogeneous in more than one direction, like tokamaks and stellarators, identification of the continuum modes is considerably more complicated than in equilibria which are inhomogeneous in one dimension only. Pao[20] and Goedbloed[21] were the first to treat these problems in a tokamak equilibrium. By considering the MHD equations in orthogonal flux coordinates, Pao was able to show that the continua are specified on

each flux surface by the discrete spectra of a set of coupled differential equations involving only the operator $\vec{B}\cdot\nabla$. Though the eigenfrequencies are discrete on any particular flux surface, they again cover a continuous range of values as the flux surface is varied from the magnetic axis to the plasma edge. Similar sets of coupled differential equations for the continua have also been considered by Tataronis et al.[18,22], Hameiri[35], and Hameiri and Hammer[23] for more general toroidal equilibria, such as stellarators.

In this thesis, properties of the ideal MHD shear Alfvén wave in an axisymmetric toroidal device, such as a tokamak, will be described. An analytic representation for the shear Alfvén wave dispersion relation will be derived by directly solving the continuum eigenvalue equations using large aspect ratio expansions for the equilibrium quantities. Analyses of the results anticipated in experiments on tokamaks have previously been based on expressions for the continua which were derived using cylindrical models. Such calculations implicitly assumed that the toroidal nature of the equilibrium would not significantly alter the location, or even the existence, of singular surfaces in the plasma for appropriate oscillator frequencies and helicities. The analytic forms derived in this thesis for the continuum will be used to demonstrate that gaps appear in the continuous spectrum on, and in the immediate vicinity of, rational q surfaces, where q is the safety factor. The gap formation can be attributed to the coupling of poloidal harmonics by the periodic variations in the equilibrium due to first

order toroidicity corrections. Implications of the presence of these gaps will be discussed. Numerical representations of the shear Alfvén continuum of the Tokapole II device[11,24] will be obtained by a direct solution of the exact continuum equations, using a numerical solution[25] of the Grad-Shafranov equation for the Tokapole II equilibrium. These representations are in agreement with the qualitative model obtained using the analytic dispersion relation.

The shear Alfvén wave structure in the vicinity of a resonant surface, ϕ_o, will be analyzed using a generalization of the method of Frobenius[19,20,22]. It will be shown that the spatial singularities associated with the transform of the perturbed radial velocity are always logarithmic if the equilibrium is symmetric about the midplane, or else are of the form $(\phi-\phi_o)^{i\nu}$, when the equilibrium is not symmetric about the midplane. The parameter, ν, can then be determined by certain integrals involving equilibrium quantities. The corresponding behavior of the transforms of the perturbed fluid velocity components within the resonant surface is always non-square-integrable. A comparison with earlier results by Pao[20], Tataronis et al.[18,22], and Hameiri[35] will be presented. Finally, since the current experiments[10,11,12] involving shear Alfvén waves in axisymmetric devices all operate at very low equilibrium plasma pressures, a set of reduced MHD equations, valid in the very low beta limit, will also be derived and discussed.

This reduced set should provide a good description of these waves in these experiments.

The outline, then, of this thesis is as follows. The basic theory of shear Alfvén waves in toroidal systems is presented in Chapter 2. Analytic solutions for the shear Alfvén continuum in a large aspect ratio tokamak are derived in Chapter 3, while the numerical solutions are presented in Chapter 4. The analysis of the mode structure in the vicinity of the resonant surfaces is developed in Chapter 5. Chapter 6 contains the derivation and discussion of the set of reduced MHD equations valid in the limit of zero equilibrium pressure. Results and suggestions for further research are summarized in Chapter 7. A number of appendices containing additional details on some of the calculations in the main chapters are also provided for the convenience of the reader.

Figure 1.1 Friedrichs Diagram for the Three MHD Waves

The wavefronts formed by the three MHD waves are plotted at some instant in time following their excitation by a source localized to the origin of an x-z coordinate system. The equilibrium magnetic field points in the x-direction. Note that propagation of the shear Alfvén and cusp waves is localized to a cone but the propagation of the fast wave is isotropic.

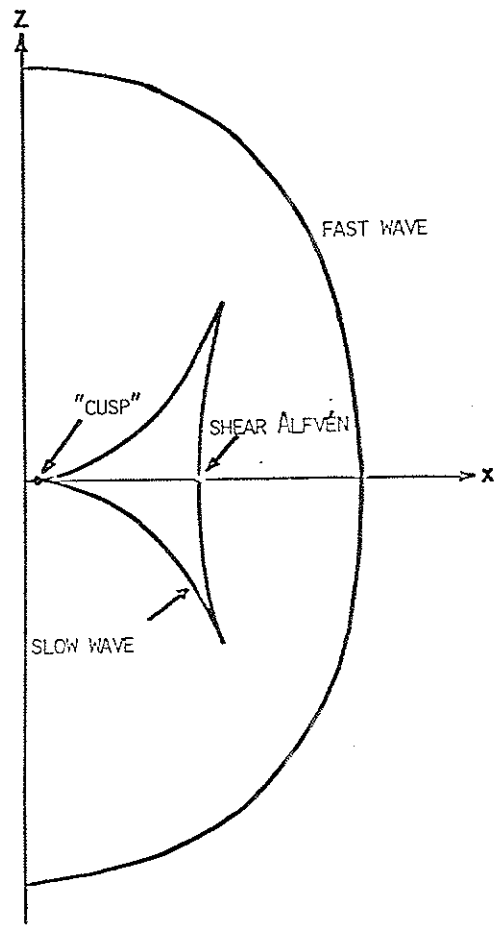

FIGURE 1.1

Figure 1.2 Dispersion Diagram for the Three MHD Waves

Solutions to the dispersion relation, Eq. (1.1), for the three MHD waves are plotted for a fixed value of $k_\parallel$. Note that the shear Alfvén and cusp waves exhibit resonances at $\omega=k_\parallel V_A$ and $\omega=k_\parallel V_C$, respectively.

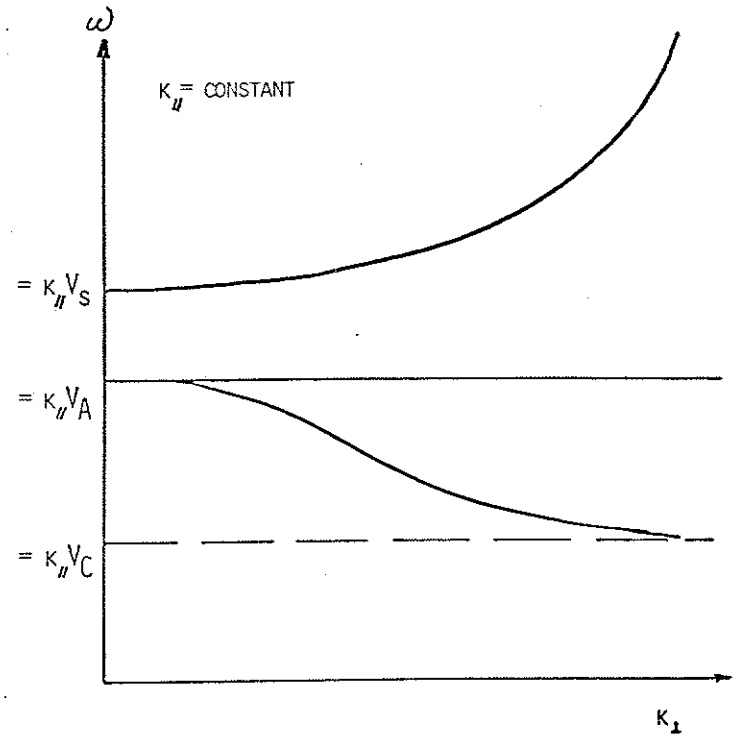

FIGURE 1.2

CHAPTER 2

THE MHD DESCRIPTION OF SHEAR ALFVÉN WAVES IN TOROIDAL EQUILIBRIA

According to ideal MHD theory, a plasma may be heated with RF power by excitation of the singular shear Alfvén wave. The prediction of RF energy absorption via this mode is based on the idea that the Alfvén wave lies in the continuous spectrum of the linearized ideal MHD equations and consequently exhibits spatially non-square-integrable singularities at particular locations in an inhomogeneous plasma. An implication of the singularity, or resonance, is that energy from an external source can be transferred to the Alfvén wave, and hence to the plasma. To determine whether it is possible to utilize this heating scheme on a plasma in a particular equilibrium configuration, it is necessary to determine first if the ideal MHD equations yield a continuum for the chosen equilibrium, i.e.,whether or not it is possible to satisfy all appropriate boundary conditions with a mode in the continuum of the equilibrium. If the chosen equilibrium is spatially inhomogeneous in one direction only, then the continuous spectra and associated wave structure may be obtained analytically. For example, in the cylindrical screw pinch, Fourier analysis in the directions of symmetry θ,z allows the MHD equations to be reduced to a single ordinary differential equation in the radial coordinate, r:[14]

$$\frac{d}{dr}\left[\frac{1}{b_2}\frac{d}{dr}(r\hat{\xi}_r)\right] - \left[b_1 + \frac{b_o^2}{b_2} - \frac{d}{dr}\left(\frac{b_o}{b_2}\right)\right](r\hat{\xi}_r) = 0 \quad . \tag{2.1}$$

In Eq. (2.1), the dependent variable, $\hat{\xi}_r$, is the Laplace transform of the radial component of the linearized fluid displacement, $\vec{\xi}$, defined as

$$\vec{\xi}(\vec{r},t) = \int_o^t dt'\vec{v}(\vec{r},t') \quad .$$

The coefficients b_o, b_1, and b_2 are defined as follows:

$$b_o = \frac{-1}{A}\left[\frac{2B_p}{\mu_o r}\right]\left[\frac{m}{r}F + \frac{\rho^2\omega^4 B_p}{C}\right]$$

$$b_1 = \frac{1}{r}\left[A - \frac{2B_p}{\mu_o r}r\frac{d}{dr}\left(\frac{B_p}{r}\right) - \left(\frac{2B_p}{\mu_o r}\right)^2\frac{F^2}{A} - \left(\frac{2B_p}{\mu_o r}\right)^2\frac{\rho^2\omega^4 B_p^2}{AC}\right]$$

$$b_2 = \frac{-rD}{AC} \quad ,$$

where B_p and B_z are the equilibrium azimuthal and longitudinal magnetic fields and where

$$A = -\rho\omega^2 + \frac{F^2}{\mu_o}$$

$$C = -\left[\gamma P_o + \frac{B^2}{\mu_o}\right]\rho\omega^2 + \gamma P_o \frac{F^2}{\mu_o}$$

$$D = \rho^2\omega^4 + \left(\frac{m^2}{r^2} + k^2\right)C$$

$$F = \frac{m}{r} B_p + kB_z$$

The azimuthal and longitudinal mode numbers are m and k, respectively, γ is the ratio of specific heats, P_o is the equilibrium fluid pressure, ρ is the equilibrium mass density, and μ_o is the vacuum permeability. The continua are specified algebraically by the singular points of the coefficients in the radial equation. The shear Alfvén continuum in the screw pinch is given by

$$\omega_A^2 = \frac{\left(\frac{mB_p}{r} + k\,B_z\right)^2}{\mu_o\rho} \quad . \tag{2.2}$$

Since the equilibrium quantities are functions of the radius, r, Eq. (2.2) predicts a continuous range of resonant frequencies corresponding to $0 < r < a$, where a is the plasma radius, at which the Alfvén wave propagates. For any frequency, ω_o, in this range, the radial eigenfunction in a compressible plasma exhibits a logarithmic singularity at the resonant surface, r_o, where $\omega_o^2 = \omega_A^2(r_o)$[14,22].

The procedure for obtaining the continuous spectra and for determining the nature of the radial wave structure about the resonant surfaces in an axisymmetric tokamak is considerably more complicated because there is one less degree of symmetry. Pao[20] and Goedbloed[21] were the first to treat these problems. By considering the MHD equations in orthogonal flux coordinates, Pao demonstrated that the continua in an axisymmetric tokamak are determined by the eigenvalues of a set of coupled first order ordinary differential equations on each flux surface. Though the eigenvalues are discrete on any particular flux surface, they again cover a continuous range of values as the flux surface is varied from the axis to the plasma edge. For a given frequency, ω_o, in this range, the radial eigenfunction can be shown to be singular at the resonant surface, ϕ_o, where $\omega_o^2 = \omega_A^2(\phi_o)$. Though Pao specified a criterion on the solutions which implies that the spatial singularities in the radial direction are logarithmic in nature, in fact this criterion is satisfied absolutely only for compressible plasmas in an up-down symmetric equilibrium. In this thesis, it will be shown in

Chapter 5 that the wave structure in the vicinity of a resonant surface is always spatially singular in an axisymmetric tokamak, where the exact nature of the singularity depends on the particular characteristics of the equilibrium being considered.

Similar sets of coupled differential equations for the ideal MHD continua have also been considered by Tataronis, Talmadge, and Shohet[18], Tataronis and Salat[22], Hameiri [35], and Hameiri and Hammer[23] for more general toroidal equilibria. However, analytic representations for the continua in a toroidal equilibrium were not derived in any of these studies. In this thesis, analytic representations, for the shear Alfvén continuum of a large aspect ratio tokamak, which were obtained using the formalism of Tataronis et al.[18], will be derived and discussed in Chapter 3.

Tataronis et al.[18] have generalized Pao's approach to include toroidal equilibria with closed, nested flux surfaces, which may or may not be axisymmetric. Their analysis is based on the usual linearized equations of ideal MHD theory,

$$i\omega\rho\vec{v} = \frac{1}{\mu_o}(\vec{B}\cdot\nabla)\vec{B} + \frac{1}{\mu_o}(\vec{b}\cdot\nabla)\vec{B} - \nabla p^* \quad , \tag{2.3}$$

$$i\omega\vec{b} = (\vec{b}\cdot\nabla)\vec{v} - (\vec{v}\cdot\nabla)\vec{B} - \vec{B}\nabla\cdot\vec{v} \quad , \tag{2.4}$$

$$i\omega p = -\vec{v}\cdot\nabla P_o - \gamma P_o \nabla\cdot\vec{v} \quad , \tag{2.5}$$

where the total perturbed pressure is $p^* = p + \vec{B}\cdot\vec{b}/\mu_o$ and γ is the ratio of specific heats. The equilibrium mass density, magnetic field and pressure are denoted respectively by ρ, $\vec{B}$ and P_o, while the perturbed pressure, magnetic field and plasma velocity are denoted respectively by p, $\vec{b}$, and $\vec{v}$. A time dependence of $\exp(i\omega t)$ has been assumed. Identification of the continuous spectra is facilitated by transformation to general flux coordinates ψ, θ, ϕ, in which Equations (2.3)–(2.5) may be written in the following form[18]:

$$\frac{\partial\vec{X}}{\partial\psi} = \vec{A}\cdot\vec{X} + \vec{C}\cdot\vec{Y} \quad , \tag{2.6}$$

$$\vec{X}\cdot\vec{Y} = \vec{K}\cdot\vec{X} \quad , \tag{2.7}$$

$$i\omega b^1 = \vec{B}\cdot\nabla v^1 \quad , \tag{2.8}$$

where

$$\vec{X} = \begin{bmatrix} v^1 \\ \\ \\ i\omega p^* \end{bmatrix} , \quad \vec{Y} = \begin{bmatrix} v^2 \\ \\ v^3 \\ \\ i\omega b^2 \\ \\ i\omega b^3 \end{bmatrix} , \qquad (2.9)$$

and $\vec{\vec{A}}$, $\vec{\vec{C}}$, $\vec{\vec{X}}$ and $\vec{\vec{K}}$ are matrices whose elements are linear combinations of first derivatives with respect to θ and ϕ only, with ϕ appearing as parameter. Explicit forms for these matrices, valid for an axisymmetric toroidal equilibrium described by general flux coordinates, are given in Appendix B. The vectors $\vec{v}$, $\vec{B}$ are expressed in contravariant form in which $v^i \equiv \vec{v}\cdot\nabla u^i$, where $u^i = (\phi,\theta,\phi)$. A formal solution to Eqs. (2.6)-(2.8) is obtained by first solving Eq. (2.7) for $\vec{Y}$,

$$\vec{Y} = \vec{\vec{X}}^{-1}\cdot\vec{\vec{K}}\cdot\vec{X} \quad , \qquad (2.10)$$

and then eliminating $\vec{Y}$ from Eq. (2.6) to obtain an equation which can be solved for $\vec{X}$. Admissible solutions must be periodic in θ, ϕ (since the flux surfaces are nested closed tori), regular about the magnetic axis, and must satisfy the appropriate continuity

conditions at the plasma-vacuum interface[26]. This procedure will fail on a flux surface, ϕ_o, if, for a given ω, the inverse of $\vec{\vec{X}}$ does not exist. The condition for the nonexistence of $\vec{\vec{X}}^{-1}$ is that a non-trivial vector $\vec{g}(\phi,\theta,\phi)$ exists which is periodic in θ and ϕ on the surface, ϕ_o, and which satisfies

$$\vec{\vec{X}}\cdot\vec{g} = 0 \quad . \qquad (2.11)$$

Equation (2.11) is a system of linear partial differential equations in terms of the operator $\vec{B}\cdot\nabla$, with ϕ_o and ω appearing only as parameters. Consequently, the system together with the periodic boundary conditions maybe regarded as an eigenvalue problem on each magnetic surface for the frequencies, ω, and the vector $\vec{g}$. The sets of frequencies so determined form the continuous spectrum for the equilibrium. The surface, $\phi=\phi_o(\omega)$, is singular in the sense that Eqs. (2.6), (2.7), and (2.8) may possess singular solutions about that surface[18,20-23,25].

An analysis of the behavior of the wave functions about the resonant surfaces, ϕ_o, yields the form of the singularities. A generalization[18,20,22,35] of the method of Frobenius[19,36], which is used to solve an ordinary differential equation in the vicinity of a singular point, such as Eq. (2.1), may be constructed. The nature of the functions $\vec{X}$ and $\vec{Y}$ about a singular surface, ϕ_o, may be determined by considering expansions of the following form[18,22,23,35]:

$$\vec{X}(\phi,\theta,\phi) = (\phi-\phi_o)^{\nu}[\vec{f}_o(\theta,\phi) + (\phi-\phi_o)\vec{f}_1(\theta,\phi) + \cdots]$$

$$\vec{Y}(\phi,\theta,\phi) = (\phi-\phi_o)^{\nu-1}[\vec{g}_o(\theta,\phi) + (\phi-\phi_o)\vec{g}_1(\theta,\phi) + \cdots] \quad , \tag{2.12}$$

where the coefficients $\vec{f}_i(\theta,\phi)$ and $\vec{g}_i(\theta,\phi)$ are periodic in θ, ϕ and ν is a constant. Upon substitution of these expressions into Eqs. (2.6) and (2.7), expansion of the matrices $\vec{\vec{A}}$, $\vec{\vec{C}}$ $\vec{\vec{\chi}}$ and $\vec{\vec{K}}$ in powers series in ϕ and about ϕ_o, ($\vec{\vec{A}} = \vec{\vec{A}}_o + (\phi-\phi_o)\vec{\vec{A}}_1 + \cdots$ etc.), and the equating of the coefficients of like powers of $(\phi-\phi_o)$, a hierarchy of equations for the functions $\vec{f}_i$ and $\vec{g}_i$ is obtained. The equations which arise from the $(\phi-\phi_o)^{\nu-1}$ and $(\phi-\phi_o)^{\nu}$ coefficients are,

$$\vec{\vec{\chi}}_o \cdot \vec{g}_o = 0 \quad , \tag{2.13}$$

$$\nu\vec{f}_o = \vec{\vec{C}} \cdot \vec{g}_o \quad , \tag{2.14}$$

$$\vec{\vec{\chi}}_o \cdot \vec{g}_1 = (\vec{\vec{K}}_o \cdot \vec{\vec{C}}_o/\nu - \vec{\vec{\chi}}_1)\,\vec{g}_o \quad . \tag{2.15}$$

If Eq. (2.13) can be satisfied by a non-trival vector $\vec{g}_o$, which is periodic in θ, ϕ, then the surface ϕ_o is singular. Moreover, it follows that $\vec{\vec{\chi}}_o$ is a singular operator, since the inverse $\vec{\vec{\chi}}_o^{-1}$ does

not exist. Hence, Eq. (2.15) is a singular equation for $\vec{g}_1$, which can be solved only if the right-hand side satisfies a set of compatibility conditions[27], to be described more completely in Chapter 4. These conditions are

$$\langle\vec{u}_i|(\vec{\vec{K}}_o\cdot\vec{\vec{C}}_o - \nu\vec{\vec{\chi}}_1)\cdot\vec{g}_o\rangle = 0 \tag{2.16}$$

where $\langle\vec{a}|\vec{b}\rangle$ denotes the inner product between the vectors $\vec{a}$ and $\vec{b}$ over the singular surface, and $\vec{u}_i$, $i = 1,\cdots,n$, comprise the set of basis vectors of the null space of $\vec{\vec{\chi}}_o$. Expanding $\vec{g}_o$ in terms of $\vec{u}_i$'s yields the following eigenvalue problem for the parameter, ν:

$$(\vec{\vec{R}}-\nu\vec{\vec{S}}) \cdot \vec{v} = 0 \quad , \tag{2.17}$$

where $\vec{\vec{R}}$ and $\vec{\vec{S}}$ are matrices whose elements are given by

$$R_{ij} = \langle\vec{u}_i|\vec{\vec{K}}_o\cdot\vec{\vec{C}}_o|\vec{u}_j\rangle \tag{2.18}$$

and

$$S_{ij} = \langle\vec{u}_i|\vec{\vec{\chi}}_1|\vec{u}_j\rangle \tag{2.19}$$

respectively. That the solution for ν may be formulated as an eigenvalue problem was not considered in previous treatments[18,20,22,23,35]. The behavior of any possible spatial singularities of the wave functions is effectively determined by the

values of ν which satisfy this eigenvalue problem. If the implied spatial singularities are non-square-integrable, then the concept of RF energy absorption by the continuum is valid. However, if the solutions for ν indicate that $\vec{X}$ and $\vec{Y}$ do not exhibit non-square-integrable spatial singularities, then the modes do not belong to a continuous spectrum and the possibility of heating the plasma by absorption in the continuum is questionnable. The criterion given by Pao is equivalent to the one above when $\nu = 0$ is the only possible solution. In reference 22, Tataronis and Salat indicate that if $\nu = 0$ only, then it can be shown that $\vec{X}$ and $\vec{Y}$ contain logarithmic singularities about the surface, ϕ_o. More generally, if any solution for ν is $\nu = 0$, then it will be shown in Chapter 4 that logarithmic singularities in $(\phi-\phi_o)$ are present in solutions for $\vec{X}$ and $\vec{Y}$. For equilibria which are inhomogeneous in one direction only, the analog of Eq. (2.17) can be solved. For a compressible plasma in a cylindrical screw pinch, ν can be shown to be equal to zero[22], while for an incompressible plasma in a cylindrical screw pinch, ν can be shown to be purely imaginary[22]. In Chapter 5 of this thesis, ν will be shown to be either zero or imaginary for an axisymmetric, but otherwise arbitrary, tokamak plasma.

At this point, it is useful to examine in more detail the solutions for the continua and associated spatial singularities in a cylindrical screw pinch configuration[4,13,14]. In terms of cylindrical coordinates (r,θ,z), the linearized MHD equations have

the form of Eqs. (2.6)-(2.9), where ϕ is replaced by r, and the toroidal coordinate is replaced by the axial coordinate, z. Because of cylindrical symmetry, the eigenvalue equations for the continuum frequencies, Eq. (2.11), become purely algebraic after a Fourier decomposition in the poloidal angle, θ, is taken. The matrix, $\overleftrightarrow{\chi}$, is thus given by

$$\begin{bmatrix} -\rho\omega^2-\left(1-\frac{B_\theta^2/\mu_o}{B_*}\right)\frac{DD}{\mu_o} & \frac{B_zB_\theta/\mu_o}{B_*}\frac{DD}{\mu_o} \\ \frac{B_\theta B_z/\mu_o}{B_*}\frac{DD}{\mu_o} & -\rho\omega^2-\left(1-\frac{B_z^2/\mu_o}{B_*}\right)\frac{DD}{\mu_o} \end{bmatrix} \tag{2.20}$$

where $D \equiv \vec{B}\cdot\nabla = \frac{mB_\theta}{r} + kB_z$, m and k are the poloidal and axial mode numbers, respectively, $B_* = \gamma P_o + |\vec{B}|^2/\mu_o$, and the vector $\vec{Y}$ now is given as

$$\begin{bmatrix} rv_\theta \\ \\ v_z \end{bmatrix} . \qquad (2.21)$$

Solving for the frequencies, ω^2, yields the shear Alfvén continuum, where

$$\omega_A^2 = \frac{\left(\frac{mB_\theta}{r} + kB_z\right)^2}{\mu_o \rho} , \qquad (2.22)$$

and the cusp, or slow wave, continuum where

$$\omega_c^2 = \frac{\gamma P_o}{B_*} \omega_A^2 . \qquad (2.23)$$

Estimates for the shear Alfvén continuum frequencies of a tokamak which are based on Eq. (2.22) cannot yield particularly accurate estimates since Eq. (2.22) is not a flux function in a toroidal equilibrium. The estimates are made by identifying B_θ with the poloidal magnetic field, B_z with the toroidal magnetic field, r with the minor radius of the flux surface, and k with n/R_o, the magnitude of the wave vector in the toroidal direction. In a tokamak, these functions all vary with the poloidal angle, θ. It becomes necessary to introduce some ad hoc flux surface averages of these quantities

in order to obtain some estimate for ω_A^2 which is constant on a flux surface. Even so, it is still not clear a priori that the toroidal nature of the problem will not significantly alter the structure of the shear Alfvén continuum away from that predicted by the straight cylindrical model. In this thesis, a strong distortion of the cylindrical model predictions which occurs about rational q surfaces will be derived in Chapter 3 and its implications for experiments discussed.

The radial structure of the shear Alfvén wave about the resonant surface, r_o, in a compressible, cylindrically symmetric, screw pinch plasma may now easily be shown to be logarithmic, using the formalism developed in Eqs. (2.16)-(2.19). The results obtained in this method are equivalent to the results obtained by aplying the method of Frobenius to Eq. (2.1)[28] and to the results obtained by direct application of Eq. (2.16)[4,14]. The analog, for the cylindrical case, of the matrix $\vec{K}_o \cdot \vec{C}_o$ in Eq. (2.16) is:

$$\begin{bmatrix} 0 & -\Delta \\ \\ \Delta & 0 \end{bmatrix} , \qquad (2.24)$$

where $\Delta \equiv 2\left(\frac{B_\theta}{r}\right)(\gamma P_o/B_*)D \frac{\partial}{\partial z}$. Because there are two vectors in the null space of $\vec{\chi}_o$ for a given ω_A^2, namely,

$$\begin{bmatrix} B_z \\ -B_\theta \end{bmatrix} a(m,k)e^{\pm i(m\theta+kz)} \qquad (2.25)$$

where $a(m,k)$ is a constant, then the eigenvalue problem of Eq. (2.17) for the parameter, ν, is of order 2. Direct solution yields $\nu = 0$ as a double root, indicating the presence of a logarithmic singularity in v_r and p^*. When the plasma is incompressible, i.e. $\gamma \to \infty$, the spatial singularity is no longer logarithmic. In this case, the shear Alfvén and cusp continua are degenerate. There are now four vectors in the null space of $\vec{\vec{\chi}}_o$; the two as given in Eq. (2.25), and the following two,

$$\begin{bmatrix} B_\theta \\ B_z \end{bmatrix} c(m,k)e^{\pm i(m\theta+kz)} \quad , \qquad (2.26)$$

where $c(m,k)$ is a constant.

One can readily verify that the radial behavior in the incompressible screw pinch is characterized by an imaginary exponent,

$$\nu = \pm 2i\left(\frac{k}{f}\right)\left(\frac{B_\theta}{r}\right)\left[\frac{\partial \ln(f^2/\rho)}{\partial r}\right]^{-1} \qquad (2.27)$$

where $f \equiv \frac{mB_\theta}{r} + kB_z$. In either case, the compressible plasma or the incompressible plasma, the radial wave structure is singular, though the exact nature of the singularity depends on the case in question. The corresponding behavior of the perturbed poloidal and axial velocities can be shown to be non-square-integrable. In this thesis, the effects of the breaking of symmetry, by toroidicity and noncircularity of the plasma cross section, on the structure of the Alfvén waves about a resonant surface in a tokamak will be investigated.

The ideal MHD continua for an axisymmetric tokamak and the corresponding behavior of the wave function along the singular surface are specified by the solution of the system of coupled partial differential equations in Eq. (2.11). When the two angle variables θ,ϕ on the singular surface, ϕ_o, are chosen to be the Hamada coordinates θ,ξ (see Appendix A for details), these equations assume the form,

$$(\mu_o\rho\omega^2)\vec{\vec{N}}(\theta) \cdot \vec{Y}(\theta,\xi) + \vec{B} \cdot \nabla[\vec{\vec{N}}(\theta)\vec{B} \cdot \nabla] \cdot \vec{Y}(\theta,\xi) = 0 \quad , \qquad (2.28)$$

where $\vec{\vec{M}}$ and $\vec{\vec{N}}$ are matrices whose elements are functions only of θ in an axisymmetric equilibrium, the differential operator $\vec{B} \cdot \nabla$ is given by

$$\vec{B} \cdot \nabla = (\vec{B}\cdot\nabla\theta)\frac{\partial}{\partial\theta} + (\vec{B}\cdot\nabla\xi)\frac{\partial}{\partial\xi} = B^2\frac{\partial}{\partial\theta} + B^3\frac{\partial}{\partial\xi} \quad , \qquad (2.29)$$

where B^2 and B^3 are the contravariant components of the equilibrium magnetic field, and the vector $\vec{Y}$ is now defined by,

$$\vec{Y} = \begin{bmatrix} v^2 \\ \\ v^3 \end{bmatrix} = \begin{bmatrix} \vec{v}\cdot\nabla\theta \\ \\ \vec{v}\cdot\nabla\xi \end{bmatrix} \quad . \tag{2.30}$$

The elements of $\vec{Y}$ are the contravariant components of the perturbed velocity in the directions $\nabla\theta$, $\nabla\xi$. The matrices $\vec{M}$ and $\vec{N}$ are defined as follows,

$$\vec{M}(\theta) = \begin{bmatrix} g_{22} & g_{23} \\ \\ g_{32} & g_{33} \end{bmatrix} \quad , \quad \vec{N}(\theta) = \vec{M} - \frac{1}{B_*^T}\begin{bmatrix} B_2B_2 & B_2B_3 \\ \\ B_3B_2 & B_3B_3 \end{bmatrix} \quad , \tag{2.31}$$

where the terms, g_{ij}, are metric tensor elements for the equilibrium, and B_2 and B_3 are covariant components of the equilibrium magnetic field. The variable, B_*^T, is given by

$$B_*^T = |B|^2\left(1 + \frac{1}{2}\gamma\beta_M\right) \quad , \tag{2.32}$$

where $|B|$ is the magnitude of the equilibrium field and β_M is the total plasma beta. In an axisymmetric tokamak, the toroidal angle, ξ, is ignorable and the matrices $\vec{M}$ and $\vec{N}$ are functions only of the poloidal angle, θ. More generally, in a non-axisymmetric device, these matrices would also depend on ξ.

To proceed further, it is particularly convenient to introduce a transformation[27] from the Hamada coordinates (θ,ξ) to (θ,β), where $\beta = q(\phi)\theta - \xi$ and $q(\phi)$ is the safety factor, $B^3(\phi)/B^2(\phi)$. Recall that in Hamada coordinates the magnetic lines of force are straight on each magnetic surface and furthermore, B^2 and B^3 are functions only of ϕ. The coordinate β is constant on a field line. Consequently, the partial differential operator $\vec{B}\cdot\nabla$ in terms of these new coordinates becomes an ordinary differential operator given by

$$\vec{B}\cdot\nabla = B^2\left.\frac{\partial}{\partial\theta}\right|_\beta \tag{2.33}$$

Using Eq. (2.33) in Eq. (2.28) yields the following equation for $\vec{Y}(\theta,\beta)$ in an axisymmetric tokamak,

$$\lambda\vec{M}(\theta)\cdot\vec{Y}(\theta,\beta) + \left.\frac{\partial}{\partial\theta}\right|_\beta\left[\vec{N}(\theta)\left.\frac{\partial}{\partial\theta}\right|_\beta\right]\cdot\vec{Y}(\theta,\beta) = 0 \quad , \tag{2.34}$$

where the eigenvalue λ is equal to

$$\lambda = \frac{\mu_o \rho}{(B^2)^2}\,\omega^2 \tag{2.35}$$

These equations are a set of coupled Sturm-Liouville equations and, with periodic boundary conditions, comprise a self-adjoint system. [See Appendix B for proof of the self-adjointness.]

In the coordinates, θ,β, toroidal periodicity is satisfied by

$$\vec{Y}(\theta,\beta+2\pi) = \vec{Y}(\theta,\beta) \quad , \tag{2.36}$$

where increasing β by 2π at constant θ is equivalent to moving once around toroidally. Poloidal periodicity is satisfied by

$$\vec{Y}(\theta,\beta) = \vec{Y}(\theta+2\pi,\beta+2\pi q) \quad , \tag{2.37}$$

which corresponds to increasing θ by 2π and then moving back toroidally to the original physical position. Since the only dependence on the coordinate β arises in the eigenvector $\vec{Y}$, a Fourier decomposition of the equation in the ignorable angle β is permitted in the following form,

$$\vec{Y}(\theta,\beta) = \sum_N \vec{\Phi}_N(\theta,\beta) = \sum_N e^{-iN\beta}\vec{\Phi}_N(\theta) \tag{2.38}$$

In the next chapter, the inverse aspect ratio, $\varepsilon \sim a/R_o$, is assumed to be small and the matrix elements of $\vec{M}$ and $\vec{K}$ in Eq. (2.34) are expanded in terms of ε, with $\vec{Y}(\theta,\beta)$ in the form given by Eq. (2.38). A perturbation solution of the resulting eigenvalue equations for the continuous spectra is then developed.

CHAPTER 3

ANALYSIS OF THE CONTINUOUS SPECTRA IN A LARGE ASPECT RATIO TOKAMAK

A description of the ideal MHD continuous spectra in a large aspect ratio tokamak provides an understanding of how toroidicity and/or noncircularity of the flux surface cross sections influence the location of the resonant surfaces where localized heating may occur. In this chapter, an analytic model for the continua is obtained by solving the eigenvalue equations, Eq. (2.33), for a general, axisymmetric tokamak equilibrium in a large aspect ratio expansion scheme. Toroidicity is treated explicitly as an order $\epsilon \sim a/R_o$ perturbation of an infinitely long periodic cylinder. Formal perturbation techniques of quantum mechanics are used to derive approximate dispersion relations. A generalization of the method to include effects of noncircularity of the flux surface cross sections follows readily from the calculations. The small inverse aspect ratio expansion scheme is developed in section 1, while the dispersion relations are derived and discussed in sections 2 and 3. Numerical solutions to the exact equations will be presented in the next chapter.

Section 1. The Perturbation Expansion

In the limit of small ϵ, the magnetic fields and radial coordinate of the tokamak are assumed to vary as

$$
\begin{aligned}
B_T &= B_{T_o}(1-\epsilon\, r/a \cos\chi) \\
B_p{}^T &= B_p(1+\epsilon\, \Lambda\, r/a \cos\chi) \\
R &= R_o(1+\epsilon\, r/a \cos\chi)
\end{aligned}
\tag{3.1}
$$

where $B_p{}^T$ is the poloidal field in the tokamak, B_p is the poloidal field at $R = R_o$, Λ is a quantity of order 1[30], a and R_o are, respectively, the minor and major radii, χ is a poloidal angle which varies uniformly from 0 to 2π, and r is a radial coordinate measured from the magnetic axis. The flux surfaces are taken to be circular under the preceding assumptions, but the effects due to non-circularity will be discussed further on. With these expansions, the metric tensor elements and equilibrium magnetic field components, which appear as elements of the matrices $\overleftrightarrow{M}$ and $\overleftrightarrow{K}$, can be readily decomposed into terms of order ϵ^o, which describe an infinitely long periodic cylinder (screw pinch), and corrections of order ϵ^1 and higher, which are due to toroidicity. The screw pinch limit is obtained by holding the quantities $qR_o = rB_{T_o}/B_p$ and ϕ/R_o fixed while allowing $\epsilon \to 0$. In this manner, the rotational transform and poloidal flux in the tokamak, which are defined on a length $2\pi R_o$, evolve into the rotational transform per unit length and the poloidal flux per unit length of an infinitely long cylinder with periodicity length $2\pi R_o$. In this limit, the poloidal Hamada angle θ differs from χ by an amount of order ϵ. In Eq. (3.1), the

angle χ may hence be replaced by θ with an error of order ϵ^2 in B_T, B_p^T and R. The expansions of the elements of $\vec{\vec{M}}$ and $\vec{\vec{N}}$ are given as follows:

$$g_{22} = r^2(1+2\ \epsilon\ \Lambda \frac{r}{a} \cos\theta) + O(\epsilon^2) \tag{3.2}$$

$$g_{23} = -2\ \epsilon\ q\ R_o^2 \frac{r}{a} \cos\theta + O(\epsilon^2)$$

$$g_{33} = R_o^2 + 2\ \epsilon\ R_o^2 \frac{r}{a} \cos\theta + O(\epsilon^2)$$

$$B_2 = rB_p(1+2\ \epsilon\Lambda \frac{r}{a} \cos\theta) - 2\ \epsilon\ q\ R_o\ B_{T_o} \frac{r}{a} \cos\theta + O(\epsilon^2)$$

$$B_3 = R_o B_{To}(1+2\ \epsilon\Lambda \frac{r}{a} \cos\theta) - 2\ \epsilon\ q\ R_o\ B_{T_o} \frac{r}{a} \cos\theta + O(\epsilon^2)$$

$$B_*^T = B_*(1-2\ \epsilon \frac{r}{a} B_W \cos\theta) + O(\epsilon^2)$$

where

$$B_W \equiv \frac{B_{T_o}^2 - \Lambda B_p^2}{B_{T_o}^2 + B_p^2} \ .$$

The ϵ^o terms correspond to a screw pinch described by coordinates ϕ, θ and $z' \equiv z/R_o$, where $2\pi R_o$ is the periodicity length of the cylinder and $qR_o = rB_{T_o}/B_p$ is the rotational transform.

Using the expansions given in Eq. (3.1), the matrices $\vec{\vec{M}}$ and $\vec{\vec{N}}$ may be similarly separated into "unperturbed" parts containing the "screw pinch" terms plus small "perturbed" parts due to first order toroidicity effects. This decomposition can be written as follows:

$$\vec{\vec{M}} = \vec{\vec{M}}^o + \epsilon\ \vec{\vec{M}}^1 + O(\epsilon^2) \tag{3.3}$$

$$\vec{\vec{L}} \equiv \frac{\partial}{\partial\theta}\Big|_\beta \vec{\vec{N}}(\theta) \frac{\partial}{\partial\theta}\Big|_\beta = \vec{\vec{L}}^o + \epsilon\ \vec{\vec{L}}^1 + O(\epsilon^2)$$

Since the operators $\vec{\vec{M}}^o$, $\vec{\vec{L}}^o$, $\vec{\vec{M}}^1$, $\vec{\vec{L}}^1$ are all Hermitian, and since $\epsilon\ \vec{\vec{M}}^1$ and $\epsilon\ \vec{\vec{L}}^1$ represent small corrections to $\vec{\vec{M}}^o$ and $\vec{\vec{L}}^o$, it is permissible to use the formal perturbation techniques of quantum mechanics to solve the equations[31]. In applying the methods, the eigenvector $\vec{Y}$ is expanded in terms of any complete set of functions. It is generally most convenient to choose as this set the eigenfunctions of the zeroth order, or unperturbed, system of equations. Thus, from Eq. (3.3), the basis functions, Φ^o_{NM}, are obtained from the following equation,

$$\lambda^o_{NM}\ \vec{\vec{M}}^o \cdot \Phi^o_{NM} + \vec{\vec{L}}^o \cdot \Phi^o_{NM} = 0 \quad , \tag{3.4}$$

where M and N are respectively poloidal and toroidal mode numbers resulting from a Fourier decomposition with respect to θ and β, and λ^o_{NM} is the eigenvalue associated with this reduced problem. Because Eq. (3.4) consists of 2 decoupled harmonic oscillator type

equations, the solutions, $\vec{\Phi}^o_{NM}$, form a complete set. Therefore, we can expand the eigenvectors in the tokamak, $\vec{\Phi}$, in terms of the screw pinch eigenvectors, $\vec{\Phi}^o_{NM}$, as follows,

$$\vec{\Phi} = \sum_{N,M} a_{NM} \vec{\Phi}^o_{NM} \equiv \sum_{\alpha} a_\alpha \vec{\Phi}_\alpha \tag{3.5}$$

Upon substituting this expansion for $\vec{\Phi}$ into Eq. (2.34) and taking inner products of the resulting expression with each of the $\vec{\Phi}^o_\alpha$'s, an infinite set of equations for the coefficients a_α is obtained. This set of equations has a nontrivial solution if and only if the determinant of the coefficients of the a_α's vanishes. Using Eq. (3.4), this determinant may be written in the form

$$\det \begin{bmatrix} \lambda-\lambda^o_\alpha+\varepsilon\langle\Phi^o_\alpha|\lambda M^1+L^1|\Phi^o_\alpha\rangle & \varepsilon\langle\Phi^o_\alpha|\lambda M^1+L^1|\Phi^o_{\alpha+1}\rangle\cdots \\ \varepsilon\langle\Phi^o_{\alpha+1}|\lambda M^1+L^1|\Phi_\alpha\rangle & \lambda-\lambda^o_{\alpha+1}+\varepsilon\langle\Phi^o_{\alpha+1}|\lambda M^1+L^1|\Phi^o_{\alpha+1}\rangle\cdots \\ \vdots & \vdots \end{bmatrix} = 0 \tag{3.6}$$

It is this equation which determines the eigenvalue λ. Notice that the terms arising from toroidal corrections are all of order ε or smaller. In the following sections, the eigenvalues for the continuous spectra in a large aspect ratio tokamak will be obtained by assuming the following expansion for λ in Eq. (3.6),

$$\lambda = \lambda^o + \varepsilon\lambda^1 + o(\varepsilon^2) \tag{3.7}$$

and systematically determining the coefficients λ^1.

Section 2. Solution of the Lowest Order Equations (Screw Pinch)

In this section, the properties of the basis functions are obtained by solving Eq. (3.4). Since the operators $\vec{M}^o$ and $\vec{L}^o$ of the screw pinch are independent of θ, the appropriate choice for the unperturbed eigenfunctions is

$$\vec{\Phi}^o_{NM} = r_{NM}\, e^{-iN\beta}\, e^{i(M+Nq)\theta}\, \vec{f}_{NM} \quad , \tag{3.8}$$

where r_{NM} is an arbitrary normalization, $\vec{f}_{NM}$ is the appropriate vector, and the phase $(M+Nq)\theta$ is chosen to satisfy poloidal and toroidal periodicity requirements. Two distinct solutions for λ^o are obtained from Eq. (3.4), corresponding to the shear Alfvén continuous spectrum,

$$\lambda^o = (M+Nq)^2, \qquad \vec{f}^{\,A}_{NM} = \begin{bmatrix} -\frac{1}{q} \\ \frac{B_{To}^2}{B_p^2} \\ 1 \end{bmatrix} , \tag{3.9}$$

and to the cusp, or slow wave, spectrum,

$$\lambda^o = \Gamma(M+Nq)^2, \qquad \vec{f}^{\,s}_{NM} = \begin{bmatrix} 1 \\ \frac{1}{q} \\ 1 \end{bmatrix} , \tag{3.10}$$

where $\Gamma \equiv \frac{1}{2}\gamma\beta_M/(1+\frac{1}{2}\gamma\beta_M)$. In the incompressible limit, $\gamma \to \infty$, the cusp and Alfvén spectra are degenerate and the vectors $\vec{f}^{\,A}$ and $\vec{f}^{\,s}$

are not uniquely specified by the ε^0 equations. Further discussion of this special case may be found in Chapter 5.

The unperturbed eigenfunctions are orthogonal to each other with respect to the matrix $\overset{\leftrightarrow}{M}^0$. For the Alfvén modes, the condition is given by

$$\langle \xi^0_{NM} | M^0 | \xi^0_{N'M'} \rangle \equiv \oint d\beta \oint d\theta \, \vec{\xi}^{\,0}_{NM} \cdot \overset{\leftrightarrow}{M}^0 \cdot \vec{\xi}^{\,0}_{N'M'}$$

$$= (2\pi)^2 |\tau_{NM}|^2 R_o^2 \left[1 + \frac{B_{To}^2}{B_p^2}\right] \delta_{M'M} \, \delta_{N'N} \qquad (3.11)$$

A similar condition may also be written for two cusp modes. The Alfvén and cusp modes are always orthogonal to each other in this order. Equation (3.11) is used to choose the normalization factor τ_{NM} so that

$$\langle \xi^0_{NM} | M^0 | \xi^0_{N'M'} \rangle = \delta_{M'M} \, \delta_{N'N} \quad . \qquad (3.12)$$

Though two distinct eigenvalues are obtained for the unperturbed state, each eigenvalue is at least two-fold degenerate. This double degeneracy arises because the modes M,N and -M,-N are both linearly independent solutions for the same eigenvalue $\lambda^0 = (M+Nq)^2$, for any value of q. Additional degeneracy will occur between modes M,N and M',N' whenever

$$(M+Nq)^2 = (M'+N'q)^2 \quad . \qquad (3.13)$$

This condition, Eq. (3.13), can be satisfied exactly only on rational surfaces, $q = q_r$, since M, N, M', and N' are all integers. It is very nearly satisfied on the neighboring flux surfaces, $q = q_r + \delta$, for $|\delta| \ll q_r$.

Note that condition (3.13) is written for degeneracy between two different Alfvén modes or two different cusp modes. Aside from the special cases $\Gamma = 1$ or $M + Nq = 0$, the cusp and Alfvén spectra are, in general, distinct. It may, however, be possible to find special values of Γ and q such that

$$(M+Nq)^2 = \Gamma(M'+N'q)^2 \qquad (3.14)$$

In this case, there would be a degeneracy between the Alfvén and cusp modes. Since it is not likely that such special cases would be of experimental interest, they will not be considered in the following discussions. Furthermore, since the experiments in progress are investigating the Alfvén modes, the following sections will deal explicitly only with the Alfvén spectrum. Analogous expressions for the cusp spectra can be easily derived.

Section 3. First Order Corrections and Mode Coupling

The first order corrections to the shear Alfvén continuous spectrum arising from toroidicity will now be considered. In nondegenerate perturbation theory, the first and second order corrections to the αth unperturbed eigenvalue are found from Eq. (3.6) in which all off-diagonal elements except those in the αth row and αth column are ignored. Solving the determinant equation then yields the expression

$$\left(\lambda - \lambda_\alpha^{\,o} + \varepsilon H_{\alpha\alpha} - \varepsilon^2 \sum_{\beta\neq\alpha} \frac{|H_{\alpha\beta}|^2}{\lambda-\lambda_\beta^{\,o}} + O(\varepsilon^3)\right)$$

$$\times \left(\lambda-\lambda_{\alpha+1}^{\,o} + \varepsilon H_{\alpha+1,\alpha+1} + O(\varepsilon^2)\right)\cdots = 0 \quad , \tag{3.15}$$

where

$$H_{\alpha\beta} \equiv \langle \Phi_\alpha^{\,o} | \lambda M^1 + L^1 | \Phi_\beta^{\,o} \rangle \quad . \tag{3.16}$$

By setting the quantity in the first parentheses equal to zero and using the method of successive approximation, the first and second order corrections to the unperturbed eigenvalue, $\lambda_\alpha^{\,o}$, may be found to be

$$\lambda_\alpha^{\,1} = -H'_{\alpha\alpha} \quad ,$$

$$\lambda_\alpha^{\,2} = \sum_{\beta\neq\alpha} \frac{|H'_{\alpha\beta}|^2}{\lambda_\alpha^{\,o} - \lambda_\beta^{\,o}} \quad , \tag{3.17}$$

where the prime signifies that λ has been replaced by $\lambda_\alpha^{\,o}$ in the term. In the case of degenerate or nearly degenerate eigenvalues, i.e., where $\lambda_\alpha^{\,o} \simeq \lambda_\beta^{\,o}$, this solution for λ_α is invalid because of the resonant denominator in the second order correction, $\lambda_\alpha^{\,2}$. This difficulty can be traced to the fact that because both $\vec{\Phi}_\alpha^{\,o}$ and $\vec{\Phi}_\beta^{\,o}$ are linearly independent functions leading to the same eigenvalue, the correct zeroth order approximations to the total eigenfunctions, $\vec{\Phi}$, are not $\vec{\Phi}_\alpha^{\,o}$ and $\vec{\Phi}_\beta^{\,o}$ but rather some particular linear combinations of them. To obtain the correct linear combinations along with the first order corrections to the eigenvalues, it is necessary to diagonalize the submatrix containing only those states belonging to the degenerate, or nearly degenerate, eigenvalue[31].

From the discussion in Section 2, it is clear that first order corrections to the shear Alfvén continuous spectrum will arise only from terms, $H_{\alpha\beta}$, in which both eigenvectors, $\vec{\Phi}_\alpha^{\,o}$ and $\vec{\Phi}_\beta^{\,o}$, correspond to shear Alfvén eigenfunctions. Using the solutions for these eigenvectors from Eq. (3.9) in Eq. (3.16), the matrix elements, $H_{\alpha\beta}$, are given by

$$H_{\alpha\beta} = \frac{r}{a}(2+A)\delta_{N_\alpha N_\beta}\,\delta_{M_\alpha, M_\beta \pm 1}\left\{\lambda - \lambda_\beta^{\,o} \pm (M_\beta + N_\beta q)\right\} \quad . \tag{3.18}$$

From this expression, it is clear that in first order, the effect of toroidicity is to couple degenerate, or nearly degenerate, modes with the same toroidal mode numbers but with poloidal wave numbers differing by one. It is also clear that if there were no degeneracies in the unperturbed solutions, the first order corrections, as given in Eq. (3.17), would all vanish. Had higher harmonics of cos θ, for example, cos pθ, been retained earlier to model the effects of noncircularity, then degenerate modes with $N' = N$ and $M' = M \pm p$ would also have been coupled in this order. The conditions on M,N and M′,N′ for coupling in first order would then be written as

$$M + Nq = \pm \frac{p}{2} \quad , \tag{3.19}$$

where the + sign holds for $M' = M - p$ and the − sign holds for $M' = M + p$. The significance of this expression will be discussed further on.

Let us now examine in more detail the mode coupling. Consider first the case when the screw pinch modes are doubly degenerate, i.e., M,N and −M,−N belong to the same eigenvalue λ^o. From Eqs. (3.6), (3.18), the submatrix determining λ is then of the form

$$\begin{bmatrix} \lambda - \lambda_{NM}^{\,o} & 0 \\ 0 & \lambda - \lambda_{-N,-M}^{\,o} \end{bmatrix} \quad . \tag{3.20}$$

So clearly, $\lambda^1 = 0$ and these modes do not couple in first order. Hence, the correction to the unperturbed eigenvalues for these states is of second order in ε.

Consider now two modes M,N and M−1,N which satisfy Eq. (3.19) with p = 1 exactly on a particular rational surface, q_r, and approximately on neighboring flux surfaces, $q = q_r + \delta$, where $|\delta| \ll |q_r|$. From Eq. (3.9), it follows that $\lambda^o \simeq \frac{1}{4}$. Though the modes −M,−N and −M+1,−N belong to the same degenerate eigenvalue, λ^o, it is not necessary to include them in the matrix that is to be diagonalized since, from Eq. (3.20), they are not connected by the perturbation to the modes M,N and M−1,N. The first order corrections to the eigenvalues for the modes M,N and M−1,N can be found by diagonalizing the following matrix:

$$\begin{bmatrix} \lambda - \lambda_{NM}^{\,o} & \varepsilon \frac{r}{a}(2 + A)[\lambda - \lambda_{NM}^{\,o} + (M+Nq)] \\ \varepsilon \frac{r}{a}(2 + A)[\lambda - \lambda_{NM}^{\,o} + (M+Nq)] & \lambda - \lambda_{N,M-1}^{\,o} \end{bmatrix} \quad , \tag{3.21}$$

with the result

$$\lambda = \frac{\lambda^{o}_{NM} + \lambda^{o}_{N,M-1}}{2}$$

$$\pm \frac{1}{2}\sqrt{(\lambda^{o}_{NM} - \lambda^{o}_{N,M-1})^2 + 4\epsilon^2(\frac{r}{a})^2(2+\Lambda)^2(M+Nq)^2} \quad . \qquad (3.22)$$

In the case of exact degeneracy, $\lambda^{o}_{NM} = \lambda^{o}_{N,M-1} = \frac{1}{4}$ and $q = q_r$ so Eq. (3.22) reduces to

$$\lambda = \lambda^{o}_{NM}(1 \pm 2\epsilon(\frac{r}{a})(2+\Lambda)) = \lambda^{o}_{NM}(1 \pm \epsilon\Delta) \quad . \qquad (3.23)$$

When the modes are nearly degenerate, Eq. (3.22) may be written in the form

$$\lambda = (M+Nq_r)^2 + N^2\delta^2$$

$$\pm \frac{1}{2}\sqrt{(2N\delta)^2+4\epsilon^2(\frac{r}{a})^2(2+\Lambda)^2(M+Nq_r+N\delta)^2} \quad , \qquad (3.24)$$

thereby demonstrating that λ depends quadratically on δ when the modes are very nearly degenerate. This is the case when the splitting due to the perturbation, $\epsilon\frac{r}{a}(2+\Lambda)(M+Nq_r+N\delta)$, is larger than the splitting of the unperturbed eigenvalues, $N^2\delta^2$. When the splitting due to the perturbation is smaller than the splitting of the unperturbed eigenvalues, Eqs. (3.22) and (3.24) show that the solutions for λ are the unperturbed eigenvalues plus corrections of

$O(\epsilon^2)$. This is true because the two modes are no longer approximately degenerate. Upon following the above procedure for the modes $-M,-N$ and $-M+1, -N$, the eigenvalues are again found to be given by Eqs. (3.22)-(3.24). Hence, the effect of toroidicity has been to reduce the degeneracy of the eigenvalue from 4 to 2.

Figure 3.1 displays the behavior of the perturbed and unperturbed eigenvalues over a range of q about q_r. Solid lines indicate the unperturbed spectrum, while the dotted lines indicate the first order corrections. The first order corrections are significant in a range $\delta_T \simeq \frac{\Delta}{2}$ about q_r. In this range, the splitting due to the perturbation is larger than or comparable to the splitting between the unperturbed, nearly degenerate levels. Note that the effect of toroidicity is to create a gap in the spectrum around the flux surface, q_r. This gap, which arises due to poloidal coupling of degenerate modes, is analogous to the gap which appears in the energy spectrum of an electron in a periodic crystal lattice. The gaps in the electron energy spectrum occur because Bragg reflection of a travelling electron wave off the crystal lattice results in standing electron waves which are localized either in the "well" between the ions or else at the top of the "well" near the ions. For the Alfvén waves, the gap appears because the periodic variation in the magnetic field causes poloidal mode coupling which results in waves which are localized in regions of good or bad curvature. This can be shown explicitly by solving for

the unperturbed wave functions, Φ^o. For $\lambda = \lambda^o(1+\varepsilon\Delta)$, the wave is two-fold degenerate and is given by

$$\Phi \sim e^{\mp iN\beta}\, e^{\pm i(M+Nq)\theta}\, e^{\mp i\,\theta/2}\, \sin\theta/2\, \hat{f} \quad , \tag{3.25}$$

while for $\lambda = \lambda^o(1-\varepsilon\Delta)$, the function is given by

$$\Phi \sim e^{\mp iN\beta}\, e^{\pm i(M+Nq)\theta}\, e^{\pm i\,\theta/2}\, \cos\theta/2\, \hat{f} \quad . \tag{3.26}$$

The wave with the higher frequency is localized in the good curvature region at $\theta = \pi$, where the field strength is increased by the perturbation. The wave with the lower frequency is localized on the outside of the torus, $\theta = 0$, where the curvature is bad and the field strength is decreased by the perturbation.

By inverting Eq. (2.35) to obtain ω^2 and using the results of the perturbation calculations, the shear Alfvén continuum is given approximately by

$$\omega_A^2 \simeq \frac{(B^2)^2}{\mu_o \rho}\,(M+Nq)^2(1+O(\varepsilon^2)) \tag{3.27}$$

on the flux surfaces for which no poloidal coupling occurs, and by

$$\omega_A^2 \simeq \frac{(B^2)^2}{\mu_o \rho}\left\{(M+Nq_r)^2 + N^2\delta^2 \pm \frac{1}{2}\sqrt{(2N\delta)^2+\varepsilon^2\Delta^2(M+Nq_r+N\delta)^2}\right\} \tag{3.28}$$

on and in the vicinity of a rational flux surface, q_r, on which poloidal coupling does occur. These expressions have been evaluated for the Tokapole II experiment, using a numerical equilibrium code[25] to obtain the equilibrium field parameters, and a model density profile which agrees with the experimental profile within the accuracy bounds of the measurements[11]. The calculated q profile for the device is shown in Figure 4.2. An internal separatrix is located at the peak of the profile around r ≃ 8 cm. Experimental values for the toroidal field on axis and the plasma current were used in calculating the equilibrium. The numerical equilibrium agrees well with experimentally measured equilibria. When evaluating the perturbed spectrum with Eq. (3.28), the parameter ε was set equal to 0.16 in order to model the tokamak-like portion of the discharge and the parameter Δ was set equal to -1. The Alfvén continuum for modes with M = -1,-2 and N = 1 are displayed in Figure 3.3. Again, solid lines depict the unperturbed eigenfrequencies, with the toroidal corrections indicated by dotted lines. The two crossing points in the unperturbed spectrum occur on the rational surface $q_r = \frac{3}{2}$.

Toroidicity strongly affects the nature of the continuum near these degeneracy points. For the inner crossing, toroidicity effectively eliminates any resonance possibility within the spearatrix for a frequency equal to that of the unperturbed crossing points. For the outer crossing, toroidicity splits the degenerate resonance so the location of the -2,1 resonance is shifted inwards

while the location of the -1,1 resonance is shifted outwards. Away from the points of degeneracy, the continua are unaffected by the perturbation.

The results in Figures 3.1 and 3.3, obtained with the perturbation analysis given above, provide a qualitative picture of the shear Alfvén continuous spectrum for Tokapole II. A more accurate description of the spectrum requires a numerical evaluation of Eq. (2.34). The results of these computations are described in the next chapter.

Figure 3.1 Coupling of the (-1,1) and (-2,1) Modes at q=3/2 Surface
The behavior of the perturbed (••••) and unperturbed(-----) eigenvalues for the modes (-1,1) and (-2,1) in the vicinity of the rational surface, q_r=3/2, on which they couple, is displayed.

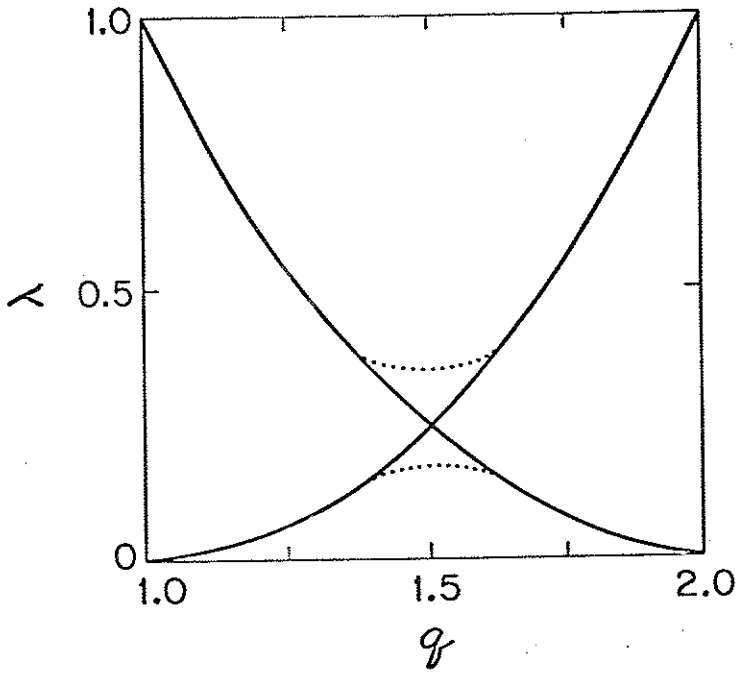

FIGURE 3.1

Figure 3.2 Shear Alfvén Continuum Frequencies vs. Minor Radius on Midplane for the Tokapole II Device

The shear Alfvén wave resonant frequencies, corresponding to the eigenvalues in Fig. 3.1, are plotted vs. minor radius on midplane for the Tokapole II equilibrium given in Fig. 4.1. The solid lines depict the lowest order solutions, Eq. (2.27), while the dotted lines indicate the first order corrections, Eq. (2.28), arising from toroidicity.

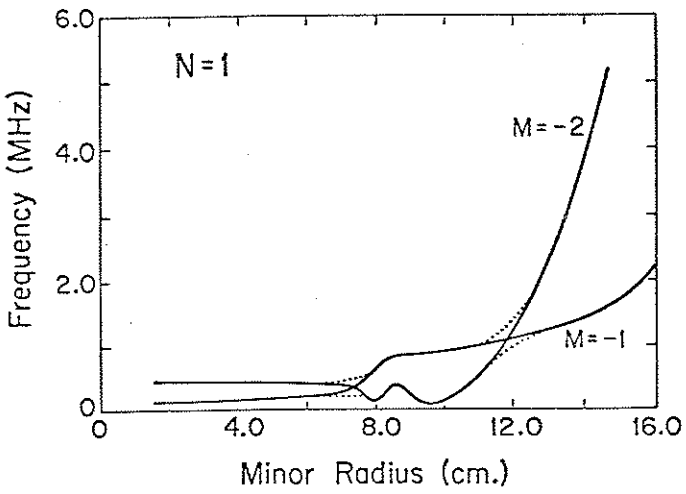

FIGURE 3.2

CHAPTER 4

NUMERICAL STUDY OF THE SHEAR ALFVÉN CONTINUOUS SPECTRUM OF THE TOKAPOLE II DEVICE

Radio frequency heating of a tokamak plasma by means of resonant excitation of shear Alfvén waves is currently being attempted on the Tokapole II device[11] at the University of Wisconsin-Madison and on other tokamaks[10,12].

The Tokapole II device[24] is a small tokamak which features an internal separatrix and a natural, four-null poloidal divertor. The separatrix and divertor regions are formed by the presence of four internal conducting rings, situated near the corners of the square vacuum vessel, which are driven inductively along with the plasma to form the "PDX-type" equilibrium. The major radius of the device is 0.5 m and one side of the vacuum vessel measures 0.44 m in length. Within the separatrix is the tokamak channel of the discharge, which measures 8-10 cm in minor radius, carries a total current of about 20 kA in these experiments, and is characterized by flux surface cross sections which become increasingly noncircular with radial distance away from the magnetic axis. Typically, the toroidal field on axis is about 0.4 tesla. A numerical solution for the equilibrium, which is generated from the Tokapole II equilibrium code, TOPEC,[25] and which is consistent with experimentally measured equilibria, is displayed in Fig. 4.1.

According to ideal MHD theory, the shear Alfvén wave may exhibit spatial singularities at particular locations in an inhomogeneous plasma where the oscillator frequency matches the local frequency of a mode belonging to the shear Alfvén continuum of the equilibrium. On the Tokapole II device, the spatial location of the resonances and the associated poloidal and toroidal mode structure are being determined experimentally using magnetic pickup coils[11]. In order to correlate the experimental findings with the theoretical description, it is necessary to solve the ideal MHD equations in axisymmetric toroidal geometry for the shear Alfvén continuum. An analytic model has been developed in the previous chapters which incorporates effects due to toroidicity and/or noncircularity of the plasma cross section by utilizing a large aspect ratio, circular cross section expansion scheme. A description based on this model indicates that the shear Alfvén continuum is given approximately by the "screw pinch" dispersion relation except in the vicinity of certain rational q surfaces, where coupling of poloidal harmonics results in the formation of gaps in the continuum. In this chapter, numerical solutions for shear Alfvén continuum in a Tokapole II equilibrium, which have been previously presented in part at the 1981 A.P.S. meeting in New York[33] and at the Third Annual Joint Grenoble-Varenna International Symposium on Heating in Toroidal Plasmas in Grenoble in 1982[34], are summarized. The numerical solutions are in qualitative agreement with the description obtained from the analytic model except in the

region close to the internal separatrix, which defines the edge of the tokamak channel in the device. This region is characterized by extremely high shear and highly noncircular flux surfaces and hence is effectively out of the regime of validity of the analytic study.

In section 1, the system of equations which determines the continuum in a tokamak and the numerical procedure chosen to solve the system are described. Numerical results are presented and discussed in section 2.

Section 1. Numerical Procedure

In an axisymmetric toroidal equilibrium, where there is only one degree of symmetry, the ideal MHD continua are specified by the eigenvalues of a set of coupled ordinary differential equations, Eq. (2.11), which are to be solved on each flux surface. Using the formalism of Tataronis et al.[18,22] and choosing as coordinates the Hamada coordinates ϕ, θ, and $\beta \equiv q\theta - \xi$[29], where ϕ is the poloidal flux divided by 2π, θ and ξ are the poloidal and toroidal angles, respectively, and q is the safety factor, the eigenvalue equations may be conveniently written in the form given in Eq. (2.34):

$$\lambda \vec{\vec{M}}(\theta) \cdot \vec{Y}(\theta,\beta) + \frac{\partial}{\partial\theta}\Big|_{\beta} \left[\vec{\vec{N}}(\theta)\frac{\partial}{\partial\theta}\Big|_{\beta}\right] \cdot \vec{Y}(\theta,\beta) = 0 \quad .$$

The eigenvalue, λ, is related to the continuum frequency, ω, by Eq. (2.35):

$$\lambda = \frac{\mu_o \rho}{(B^2)^2}\,\omega^2 \quad ,$$

where μ_o is the vacuum permeability, ρ is the plasma density, and $B^2 \equiv B^2(\phi) = \vec{B} \cdot \nabla\theta$. The eigenvector, $\vec{Y}$, contains the surface components of the perturbed fluid velocity,

$$\vec{Y}(\theta,\beta) = \begin{bmatrix} \vec{v}\cdot\nabla\theta \\ \\ \vec{v}\cdot\nabla\xi \end{bmatrix} \quad . \tag{4.1}$$

In this representation, the requirements of poloidal and toroidal periodicity of the eigenfunctions are given by Eq. (2.37),

$$\vec{Y}(\theta,\beta) = \vec{Y}(\theta+2\pi,\beta+2\pi q) \quad ,$$

and Eq. (2.36) ,

$$\vec{Y}(\theta,\beta+2\pi) = \vec{Y}(\theta,\beta) \quad ,$$

respectively.

A totally real representation for the eigenvector $\vec{Y}$ is more suitable for numerical computations than the complex one which was utilized in the previous chapters. For a fixed toroidal mode number, N, the vector, $\vec{Y}$, can be represented as

$$\vec{Y}(\theta,\beta) = \vec{A}(\theta)\cos N\beta + \vec{C}(\theta)\sin N\beta \quad , \tag{4.2}$$

where consideration of a single value of N is permissible because of axisymmetry of the device. Substitution of this expression into Eq. (2.34) indicates that $\vec{A}$ and $\vec{C}$ each satisfy equations of the form (2.34) with $\vec{Y}$ replaced by either $\vec{A}$ or $\vec{C}$. However, substitution of this form into the boundary conditions, Eq. (2.35) and (2.36), indicates that $\vec{A}$ and $\vec{C}$ are connected by specific phase relations, namely,

$$\begin{aligned}
\vec{A}(\theta+2\pi) &= \vec{A}(\theta)\cos 2\pi Nq - \vec{C}(\theta)\sin 2\pi Nq \\
\vec{A}'(\theta+2\pi) &= \vec{A}'(\theta)\cos 2\pi Nq - \vec{C}'(\theta)\sin 2\pi Nq \\
\vec{C}(\theta+2\pi) &= \vec{A}(\theta)\sin 2\pi Nq + \vec{C}(\theta)\cos 2\pi Nq \\
\vec{C}'(\theta+2\pi) &= \vec{A}'(\theta)\sin 2\pi Nq + \vec{C}'(\theta)\cos 2\pi Nq \quad ,
\end{aligned} \tag{4.3}$$

where the prime denotes differentiation with respect to θ at constant ϕ and β, and the factors involving $2\pi Nq$ arise from the phase shifts accumulated as the wave moves along the field line. Had the use of the complex representation been chosen, it would have been found that the real and imaginary portions of the vector would have satisfied the same equations as the vectors $\vec{A}$ and $\vec{C}$ above.

Evaluation of the coefficient matrices $\vec{\vec{M}}$ and $\vec{\vec{N}}$ is facilitated by the use of the Tokapole II equilibrium code.[25] Output from the equilibrium code is used to calculate the elements of $\vec{\vec{M}}$ and $\vec{\vec{N}}$ as functions of θ on each flux surface, using the code MATRIX (see Appendix D). The elements of $\vec{\vec{M}}$ and $\vec{\vec{N}}$ are given by Eq. (2.31):

$$\vec{\vec{M}}(\theta) = \begin{bmatrix} g_{22} & g_{23} \\ g_{32} & g_{33} \end{bmatrix}, \vec{\vec{N}}(\theta) = \vec{\vec{M}} - \frac{1}{B_*^T} \begin{bmatrix} B_2B_2 & B_2B_3 \\ B_3B_2 & B_3B_3 \end{bmatrix} ,$$

where g_{ij} are the metric tensor elements in the surface, B_i is the i^{th} covariant component of the equilibrium magnetic field, and $B_* = |B|^2(1+\frac{1}{2}\gamma\beta_m)$, where $|B|$ is the magnitude of the equilibrium magnetic field, γ is the ratio of specific heats, and β_m is the total plasma beta.

Numerical solutions for the eigenvalues, λ, and the associated wavestructures, $\vec{\Upsilon}$, are obtained by a variation[34] of the method of Stodola and Vianello[19], using the code FREQ (see Appendix D). In this method, an iteration scheme is developed in which approximations to the eigenvalue, λ^i, and eigenfunction, $\vec{\Upsilon}_i$, after i iterations are given as

$$\lambda_o \vec{\vec{M}} \cdot \vec{\Upsilon}_i + \frac{\partial}{\partial\theta}\Big|_{\phi,\beta} \vec{\vec{N}}(\theta) \frac{\partial}{\partial\theta}\Big|_{\phi,\beta} \cdot \vec{\Upsilon}_i = -\vec{\vec{M}} \cdot \vec{\Upsilon}_{i-1} \qquad (4.4)$$

and

$$\lambda^{(i)} = \lambda_o + \delta^{(i)} \quad , \qquad (4.5)$$

with

$$\delta^{(i)} = \frac{\oint d\theta d\beta \vec{\Upsilon}^T_i \cdot \vec{\vec{M}} \cdot \vec{\Upsilon}_{i-1}}{\oint d\theta d\beta \vec{\Upsilon}^T_i \cdot \vec{\vec{M}} \cdot \vec{\Upsilon}_i} \quad , \qquad (4.6)$$

and where $\vec{\Upsilon}^T_i$ is the transpose of $\vec{\Upsilon}_i$. At each iteration, four linearly independent solutions to the homogeneous equation for $\vec{\Upsilon}_{i+1}$ and one particular solution to the inhomogeneous equation are generated. Linear combinations of these are then chosen for both $\vec{A}$ and $\vec{C}$ using the phase relations in Eq. (4.3).

The success of the method depends on providing a good initial guess to the eigenvalue. For the shear Alfvén eigenvalues, the initial guesses are obtained using the analytic model. The iteration scheme is then designed to converge to the eigenvalue which is closest to the initial guess. Convergence is obtained after i iterations when the parameter, eps, defined by

$$\text{eps} \equiv \frac{|\delta^{(i)} - \delta^{(i-1)}|}{|\lambda_o + \delta^{(i)}|} \quad , \qquad (4.7)$$

is less then or equal to a specified tolerance level. For the solutions presented in this thesis, the tolerance is typically set at 10^{-5} and convergence is usually achieved after a very small number of iterations, $\lesssim 5$. For the cases in which the eigenvalues corresponding to different shear Alfvén modes closely approach each other, more iterations, on the order of 50, are required before a convergent solution is obtained.

Numerical difficulties are encountered on flux surfaces which lie within one centimeter in minor radius of the internal separatrix of the Tokapole II equilibrium. The numerical solution for the equilibrium which has been used in these calculations is displayed in Fig. 4.1 while the corresponding q profile is shown in Fig. 4.2. Note the extreme shear which is present at the edge of the central tokamak channel, between r = 7 cm and r = 8 cm. Because of this extreme shear, many closely spaced modes with different poloidal and toroidal mode numbers are present in this region, rendering convergence difficult. Similar problems would also have been encountered if a variational approach, using a Galerkin method,[27] for example, had been chosen instead. In that case, a large number of terms in a finite element expansion would probably have to be kept in order to obtain a good description of the continuum in this high shear region. The method used in this study does yield convergent solutions in this region. However, because of the complicated mode structure, it is difficult to determine to which branch of the continuum each solution belongs.

Section 2. Numerical Results

The equations for the continuum, Eqs. (2.34), are solved using a numerical solution for the Tokapole II equilibrium, which is depicted in Fig. 4.1. The tokamak channel has a minor radius of about 8 cm, with the magnetic axis situated at a major radius of about 51.5 cm. The total plasma current is 20 kA and the magnetic field on axis is 5 kG, in agreement with experimentally measured parameters. A density profile which agrees qualitatively with experimental measurements has been constructed and is displayed in Fig. 4.3.

By comparing Figs. 4.4 and 4.5, numerical solutions for the shear Alfvén eigenvalues may be compared to the corresponding "screw pinch" model solutions, i.e., to the zeroth order in ε solutions of the analytic model. Poloidal mode numbers of M = 1-5 with a toroidal mode number of N = -2 are displayed in these figures. Poloidal mode numbers for the numerical solutions have been determined by examining the wave structure of each solution along a poloidal field line. It is observed that the poloidal structure of each branch varies in a continuous manner as the separatrix is approached. Modulation of the equilibrium due to toroidicity causes the coupling of the (3,-2) mode to the (2,-2) mode at a minor radius of $r \simeq 4$ cm, corresponding to $q \simeq 1.25$, as predicted by the analytic theory. This coupling results in the formation of a gap in the continuum, as can be seen by comparison with the corresponding

solutions in Fig. 4.5. An enlarged view of this mode coupling is provided in Fig. 4.6. The poloidal structure of the (3,-2) mode as the coupling surface is approached from the center of the tokamak channel is shown sequentially in Figs. 4.7-4.9, while the corresponding poloidal structure for the (2,-2) mode is shown sequentially in Figs. 4.10-4.12. The effect of the coupling is to cause the (3,-2) mode to become increasingly peaked on the inside of the torus and the (2,-2) mode to become increasingly peaked on the outside of the torus. At the coupling surface, $r \simeq 4$ cm, the two modes exhibit similar structure but are 180^{o} out of phase with each other, as predicted by the analytic model.

By comparing Fig. 4.4 with Fig. 4.5, it can be seen that the (4,-2) mode is significantly altered from the screw pinch solution near the separatrix. The difference is attributed to the strong mode coupling which occurs in this region.

The shear Alfvén continuum frequencies, corresponding to the eigenvalues shown in Fig. 4.4, are displayed in Fig. 4.13. The effect of the gap formation at $r \simeq 4$ cm has been to remove the possibility of heating throughout most of the tokamak channel with a frequency of about 0.5 MHz.

The behavior of modes with N = -1 and M = 0-4 is examined in Figs. 4.14-4.24. Numerical solutions for the eigenvalues are given in Fig. 4.14 while the corresponding "screw pinch" solutions are given in Fig. 4.15. The (1,-1) mode couples to the (2,-1) mode around the surface $r \simeq 6.5$ cm, or $q \simeq 1.5$. The poloidal wave

structure for these two modes is given in Figs. 4.18-4.20, respectively, for $r \simeq 6$, 6.5, and 7 cm. The observed behavior is in agreement with the analytic model. Figures 4.16 and 4.17 display the poloidal wave structure for the M = "0" and M = 1 modes, respectively. The M = "0" mode contains a strong modulation by an M = 1 component, probably due to the M = 1 modulation of the equilibrium by toroidicity. The observed differences in the radial structure of the eigenvalues near the separatrix can be attributed to strong mode couplings in the region. Finally, the shear Alfvén continuum frequencies, corresponding to the eigenvalues in Fig. 4.14, are displayed in Fig. 4.24.

Results of the numerical solutions for the shear Alfvén continuum in the tokamak region of the Tokapole II device are in qualitative agreement with results from an analytic model developed previously. Strong mode coupling induced by extreme shear and noncircularity of the plasma cross section in the region near the separatrix significantly alters the magnitude and behavior of the continuum eigenvalues in the region, as can be seen by comparing Fig. 4.4 to Fig. 4.5 and Fig. 4.14 to Fig. 4.15. In addition, for flux surfaces which are located closer to the separatrix than to the magnetic axis, i.e., for $r \geq 4$ cm, additional shifts in magnitudes of the eigenvalues occur due to finite aspect ratio and noncircularity of the plasma cross sections. These shifts are in agreement with the analytic model. According to perturbation theory calculations, as given in Eq. (3.17), the second order corrections

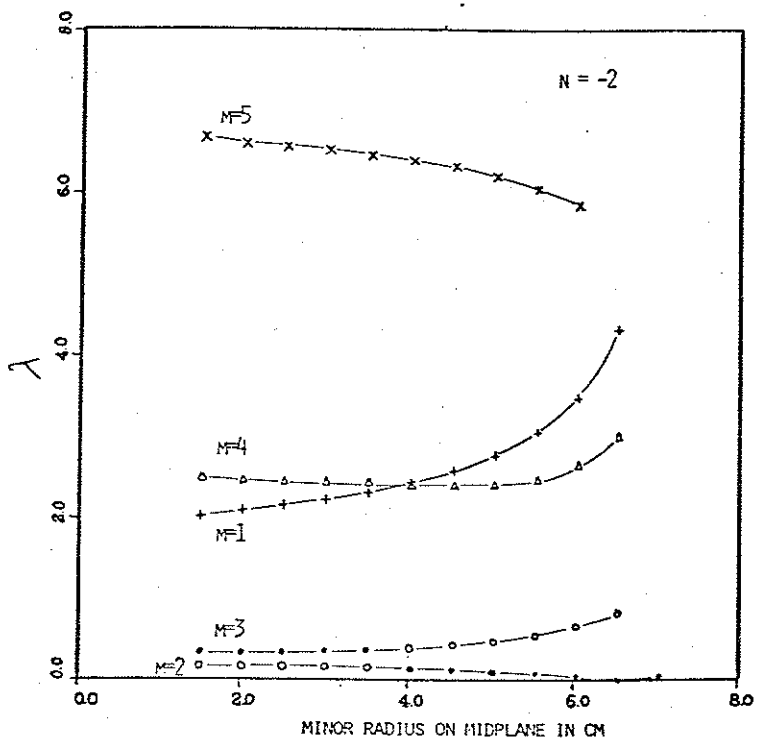

FIGURE 4.4

Figure 4.5 Shear Alfvén Eigenvalues in the Screw Pinch Approximation vs. Minor Radius on Midplane

The "screw pinch" model predictions for the modes shown in Fig. 4.4 are displayed.

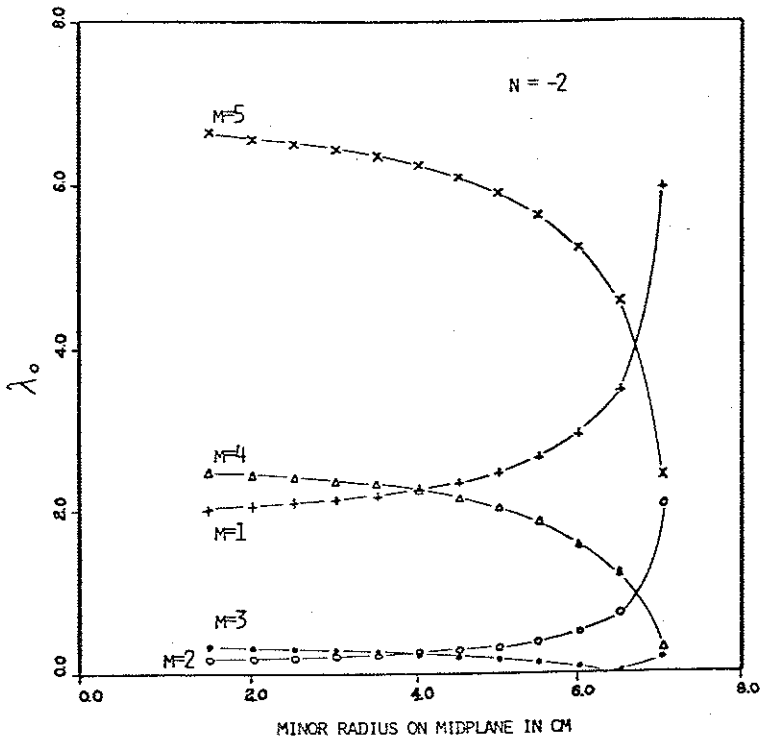

FIGURE 4.5

Figure 6 Coupling of the (3,-2) and (2,-2) Modes at the $q \simeq 1.25$ Surface

An enlarged view of the coupling between the (3,-2) and (2,-2) modes of Fig. 4.4 is given, along with the "screw pinch" model predictions for these modes.

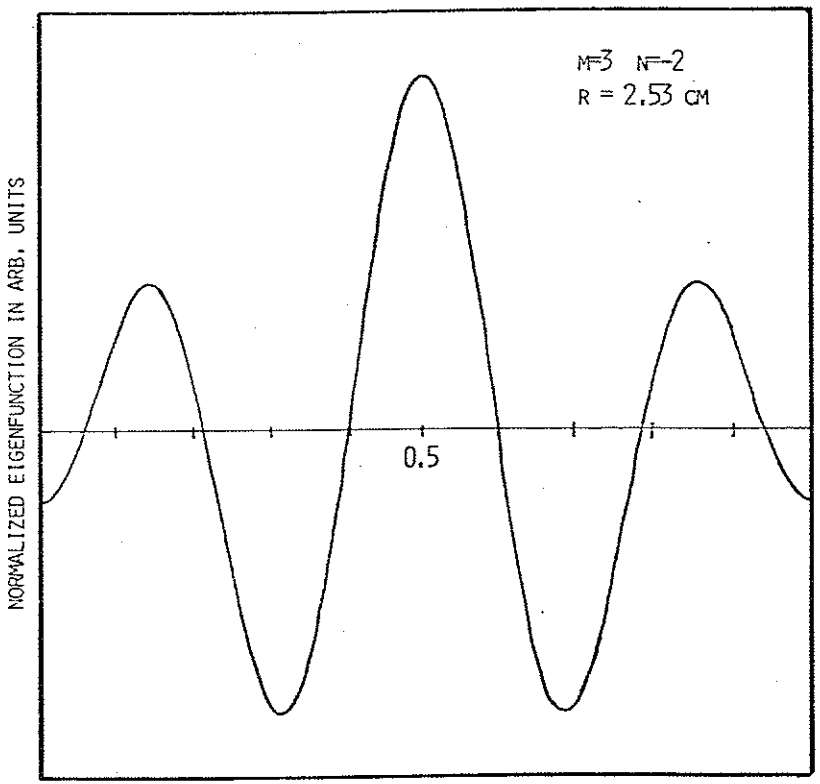

FIGURE 4.8

Figure 4.9 Poloidal Structure of the (3,-2) Mode at the Coupling Surface, r=4.03 cm

The eigenfunction corresponding to the eigenvalue in Fig. 4.6 at the top of the gap at r≅4.03 cm is displayed vs. the relative distance along a poloidal field line on the coupling surface. Note that the eigenfunction is peaked on the inside of the torus and is 180° out of phase with the eigenfunction (shown in Fig. 4.12) corresponding to the bottom of the gap.

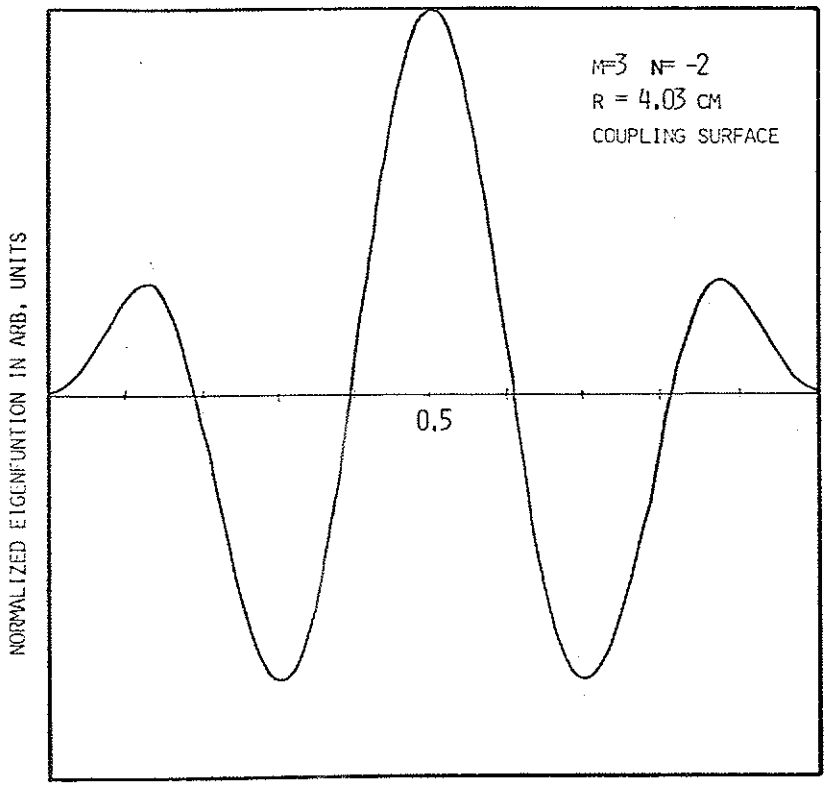

FIGURE 4.9

Figure 4.10 Poloidal Structure of the (2,-2) Mode at r=1.53 cm

The eigenfunction corresponding to the (2,-2) mode in Fig. 4.6 is displayed vs. the relative distance along a poloidal field line for a minor radius on midplane of 1.53 cm. The mode is relatively unaffected by the coupling which occurs around r=4.03 cm.

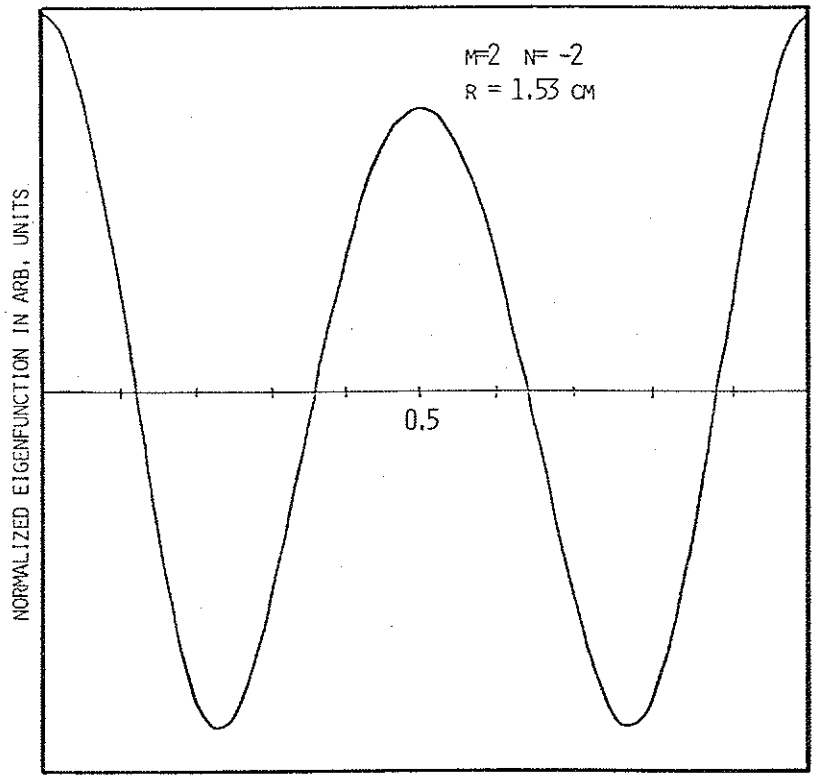

FIGURE 4.10

Figure 4.11 Poloidal Structure of the (2,-2) Mode at r=2.53 cm

The eigenfunction corresponding to the (2,-2) mode in Fig. 4.6 is displayed vs. the relative distance along a poloidal field line for a minor radius on midplane of 2.53 cm. Modulation of the mode amplitude due to coupling to the (3,-2) mode is evident on the inside of the torus.

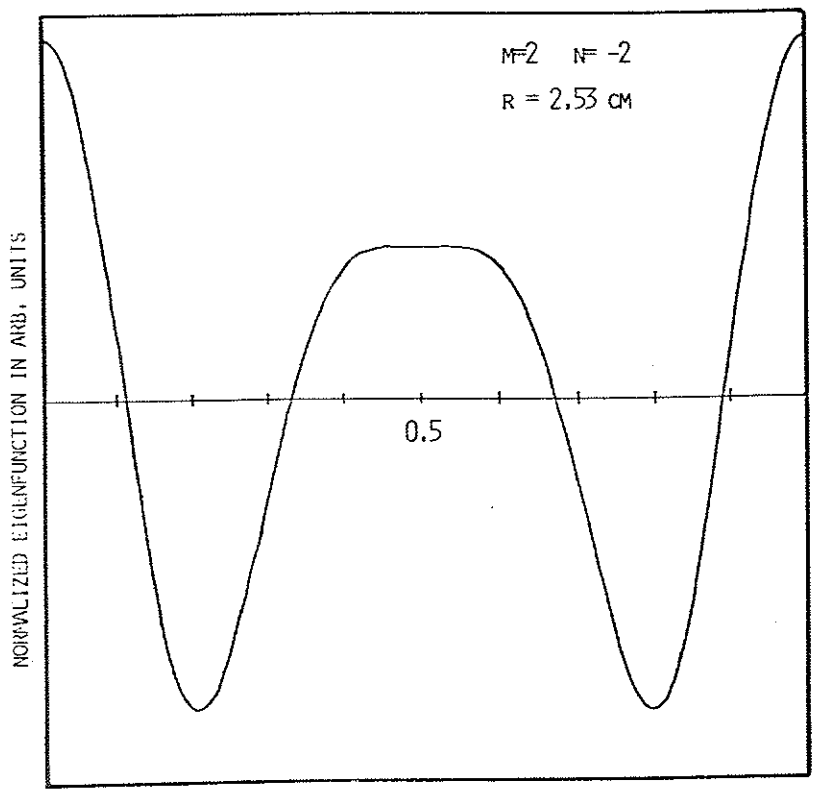

FIGURE 4.11

Figure 4.12 Poloidal Structure of the (2,-2) Mode at the Coupling Surface, r=4.03 cm

The eigenfunction corresponding to the eigenvalue in Fig. 4.6 at the bottom of the gap at r=4.03 cm is displayed vs. the relative distance along a poloidal field line on the coupling surface. Note that the eigenfunction is peaked on the outside of the torus and that it is 180° out of phase with the eigenfunction (shown in Fig. 4.9) corresponding to the top of the gap.

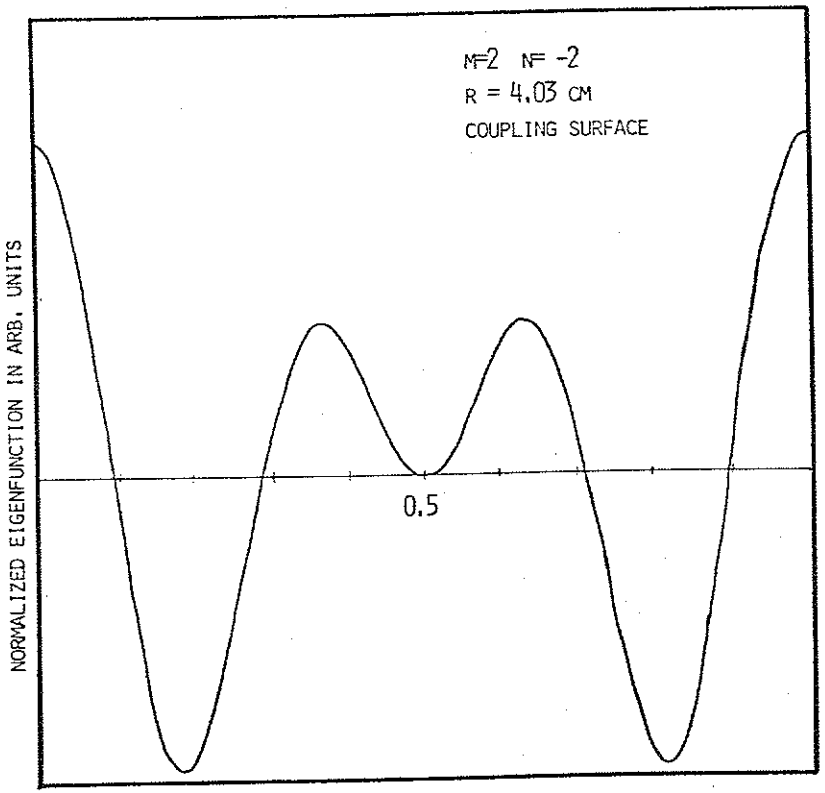

FIGURE 4.12

Figure 4.13 Shear Alfvén Continuum Frequencies vs. Minor Radius on Midplane

The shear Alfvén continuum frequencies corresponding to the modes displayed in Fig. 4.4 are shown.

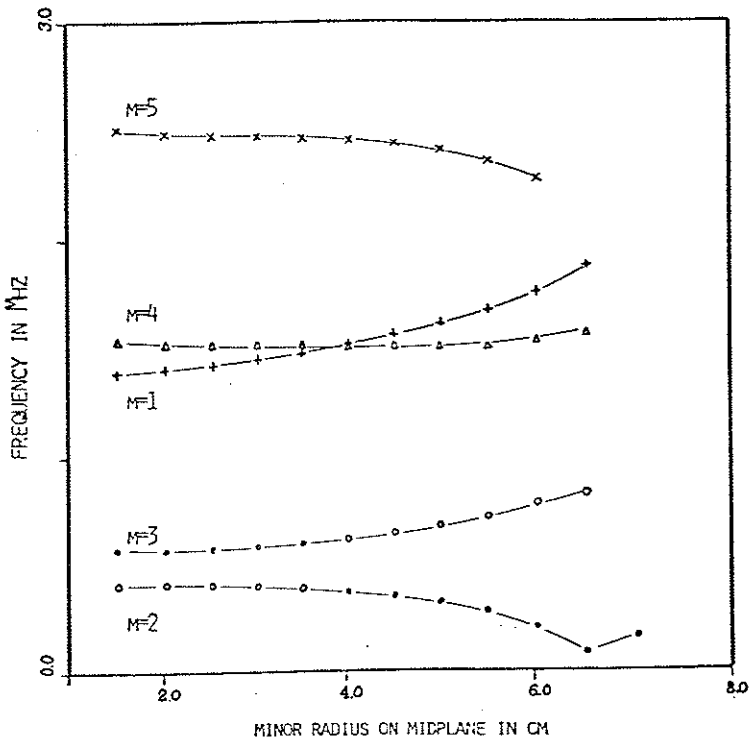

FIGURE 4.13

Figure 4.14 Shear Alfvén Eigenvalues vs. Minor Radius on Midplane

The eigenvalues corresponding to the modes M = 4,3,2,1,0 and N = -1 in the analytic model are displayed. Mode coupling has occurred at $r \simeq 6.53$ cm between the (2,-1) and (1,-1) modes.

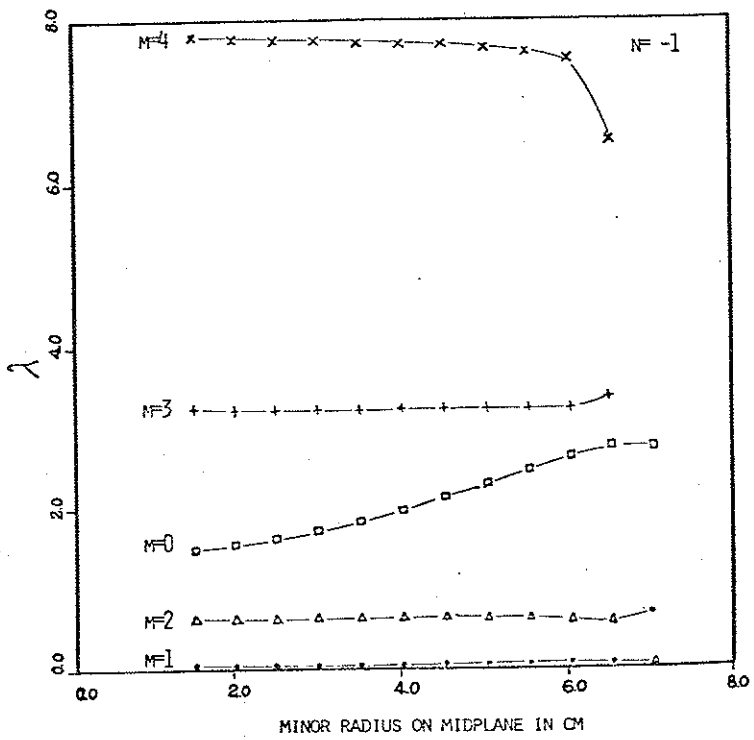

FIGURE 4.14

Figure 4.15 Shear Alfvén Eigenvalues in the Screw Pinch Approximation vs. Minor Radius on Midplane

The screw pinch model predictions for the modes shown in Fig. 4.14 are displayed.

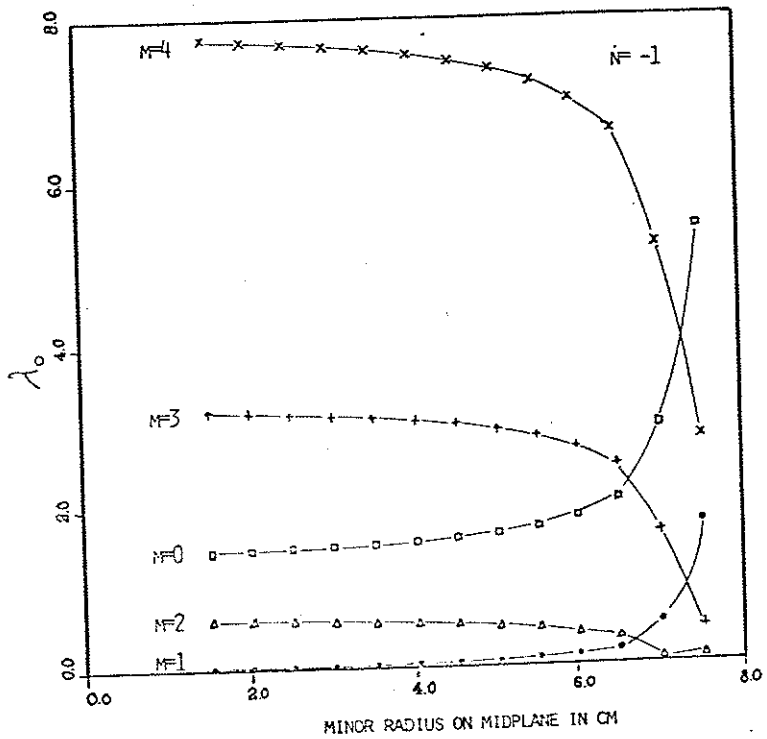

FIGURE 4.15

Figure 4.16 M=0 Eigenfunctions vs. Relative Distance Along Poloidal Field Line

The eigenfunction corresponding to the M=0, N=-1 mode is displayed for three different minor radii. Note the modulation of the mode caused by the 1/R dependence of the equilibrium fields.

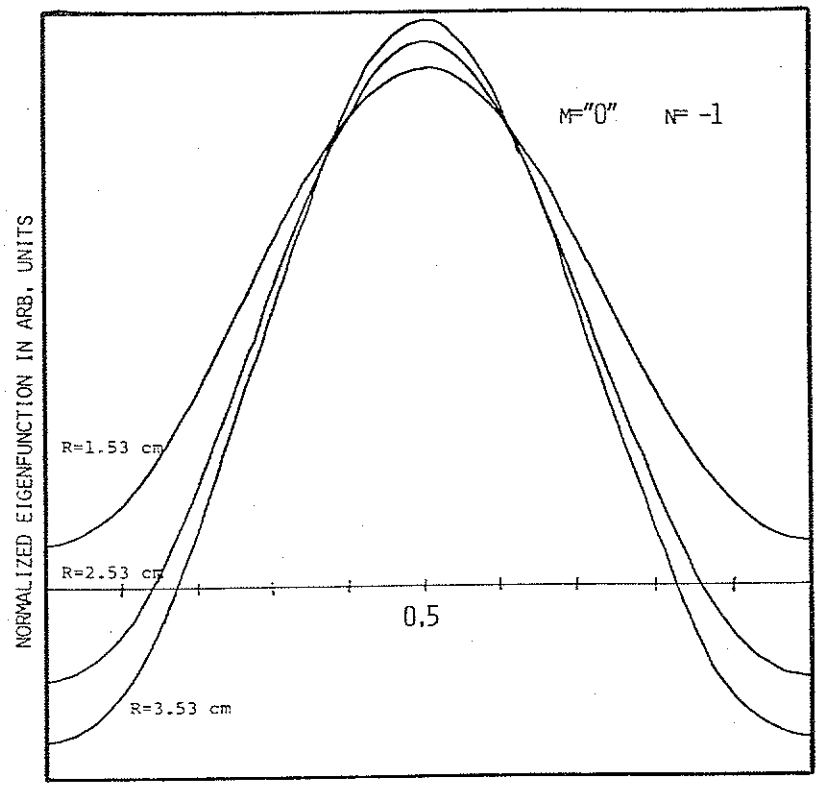

FIGURE 4.16

Figure 4.17 M=1 Eigenfunctions vs. Relative Distance Along Poloidal Field Line

The eigenfunction corresponding to the M=1, N=-1 mode is displayed for a minor radius of r=2.53 cm.

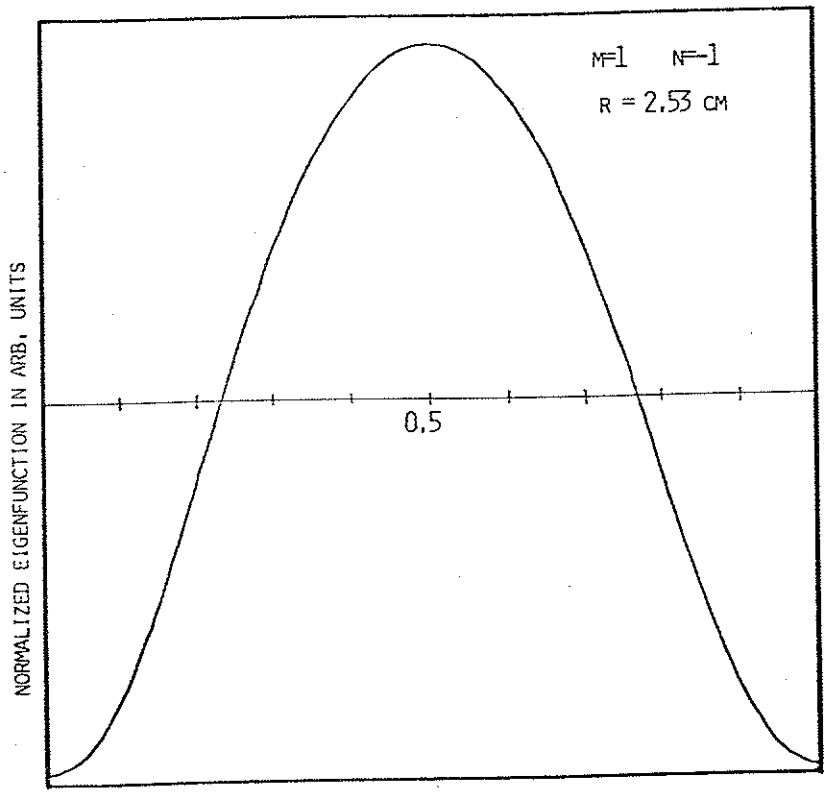

FIGURE 4.17

Figure 4.18 Poloidal Structure of the (1,-1) Mode at r=6.03 cm

The eigenfunction corresponding to the (1,-1) mode in Fig. 4.14 is displayed vs. the relative distance along a poloidal field line for a minor radius on midplane of r=6.03 cm. Modulation of the wave amplitude due to coupling to the (2,-1) mode is evident on the inside of the torus.

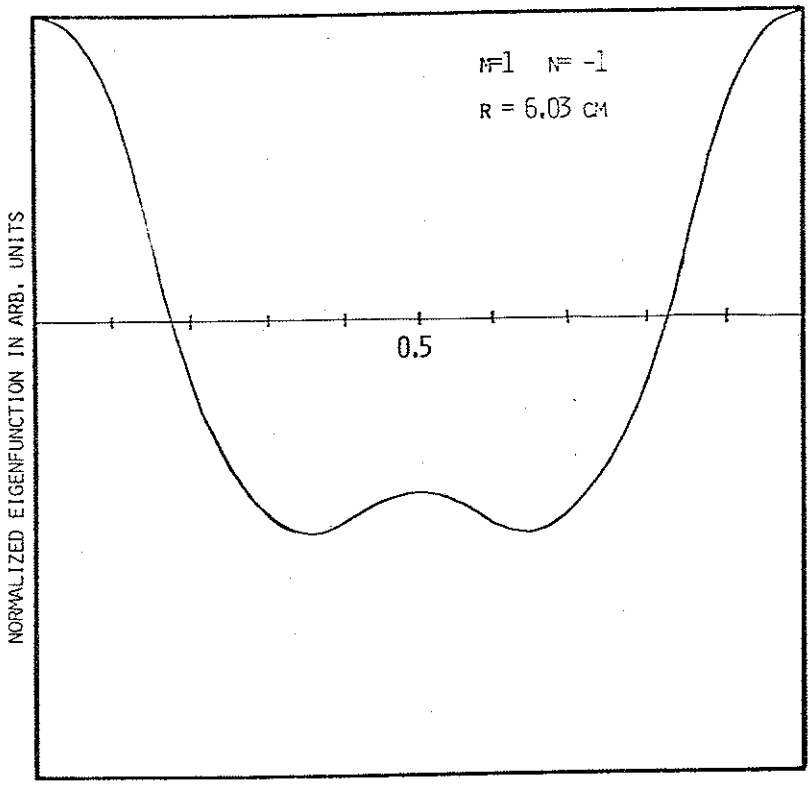

FIGURE 4.18

Figure 4.19 Poloidal Structure of the (1,-1) Mode at the Coupling Surface, r=6.53 cm

The eigenfunction corresponding to the bottom of the gap at r=6.53 cm is displayed vs. the relative distance along a poloidal field line close to the coupling surface. Note that the mode is peaked on the outside of the torus.

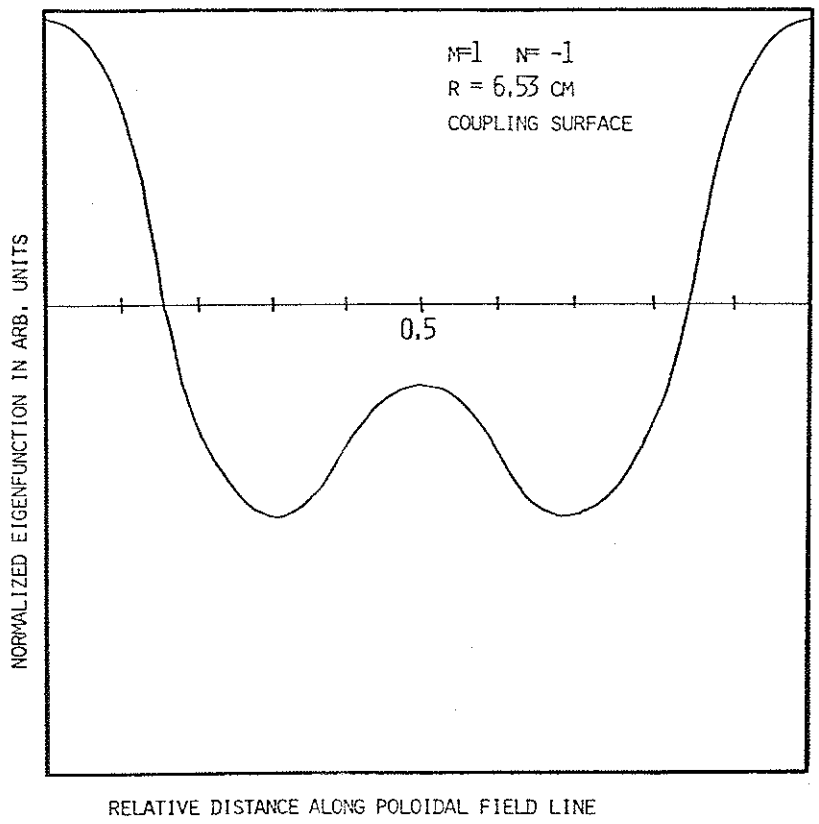

FIGURE 4.19

Fig. 4.20 Poloidal Structure of the (1,-1) Mode at r=7.03 cm

The eigenfunction corresponding to the mode which has a (1,-1) character near the magnetic axis is displayed vs. relative distance along a poloidal field line at r=7.03 cm. A large M=2 component is present in the mode, due to the coupling to the (2,-2) mode around r=6.53 cm.

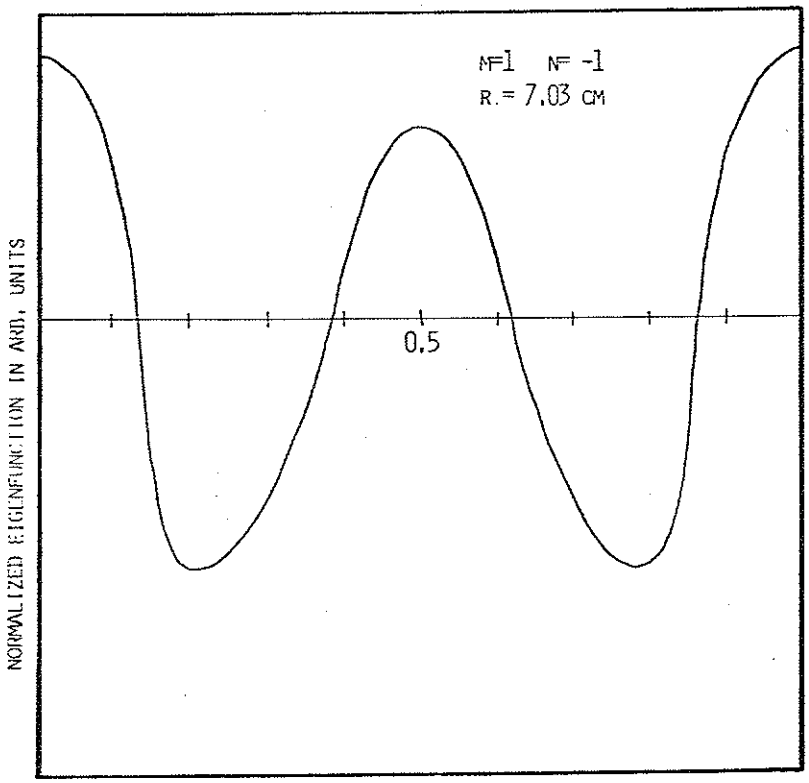

FIGURE 4.20

Figure 4.21 Poloidal Structure of the (2,-1) Mode at r=6.03 cm

The eigenfunction corresponding to the mode which has a (2,-1) character near the magnetic axis is displayed vs. relative distance along a poloidal field line r=6.03 cm. Significant coupling to the (1,-1) mode is already evident at this radius.

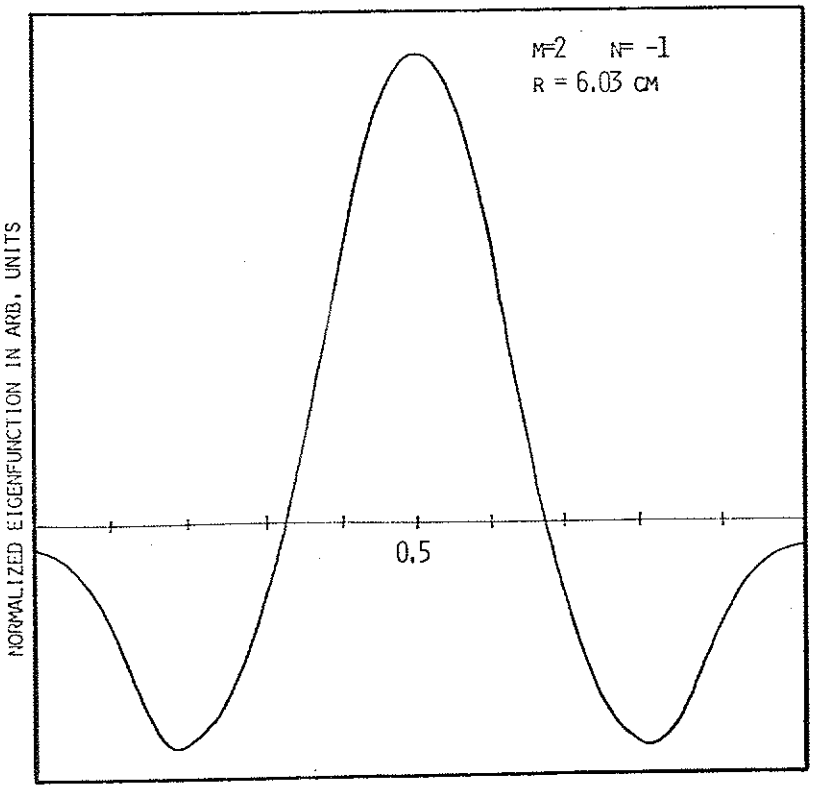

FIGURE 4.21

Figure 4.22 Poloidal Structure of the (2,-1) Mode at the Coupling Surface, r=6.53 cm

The eigenfunction corresponding to the top of the gap at r=6.53 cm is displayed vs. the relative distance along a poloidal field line close to the coupling surface. Note that the mode is peaked on the inside of the torus.

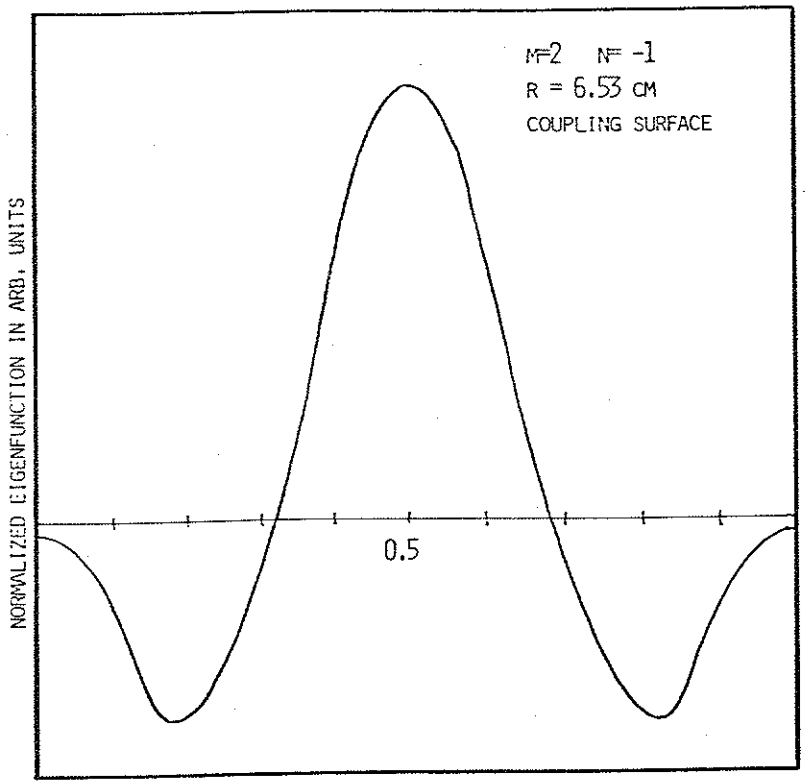

FIGURE 4.22

Figure 4.23 Poloidal Structure of the (2,-1) Mode at r=7.03 cm

The eigenfunction corresponding to the mode which has a (2,-1) character near the magnetic axis is displayed vs. the relative distance along a poloidal field line at r=7.03 cm. A large M=1 component is present in the mode, due to the coupling to the (1,-1) mode around r=6.53 cm. The sharpness of the outer peaks in the eigenfunction is attributed to the distortion of the flux surface near the poloidal field nulls.

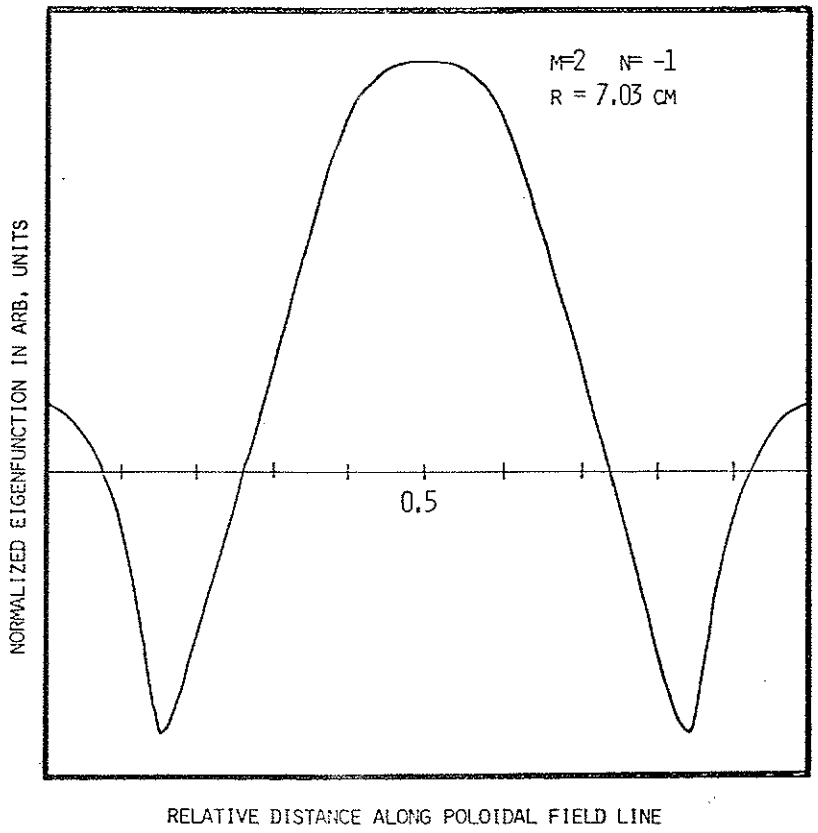

FIGURE 4.23

Figure 4.24 Shear Alfvén Continuum Frequencies vs. Minor Radius on Midplane

The shear Alfvén continuum frequencies corresponding to the modes displayed in Fig. 4.15 are shown.

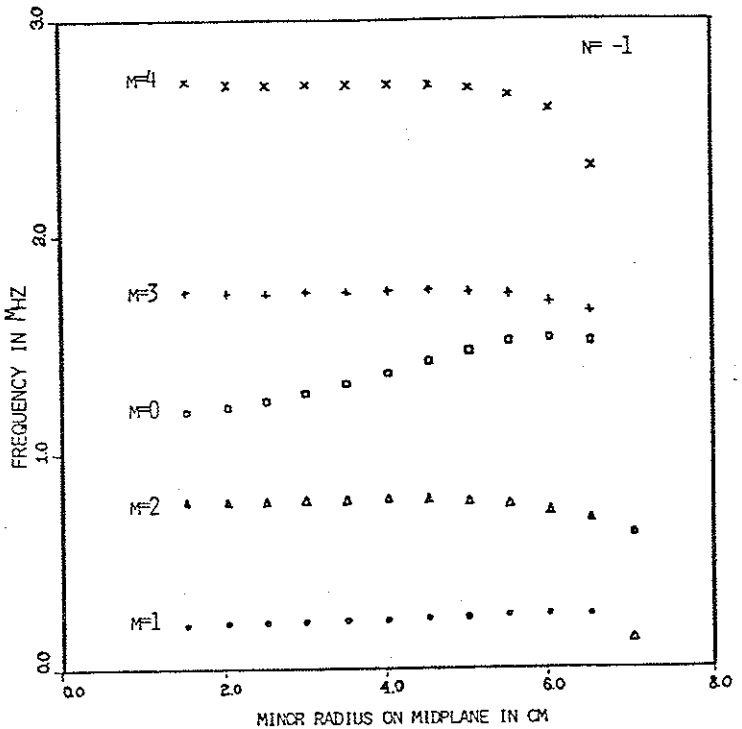

FIGURE 4.24

CHAPTER 5

ANALYSIS OF THE WAVE STRUCTURE ABOUT THE RESONANT SURFACES

The theory of RF energy absorption in a plasma via the resonant excitation of the singular shear Alfvén wave is predicated on two key concepts. The first is that the ideal MHD equations for an inhomogeneous equilibrium admit solutions for the shear Alfvén wave which are characterized by a continuous spectrum. In the previous two chapters, the presence and structure of the shear Alfvén continuum in an axisymmetric tokamak has been investigated analytically, using large aspect ratio expansion schemes, and numerically, by directly solving for the continuum in a Tokapole II equilibrium. The second concept is that the wave structure associated with a mode in the continuum is non-square-integrable about the surfaces where resonance between the external oscillator and the local shear Alfvén wave is achieved. The rate at which energy is absorbed by the localized Alfvén wave is determined by the nature of the spatial singularity of the radial component of the plasma velocity[3,4,14]. In a straight cylindrical screw pinch configuration, the radial structure has been shown to be either a logarithmic or else of the form $(r-r_o)^{iv}$ according to whether the plasma motion is compressible or incompressible[22]. In toroidal geometry, the nature of singularity is determined by the solvability conditions on a singular system of inhomogeneous equations, as discussed in Chapter 2. The solvability conditions are examined in

this chapter to determine the spatial form of shear Alfvén wave about the resonant surfaces in axisymmetric tokamak geometry. Effects due to plasma compressibility/incompressibility and of up-down symmetry/asymmetry of the equilibrium with respect to reflection about the midplane are deduced. Results are compared to previous analyses by Pao[20], Hameiri[35], and Tataronis and Salat[22].

Section 1. Radial Structure of Waves and Solvability Conditions

The linearized ideal MHD equations for an axisymmetric tokamak may be written in the following convenient form, given in Chapter 1 and Appendix B:

$$\frac{\partial \vec{X}}{\partial \Phi} = \vec{\vec{A}} \cdot \vec{X} + \vec{\vec{C}} \cdot \vec{Y} \tag{5.1}$$

$$\vec{\vec{X}} \cdot \vec{Y} = \vec{\vec{K}} \cdot \vec{X} \quad . \tag{5.2}$$

In this system, $\vec{X}$ and $\vec{Y}$ are vectors with elements defined by the expressions,

$$\vec{X} = \begin{bmatrix} v^1 \\ \\ i\omega p^* \end{bmatrix} \tag{5.3}$$

and

$$\vec{Y} = \begin{bmatrix} v^2 \\ \\ v^3 \end{bmatrix} , \tag{5.4}$$

and $\vec{\vec{X}}$, $\vec{\vec{A}}$, $\vec{\vec{C}}$, $\vec{\vec{K}}$ are matrix differential operators. The matrix $\vec{\vec{X}}$ is self-adjoint and the elements of $\vec{\vec{K}}$ and $\vec{\vec{C}}$ are related in the following manner,

$$K_{11} = -C_{21}^{+} \qquad K_{12} = C_{11}^{+}$$

$$K_{21} = -C_{22}^{+} \qquad K_{22} = C_{12}^{+} \tag{5.5}$$

In Eq. (5.5), the superscript + denotes the adjoint of the operator.

Resonant surfaces, Φ_o, and consequently the continua are identified if the inverse of the matrix $\vec{\vec{X}}$ does not exist, i.e., if a nontrivial vector $\vec{Y}$ exists which satisfies the relation

$$\vec{\vec{X}} \cdot \vec{Y} = 0 \tag{5.6}$$

and the periodic boundary conditions specified in Eq. (2.36)-(2.37). The behavior of solutions for $\vec{X}$ and $\vec{Y}$ about the resonant surface, Φ_o, may be obtained using a generalization of the method of

Frobenius[18,19,20,22,35], wherein $\vec{X}$ and $\vec{Y}$ are expressed by a power series in $(\psi-\psi_o)^\nu$. The parameter ν is determined as a solvability condition on the resulting hierarchy of equations. Following the discussions in Chapter 2, appropriate forms for the expansion are the following,

$$\vec{X} = r^\nu[\vec{f}_o(\theta,\beta) + r\vec{f}_1(\theta,\beta) + \cdots]$$

$$\vec{Y} = r^{\nu-1}[\vec{g}_o(\theta,\beta) + r\vec{g}_1(\theta,\beta + \cdots] \quad , \tag{5.7}$$

where $r \equiv \psi-\psi_o$ and the coefficients $\vec{f}_i(\theta,\beta)$ and $\vec{g}_i(\theta,\beta)$ satisfy the periodicity conditions given in Eqs. (2.36)-(2.37). Upon substitution of these expressions into Eqs. (5.1)-(5.2), expansion of the matrices $\ddot{A}$, $\ddot{C}$, $\ddot{\chi}$ and $\ddot{K}$ in power series with respect to r in the form $\ddot{A}=\ddot{A}+r\ddot{A}_1+\cdots$, and equating coefficients of like powers of r, a hierarchy of equations for the functions $\vec{f}_i$ and $\vec{g}_i$ is obtained. One equation, Eq. (5.8), arises from the order $r^{\nu-1}$ coefficients of Eq. (5.2), while two equations, Eq. (5.9)-(5.10), arise from the order r^ν coefficients of Eq. (5.1) and (5.2) respectively:

$$\ddot{\chi}_o \cdot \vec{g}_o = 0 \tag{5.8}$$

$$\nu\vec{f}_o = \ddot{C}_o \cdot \vec{g}_o \tag{5.9}$$

$$\nu\ddot{\chi}_o \cdot \vec{g}_1 = (\ddot{K}_o\cdot\ddot{C}_o-\nu\ddot{\chi}_1)\cdot\vec{g}_o \quad . \tag{5.10}$$

Equation (5.9) has already been incorporated into Eq. (5.10).

The set of equations in Eq. (5.8) is recognized as consisting of the continuum eigenvalue equations which have been solved in the preceding chapters. Examination of Eqs. (2.31 and (2.34), in which the explicit form of the continuum equations is given, reveals that Eq. (5.8) comprise a set of coupled Sturm-Liouville equations in which all coefficients in the matrices are real. It has been previously proven by Tataronis et al.[18] that the eigenvalues of Eqs. (5.8) are all real and nonnegative. Since all quantities appearing in Eq. (5.8) are real and the boundary conditions in Eq. (2.36)-(2.37) are periodicity conditions, the corresponding orthonormal characteristic functions may be chosen to be purely real. Let λ_o be the eigenvalue which corresponds to the frequency of the external oscillator and let $\vec{w}_i$ where i = 1, $\cdots$n, be the linearly independent eigenvectors with eigenvalue, λ_o, i.e.,

$$\ddot{\chi}_o(\lambda_o) \cdot \vec{w}_i = 0 \qquad i = 1, \cdots, n \quad . \tag{5.11}$$

The vectors, $\vec{w}_i$, form the basis for the null space of $\ddot{\chi}_o$. Floquet theory will be used later on in this chapter to determine the number, n, of linearly independent eigenfunctions, $\vec{w}_i$, which satisfy Eq. (5.11) along with the boundary conditions (2.36)-(2.37).

Because the system of Eq. (5.8) consists of two coupled, second order differential equations, there can be at most four linearly independent vectors $\vec{w}_i$ in the null space of $\overleftrightarrow{\chi}_o$ for a given eigenvalue, λ_o. A general solution for the function $\vec{g}_o$ corresponding to the eigenvalue λ_o can be expressed as a linear combination of the n independent vectors $\vec{w}_i$, namely,

$$\vec{g}_o = \sum_{i=1}^{n} a_i \vec{w}_i \quad . \tag{5.12}$$

The first term, $\vec{f}_o$, in the expansion of the vector $\vec{X}$ is provided by Eq. (5.9). Note that $\vec{f}_o$ is specified in terms of the as yet undetermined parameter, ν. If it is found that $\nu=0$, then Eq. (5.9) does not define $\vec{f}_o$ but rather provides a constraint on $\vec{g}_o$, namely that $\vec{g}_o$ must also be null vector of the operator $\overleftrightarrow{C}_o$. Examination of the elements of $\overleftrightarrow{C}_o$, as given in Appendix B in Eqs. (B.53) to (B.55), reveals that it is highly unlikely that $\vec{g}_o$ will also be a null vector of the operator, $\overleftrightarrow{C}$. It is therefore reasonable to conclude that the series expansion as assumed in Eq. (5.7) is not valid when $\nu=0$, and, as will be shown later, an alternate expansion involving the logarithm of $(\phi-\phi_o)$ must be chosen.

Equation (5.10) consists of a set of inhomogeneous differential equations for the function $\vec{g}_1$, involving the singular operator, $\overleftrightarrow{\chi}_o(\lambda_o)$, and the unknown parameter, ν. Equation (5.8) implies that $\overleftrightarrow{\chi}_o(\lambda_o)$ is a singular operator. Therefore, the inhomogeneous term

must satisfy certain solvability conditions[27], to be discussed in the following paragraphs, in order for solutions for $\vec{g}_1$ to exist. The parameter, ν, is chosen in order that these solvability conditions are satisfied.

The solvability conditions on Eq. (5.10) are readily obtained by first substituting the expansion, Eq. (5.12), for $\vec{g}_o$ and then taking the inner product of the resulting expressions with each of the null vectors, $\vec{w}_i$, of $\overleftrightarrow{\chi}_o$. Since each of the $\vec{w}_i$'s is also in the null space of the operator $\overleftrightarrow{\chi}_o^{\dagger}$, it follows that

$$\langle \vec{w}_i | \overleftrightarrow{\chi}_o | \vec{g}_1 \rangle = 0 \tag{5.13}$$

for all vectors, $\vec{w}_i$, in the null space of $\overleftrightarrow{\chi}_o$. The inner product of the inhomogeneous term in Eq. (5.10) with each of the $\vec{w}_i$'s must therefore satisfy the conditions,

$$\sum_j a_j \left[\langle \vec{w}_i | \overleftrightarrow{K}_o \cdot \overleftrightarrow{C}_o | \vec{w}_j \rangle - \nu \langle \vec{w}_i | \overleftrightarrow{\chi}_1 | \vec{w}_j \rangle \right] = 0 \quad , \tag{5.14}$$

in order for a solution to Eq. (5.10) to exist. The n equations, Eq. (5.14), in the n unknowns, a_j, comprise a set of eigenvalue equations which provide the values of ν for which solutions of the form (5.7) may be found for Eq. (5.1)-(5.2). By defining matrices $\overleftrightarrow{R}$ and $\overleftrightarrow{S}$ such that

$$R_{ij} \equiv \langle \vec{w}_i | \overleftrightarrow{K}_o \cdot \overleftrightarrow{C}_o | \vec{w}_j \rangle \tag{5.15}$$

and

$$S_{ij} \equiv \langle \vec{w}_i | \ddot{\chi}_1 | \vec{w}_j \rangle \tag{5.16}$$

then the n equations of Eq. (5.14) may be written more succinctly as

$$[\ddot{R} - \nu \ddot{S}] \cdot \vec{a} = 0 \quad . \tag{5.17}$$

The vector $\vec{a}$ is defined as follows:

$$\vec{a} = \begin{bmatrix} a_1 \\ \cdot \\ \cdot \\ \cdot \\ a_n \end{bmatrix} \quad . \tag{5.18}$$

In the case where there is only one vector in the null space of the operator, $\ddot{\chi}_0(\lambda_0)$, then n = 1, $\vec{g}_0 = \vec{w}_1$, and the form of the solvability conditions used by Tataronis et al.[22] is recovered:

$$\langle \vec{g}_0 | \ddot{K}_0 \cdot \vec{C}_0 - \nu \ddot{\chi}_1 | \vec{g}_0 \rangle = 0 \quad . \tag{5.19}$$

For this case, Eq. (5.19) can be readily solved for the parameter ν:

$$\nu = \frac{\langle \vec{g}_0 | \ddot{K}_0 \cdot \vec{C}_0 | \vec{g}_0 \rangle}{\langle \vec{g}_0 | \ddot{\chi}_1 | \vec{g}_0 \rangle} \quad . \tag{5.20}$$

However, when there is more than one linearly independent vector in the null space of $\ddot{\chi}_0(\lambda_0)$, then the allowed values of ν must satisfy simultaneously equations of the form (5.19), with $\vec{g}_0$ replaced by appropriate pairs of the $\vec{w}_i$'s. These equations are generated by expanding $\vec{g}_0$ in Eq. (5.10) in terms of the $\vec{w}_i$'s, according to Eq. (5.12), and subsequently taking the inner product of the resulting expression with each of the $\vec{w}_i$'s. An example of this procedure is given in the analysis of the screw pinch in Chapter 2. These conditions, of course, are just those given in the eigenvalue equations (5.17). The parameter, ν, is now determined by requiring the determinant of the coefficients for the $\vec{a}_i$'s to vanish. If n distinct values for ν are found, then n distinct sets of a_i's are also determined, up to a normalization constant which is set by boundary conditions at the plasma edge. If some of the values for ν are degenerate, then the correct choice for the corresponding a_i's may be set by the higher order equations in the hierarchy in the power series expansion in $(\phi - \phi_0)$. In general, the denominator in Eq. (5.20) will be real and nonzero, since $\ddot{\chi}_1$ is a self-adjoint operator consisting of a sum of terms, which yield nonzero expectation values with $\vec{g}_0$.

The self-adjointness of $\overleftrightarrow{\chi}_1$ is readily established by taking the partial derivative with respect to ϕ of the elements of $\overleftrightarrow{\chi}$, as given in Appendix B in Eqs. (B.53)-(B.55), evaluating the result at $\phi=\phi_o$, using the self-adjointness of $\overleftrightarrow{\chi}_o$. $\overleftrightarrow{\chi}_1$ is then expressed as the following sum of self-adjoint matrices,

$$\overleftrightarrow{\chi}_1 = \rho\omega_o^2 \frac{\partial \ln\rho}{\partial\phi}\Big|_{\phi=\phi_o} \vec{\hat{n}}_o + \rho\omega_o^2 \begin{bmatrix} \frac{\partial g_{22}}{\partial\phi} & \frac{\partial g_{23}}{\partial\phi} \\ \frac{\partial g_{32}}{\partial\phi} & \frac{\partial g_{33}}{\partial\phi} \end{bmatrix}_{\phi=\phi_o} \tag{5.21}$$

$$+ \frac{\partial}{\partial\theta} \begin{bmatrix} \frac{\partial N_{11}}{\partial\phi} & \frac{\partial N_{12}}{\partial\phi} \\ \frac{\partial N_{21}}{\partial\phi} & \frac{\partial N_{22}}{\partial\phi} \end{bmatrix}_{\phi=\phi_o} \frac{\partial}{\partial\theta}$$

where $\omega_o=\omega_A^2(\phi_o)$ and the elements N_{ij} are defined in Eq. (2.31). Equilibria of experimental interest have nonzero density and magnetic field gradients. From the explicit expressions for g_{ij} and N_{ij}, as given in Eq. (2.31) and Appendix A, one can see that the expectation value of $\vec{g}_o$ with the terms of $\overleftrightarrow{\chi}_1$ will not necessarily be equal to zero. It is reasonable to conclude that $\langle\vec{g}_o|\overleftrightarrow{\chi}_1|\vec{g}_o\rangle$ will be nonzero and real for cases of physical significance.

The preceding solution method for $\vec{X}$ and $\vec{Y}$ will fail if $\nu = 0$ as previously mentioned. This occurs when

$$\langle\vec{w}_i|\vec{\hat{K}}_o \cdot \overleftrightarrow{C}_o|\vec{w}_j\rangle = 0 \quad . \tag{5.22}$$

Self-consistent expansions for $\vec{X}$ and $\vec{Y}$ are found if logarithmic singularities in $(\phi-\phi_o)$ are included in the power series expansions[22] of $\vec{X}$ and $\vec{Y}$, in analogy with results from the method of Frobenius for a single second order differential equation with a regular singular point[19,39]. The appropriate expansions for $\vec{X}$ and $\vec{Y}$ are now given by

$$\vec{X} = [\vec{f}_o(\theta,\beta) + r\vec{f}_1(\theta,\beta) + \cdots] \ln r + \alpha[\vec{d}_o(\theta,\beta) + r\vec{d}_1(\theta,\beta) + \cdots] \tag{5.23}$$

and

$$\vec{Y} = \frac{\vec{g}_o(\theta,\beta)}{r} + [\vec{\hat{n}}_o(\theta,\beta) + r\vec{\hat{n}}_1(\theta,\beta) + \cdots] \ln r + \alpha[\vec{p}_o(\theta,\beta) + r\vec{p}_1(\theta,\beta) + \cdots] \quad . \tag{5.24}$$

where $\vec{d}_i$ and $\vec{p}_i$ are nonsingular components of $\vec{X}$ and $\vec{Y}$; $\vec{f}_i$, $\vec{g}_o$ and $\vec{\hat{n}}_i$ are analytic vectors associated with the singular behavior of $\vec{X}$ and $\vec{Y}$, and the constant α is determined by the boundary conditions at the plasma edge. The lowest order terms, of order $\frac{1}{r}$, determine the dominant behavior of $\vec{X}$ and $\vec{Y}$ in the limit $\phi\to\phi_o$:

$$\overleftrightarrow{\chi}_o(\lambda_o) \cdot \vec{g}_o(\theta,\beta) = 0 \tag{5.25}$$

and

with $d = (N_{11}N_{22}-N_{12}^2)^{-1}$, and

$$\vec{S}_4 = \begin{bmatrix} \vec{S} & 0 \\ 0 & \vec{S} \end{bmatrix} \quad . \tag{5.43}$$

The submatrices, $\vec{S}$, appearing in the matrix $\vec{S}_4$ are defined as follows:

$$\vec{S} = \begin{bmatrix} 0 & -1 \\ 1 & 0 \end{bmatrix} \quad . \tag{5.44}$$

The superscript "T" in Eq. (5.42) denotes the transpose of the matrix. Any solution, $\vec{V}(\theta)$, of Eq. (5.41) may be written in terms of its initial conditions, $\vec{V}(0)$, as

$$\vec{V}(\theta) = \vec{F}(\theta) \cdot \vec{V}(0) \tag{5.45}$$

where $\vec{F}(\theta)$ is the fundamental matrix for the system. The four columns of the fundamental matrix consist of the four linearly independent solutions to Eq. (5.41) which are formed by direct integration of Eq. (5.41), starting with the initial conditions,

$$\vec{F}(0) = [\vec{V}_1(0)\ \vec{V}_2(0)\ \vec{V}_3(0)\ \vec{V}_4(0)] = I \tag{5.46}$$

where I is the identity matrix. The determinant of $\vec{F}(\theta)$, by construction, is just the Wronskian, W, of the solutions. By differentiating the Wronskian with respect to theta and using Eq. (5.41), it is easy to show that $W(\theta)$ is related to $W(0)$ by the following expression [39],

$$W(\theta) = W(0) \exp\{\int \mathrm{trace}(\vec{S}_4 \cdot \vec{H})d\theta\} = W(0) = 1 \tag{5.47}.$$

Using the explicit forms for $\vec{S}_4$ and $\vec{H}$ as given in Eqs. (5.42)-(5.43), it is trivial to show that the trace of $\vec{S}_4 \cdot \vec{H}$ vanishes. Thus, the Wronskian is always equal to its value at $\theta=0$, namely, $W(\theta)=W(0)=1$.

In accordance with Floquet theory[36,37,23], there is at least one solution, $\vec{V}(\theta)$, such that

$$\vec{V}(\theta+2\pi) = \rho\vec{V}(\theta) \quad . \tag{5.48}$$

where ρ is called the Floquet parameter. For the continuum equations, the solution, $\vec{V}(\theta)$, will satisfy the periodicity constraints, Eq. (2.36)-(2.37), if, for toroidal mode numbers, $N > 0$,

$$\rho = e^{i2\pi Nq} \quad , \tag{5.49}$$

while, for toroidal mode numbers $N < 0$,

$$\rho = e^{-i2\pi Nq} \quad . \tag{5.50}$$

By using Eqs. (5.45) and (5.46), the Floquet parameter, ρ, is determined by the condition

$$\det[\vec{\vec{P}}(2\pi)-\rho I] = 0 \quad . \tag{5.51}$$

Now, for Hamiltonian systems, such as Eq. (5.41), it is shown in Appendix E that the following invariant exists:

$$\frac{\partial}{\partial\theta}\Big|_\beta \langle\vec{V}_i|\vec{\vec{S}}_4 \cdot \vec{V}_j\rangle = 0 \quad , \tag{5.52}$$

where $\vec{V}_i$ and $\vec{V}_j$ are any two solutions to Eq. (5.41) and

$$\langle\vec{V}_i|\vec{\vec{S}}_4 \cdot \vec{V}_j\rangle \equiv \oint d\theta \vec{V}_i^T \cdot \vec{\vec{S}}_4 \cdot \vec{V}_j \quad . \tag{5.53}$$

It then follows, using Eqs. (5.48) and (5.52), that

$$\begin{aligned}\langle\vec{V}_l(0)|\vec{\vec{S}}_4 \cdot \vec{V}_k(0)\rangle &= \langle\vec{V}_l(2\pi)|\vec{\vec{S}}_4 \cdot \vec{V}_k(2\pi)\rangle \\ &= \rho_l\rho_k\langle\vec{V}_l(0)|\vec{\vec{S}}_4 \cdot \vec{V}_k(0)\rangle \quad ,\end{aligned} \tag{5.54}$$

hence,

$$(\rho_l\rho_k-1)\langle\vec{V}_l(0)|\vec{\vec{S}}_4 \cdot \vec{V}_k(0)\rangle = 0 \tag{5.55}$$

Since the $\vec{V}_k$'s form a linearly independent basis, it is not possible for $\langle\vec{V}_l|\vec{\vec{S}}_4 \cdot \vec{V}_k\rangle$ to vanish for all values of k. Hence, if ρ_k is a solution to Eq. (5.51), then so is ρ_k^{-1}, and one may conclude

$$\rho_1\rho_2\rho_3\rho_4 = 1 \tag{5.56}$$

Furthermore, $\vec{\vec{P}}(2\pi)$ is composed of totally real elements, since $\vec{\vec{P}}(0) = I$ and the elements of $\vec{\vec{H}}$ are all real. Thus, if ρ_k is a solution, then ρ_k^*, the complex conjugate of ρ_k, is also a solution. From these facts, the following possibilities arise for the four solutions, ρ_k:

$$\begin{aligned}&\text{i)} \quad \rho_k = 1 && \text{for all } k \\ &\text{ii)} \quad |\rho_k| \neq 1 && \text{for all } k \\ &\text{iii)} \quad |\rho_k| = 1 && \text{for all } k \\ &\text{iv)} \quad |\rho_k = 1 && \text{for } k = 1,2 \quad \text{and} \quad |\rho_k| \neq 1 \quad \text{for } k = 3,4\end{aligned} \tag{5.57}$$

The first two possibilities, (i) and (ii), yield solutions for ρ which cannot satisfy the periodicity constraints in Eqs. (5.49)-(5.50). Periodic solutions may be obtained as particular cases of both (iii) and (iv). Diagrams in the complex-ρ plane of these particular cases are provided in Figs. 5.1a-5.1c.

Figures 5.1a and 5.1b depict the possible solutions for the ρ_k's which lead to only one pair of ρ's which satisfy the periodicity constraints. One member of the pair, ρ_1, satisfies the periodicity constraint, Eq. (5.49), for toroidal mode number $N > 0$, while the other member, ρ_2, satisfies the periodicity constraint, Eq. (5.50), for $N < 0$. Figure 5.1c indicates the solutions when two degenerate pairs of ρ's occur such that $\rho_1 = \rho_2$ satisfy Eq. (5.49) for $N > 0$ while $\rho_3 = \rho_4$ satisfies Eq. (5.50) for $N < 0$. Hence, for a given λ, there is either one solution for ρ which yields a periodic eigenfunction, or else there is a double solution for ρ, in which case Floquet theory guarantees that there exists at least one periodic eigenfunction corresponding to the double root.

When a doubly degenerate solution for ρ satisfies the appropriate periodicity condition, Eq. (5.49) or Eq. (5.50), then the number of linearly independent periodic solutions for $\vec{V}$ is determined by the rank of the mxm matrix, $(\vec{P}(2\pi)-\rho_d I)$, where ρ_d is the double root for the Floquet parameter[37] and the order of the matrix is $m = 4$. If s denotes the rank of the matrix, then there are $n = m - s$ linearly independent eigenvectors which correspond to the solution $\rho = \rho_d$ and hence which satisfy the periodicity requirements. If the rank of the matrix is $s = 3$ then there is $n = 1$ periodic solution while if the rank of the matrix is $s = 2$, then there are $n = 2$ linearly independent periodic solutions in θ, β.

To summarize, the dimension of the null space of $\vec{\mathfrak{F}}_o(\lambda_o)$ is determined by the number, n, of linearly independent vectors, $\vec{\Psi}_1$, which satisfy the continuum equations and the appropriate poloidal and toroidal periodicity requirements. By writing the continuum equations as a Hamiltonian system of four coupled first order differential equations and considering the eigenvalues, ρ, of the fundamental matrix, $\vec{P}(\theta)$, for the system evaluated at $\theta = 2\pi$, then the existence and number of linearly independent periodic solutions are determined by the values of the Floquet parameters, ρ_k, and the rank of the corresponding matrices, $(\vec{P}(2\pi)-\rho_k I)$. In general, the fundamental matrix must be generated numerically, so the remaining quantities described must also be computed numerically.

The procedure described thus far in this section has been applied, in a modified form, to determine the number of linearly independent periodic vectors which form the basis for the null space of $\vec{\mathfrak{F}}_o$ for a given frequency in a Tokapole II equilibrium. Because the available numerical subroutines which determine the rank of a matrix require that all elements of the matrix be real, it was desirable to reformulate the preceding equations so that the periodicity conditions take the form $\rho = 1$ rather than $\rho = \exp(\pm i 2\pi N q)$. When a complex form of the boundary conditions is used, the elements of the solution vectors may also be complex. If the boundary conditions are expressed as real quantities, the corresponding solution vectors will also be real quantities, since the coefficients in the differential equations are real. By

delaying the Fourier decomposition in the toroidal direction and by using the Hamada coordinates θ, ξ, the continuum equations may be written in a form similar to Eq. (5.1) but with $\frac{\partial}{\partial\theta}$ replaced by $(\frac{\partial}{\partial\theta} + q\frac{\partial}{\partial\xi})$ and $\vec{V}(\theta)$ by $\vec{V}(\theta,\xi)$. A Fourier decomposition of the vector, $\vec{V}(\theta,\xi)$ is taken in terms of sin $(N\xi)$ and cos $(N\xi)$ as

$$\vec{V}(\theta,\xi) = \vec{A}(\theta) \cos N\xi + \vec{C}(\theta) \sin N\xi \quad . \tag{5.58}$$

The resulting eighth order Hamiltonian system is given by

$$\frac{\partial}{\partial\theta}\vec{Z} = \vec{\vec{S}}_8 \cdot \vec{\vec{H}}_8 \cdot \vec{Z} \quad , \tag{5.59}$$

where

$$\vec{Z} = \begin{bmatrix} \vec{A} \\ \\ \vec{C} \end{bmatrix} \quad , \tag{5.60}$$

$$\vec{\vec{H}}_8 = \begin{bmatrix} \vec{\vec{H}}_4 & Nq\vec{\vec{S}}_4 \\ \\ -Nq\vec{\vec{S}}_4 & \vec{\vec{H}}_4 \end{bmatrix} \quad , \tag{5.61}$$

and where $\vec{\vec{S}}_8$ is defined analogously to $\vec{\vec{S}}_4$, as in Eq. (5.43). The remainder of the analysis may now be applied to Eq. (5.59), but with the poloidal periodicity condition appropriate to the coordinates (θ,ξ), i.e.,

$$\vec{Z}(\theta+2\pi) = \vec{Z}(\theta) \quad . \tag{5.62}$$

The desired Floquet parameter signalling periodicity is now $\rho = 1$. Since, in effect, a linear combination of the functions $e^{iN\xi}$ and $e^{-iN\xi}$ has been introduced to use Eq. (5.58), a solution $\rho = 1$ is always at least a double root. When, in the complex representation $\rho = \exp(\pm i2\pi Nq)$ is a pair of single roots, then the corresponding solution for ρ in the real representation is $\rho = 1$ as a double root. Similarly, when $\rho = \exp(\pm i2\pi Nq)$ is a pair of double roots in the complex representation, then $\rho = 1$ is a quadruple degenerate root in the real representation. If $\rho = 1$ is a double root, then two real periodic solutions for $\vec{Z}$ are found, while if $\rho = 1$ is a quadruple root, then either two or four real linearly independent periodic solutions for $\vec{Z}$ exist. In the latter case, the number of linearly periodic functions may again be determined by the rank of the matrix $[\vec{\vec{P}}(2\pi)-\rho I]$, where $\rho = 1$ for the real representation.

In all cases considered for the shear Alfvén continuum frequencies in the Tokapole II device, only two periodic, real linearly independent vectors of the form Eq. (5.58) were found for any given frequency. Since such a numerical search cannot ever be

entirely complete, one cannot necessarily rule out the possibility that four real, linearly independent periodic vectors may exist for some frequency not yet considered. However, such a frequency would be out of the range of experimental interest, so its possible existence will not be contemplated further. In regards to the two real periodic solutions which were found, one is an even function of the combination θ,ξ while the other is an odd function of the combination θ,ξ. This occurs because the Tokapole II equilibrium has been idealized to be symmetric with respect to reflection about the midplane. The coefficients in the continuum equations are thus even functions of θ and the continuum equations are invariant under the simultaneous transformation $\theta \rightarrow -\theta$ and $\xi \rightarrow -\xi$. As a result, both an even function, with respect to θ,ξ, and an odd function can satisfy the equations for the same eigenfrequency. If the chosen equilibrium is not assumed to be up-down symmetric, then it is likely that an even mode and an odd mode with the same wave numbers would not share a common eigenfrequency, since each would see a different average structure of the equilibrium magnetic field.

Section 3. Applications to a Finite Pressure, Compressible Plasma in an Axisymmetric Tokamak Equilibrium

The plasmas in actual experiments involving shear Alfvén wave heating will undoubtably have some small degree of non-axisymmety and reflection asymmetry about the midplane due to the finite size of coils, nonuniformities in materials, presence of divertor

regions, etc. In this section, the spatial wave structure of a shear Alfvén continuum mode in a finite pressure, compressible, axisymmetric tokamak plasma with and without reflection symmetry about the midplane will be determined. The effect of incompressibility will be considered in Section 4 of this chapter while the effect of zero plasma beta will be examined in Chapter 6. Effects due to non-axisymmetry are outside the scope of the present study.

Following the formal developments of sections 1 and 2 of this chapter, the wave structure about the resonant surface is characterized by the exponent, ν, which appears in a generalized Frobenius-type expansion of the vectors $\vec{X}$ and $\vec{Y}$, as in Eq. (5.7). The hierachy of equations, which results by combining the expansions in Eq. (5.7) with power series expansions for the matrices $\vec{\vec{A}}$, $\vec{\vec{C}}$, $\vec{\vec{Y}}$ and $\vec{\vec{K}}$ in Eq. (5.1)-(5.2), may be solved consistently to all orders if the exponent, ν, is chosen to satisfy the compatibility conditions as expressed in Eq. (5.17), (5.15)-(5.16). The order of the eigenvalue problem, Eq. (5.17), for ν is set by the dimension of the null space of the matrix $\vec{\vec{Y}}_0$. By choosing a complex representation for the vectors $\vec{X}$ and $\vec{Y}$, the dimension of the null space of $\vec{\vec{Y}}_0$ is one, as discussed at the end of the previous section. Hence, the exponent, ν, is determined simply by Eq. (5.20), i.e.,

$$\nu = \frac{\langle \vec{g}_o | \vec{K}_o \cdot \vec{C}_o | \vec{g}_o \rangle}{\langle \vec{g}_o | \vec{X}_1 | \vec{g}_o \rangle} \quad , \tag{5.20}$$

where $\vec{g}_o$, the single vector in the null space of $\vec{X}$, is written as

$$\vec{g}_o(\theta,\beta) = \vec{A}(\theta) e^{iN\beta} \tag{5.63}$$

for a toroidal mode number $N < 0$. The denominator of Eq. (5.20) is always a real quantity, since $\vec{X}_1$ is self-adjoint, and does not vanish (unless quantities such as $\partial p/\partial\psi$ and $\partial\omega_A/\partial\psi$ vanish identically in the plasma--a situation clearly not of experimental interest). The numerator in Eq. (5.20) is always either pure imaginary or zero because of the symmetry in the matrix $\vec{F} \equiv \vec{K}_o \cdot \vec{C}_o$. From Eq. (5.5), the matrix $\vec{F}$ is anti-Hermitian, i.e.,

$$\vec{F}^+ = -\vec{F} \quad . \tag{5.64}$$

Now, by letting

$$T = \langle \vec{g}_o | \vec{F} | \vec{g}_o \rangle \tag{5.65}$$

and since

$$T^* = \langle \vec{g}_o | \vec{F}^+ | \vec{g}_o \rangle = - \langle \vec{g}_o | \vec{F} | \vec{g}_o \rangle = -T \tag{5.66}$$

it follows immediately that T is pure imaginary or zero.

The parameter, ν, is thus shown to be either pure imaginary or zero for this plasma. The corresponding wave functions exhibit non-square-integrable singularities of the form

$$\vec{Y} \sim r^{i|\nu|-1}\, \vec{g}(\theta,\beta) \tag{5.67}$$

if ν is pure imaginary, or else of the form

$$\vec{Y} = \frac{\vec{g}_o}{r} + \vec{H} \ln r + \alpha \vec{p} \tag{5.68}$$

if $\nu = 0$.

If the equilibrium under consideration exhibits up-down reflection symmetry about the midplane, i.e., $|\vec{B}(\theta)| = |\vec{B}(-\theta)|$, etc., then the coefficients in the matrix, $\vec{F}$, also exhibit a definite parity, either even or odd, with respect to the poloidal angle, θ. Using the explicit forms for the elements of $\vec{F}$, extracted from Appendix B, it is possible to show that the integrals resulting from the inner product in the numerator of Eq. (5.20) all vanish, hence $\nu = 0$. Details of this calculation are provided in Appendix F. The result is that for a finite pressure, compressible plasma in an axisymmetric, up-down symmetric tokamak, the nature of the spatial singularities about the resonant surfaces in the components of $\vec{X}$ are logarithmic in $(\psi-\psi_o)$, while those of $\vec{Y}$ are of the form

$(\phi-\phi_o)^{-1}$. If any degree of up-down asymmetry is allowed, then, in general, the form of the singularities may change to $\vec{X} \sim (\phi-\phi_o)^{i|\nu|}$ and $\vec{Y} \sim (\phi-\phi_o)^{i|\nu|-1}$, depending on the actual value assumed by the parameter, ν.

A comparison of the results for a finite pressure, compressible plasma in an axisymmetric, up-down symmetric tokamak with those given in Chapter 2 for a finite pressure, compressible plasma in a cylindrical screw pinch indicates that the toroidal nature of the equilibrium does not influence the nature of the spatial singularities of the shear Alfvén wave about the resonant surfaces in a compressible plasma. (This conclusion does not follow for an incompressible plasma, as will be discussed in the next section.) The primary effect of toroidicity in a finite pressure, compressible plasma is to introduce periodic, up-down symmetric variations in the poloidal direction which influence the nature of the continua but not the nature of the spatial singularities. Other up-down symmetric, periodic variations of the equilibrium (resulting in noncircular flux surfaces that are elliptical, etc.) likewise will influence the nature of the continua but not the spatial structure of the waves about the resonant surfaces. Conversely, these results imply that the singularities associated with the shear Alfvén wave in a finite pressure, compressible plasma in a cylindrical screw pinch with noncircular, up-down symmetric flux surfaces are the same in form as if the equilibirum was completely cylindrically symmetric. It is only when up-down asymmetric variations in the

poloidal direction are introduced that the nature of the spatial singularities may be altered from that characterizing the up-down symmetric case.

According to the results[22] summarized in Chapter 2, the shear Alfvén continuum and the cusp continuum are degenerate in an incompressible, cylindrically symmetric screw pinch. As a result of this degeneracy, the spatial singularities associated with the perturbed radial fluid velocity of a continuum mode are no longer logarithmic but are of the form $(r-r_o)^{i|\nu|}$. Mathematically, this arises because the order of the eigenvalue problem for the exponent has been doubled and the off-diagonal terms in the matrix are nonzero, leading to a value for ν which is imaginary. In the next section, shear Alfvén waves in an incompressible, finite pressure tokamak plasma will be examined to determine if the shear Alfvén and cusp continua are degenerate or distinct, and to determine the nature of the spatial singularities which may be associated with the modes.

Section 4. Application to Incompressible, Finite Pressure Plasma in an Axisymmetric Tokamak

The equations which determine the continuous spectra in an axisymmetric tokamak, Eq. (2.34), simplify in the incompressible plasma limit, when $\gamma \to \infty$, resulting in $B_*^{-1} \to 0$. In this limit, the continuum equations reduce to

$$\lambda \vec{M}(\theta) \cdot \vec{Y}(\theta,\beta) + \frac{\partial}{\partial\theta}\Big|_\beta \vec{M}(\theta) \frac{\partial}{\partial\theta}\Big|_\beta \cdot \vec{Y}(\theta,\beta) = 0 \quad , \tag{5.69}$$

where $\vec{M}(\theta)$ contains the matric tensor elements in the flux surface, which are defined in Eq. (2.31). In the cylindrically-symmetric incompressible screw pinch limit of Eq. (5.69), discussed in Chapter 2, the matrix $\vec{M}$ is independent of the theta and is diagonal, indicating the the shear Alfvén and cusp continua are mutually degenerate. As a result of this degeneracy, the character of the spatial structure of the perturbed radial velocity associated with the shear Alfvén wave is modified from logarithmic, in a compressible plasma, to $(r-r_o)^{i|v|}$ in an incompressible plasma. The theta dependence of $\vec{M}$, which arises in a tokamak because of the toroidal nature of the equilibrium, couples the two equations in Eq. (5.69) and presumably eliminates the degeneracy between the shear Alfvén and cusp modes which occurs in the incompressible cylindrically-symmetric screw pinch. This implies that in an incompressible, axisymmetric, up-down symmetric tokamak the two continua remain distinct and the analysis of the spatial wavestructure given in the preceding sections of this chapter for a compressible tokamak plasma remains valid. Specifically, the perturbed radial velocities associated with the distinct shear Alfvén and cusp continua in an incompressible, axisymmetric, up-down symmetric tokamak, exhibit logarithmic singularities about the resonant surfaces.

To demonstrate, nonrigorously, that the two continua are distinct in the incompressible limit of an axisymmetric tokamak, approximate forms for the two continua, based on the large aspect ratio expansion techniques of Chapter 3, will be developed in the remainder of this section. A more rigorous proof would entail establishing the convergence of the resulting series expansions for ω_A^2 and ω_c^2.

Proceeding as in Chapter 3, the matrix $\vec{M}$ is expanded in powers of the small inverse aspect, ε, using Eq. (3.2)-(3.3), and only first order in ε terms, arising from toroidicity, are retained. By expanding λ and $\vec{Y}$ in power series in ε as

$$\lambda = \lambda^o + \varepsilon\lambda^1 + \varepsilon^2\lambda^2 + \cdots$$

$$\vec{Y} = \vec{Y}_o + \varepsilon\vec{Y}_1 + \varepsilon^2\vec{Y}_1 + \cdots \tag{5.70}$$

and substituting the expansions into Eq. (5.69), the following hierarchy of equations results:

$$(\lambda^o\vec{M} + \vec{L}^o) \cdot \vec{Y}_o = 0 \tag{5.71}$$

$$(\lambda^o\vec{M}^o + \vec{L}^o) \cdot \vec{Y}_1 = -(\lambda^o\vec{M}^1 + \vec{L}^1) \cdot \vec{Y}_o - \lambda^1\vec{M}^o \cdot \vec{Y}_o \tag{5.72}$$

$$(\lambda^o\vec{M}^o+\vec{L}^o)\cdot\vec{Y}_2 = -(\lambda^o\vec{M}^1+\vec{L}^1)\cdot\vec{Y}_1 - \lambda^1\vec{M}^o\cdot\vec{Y}_1 - \lambda^2\vec{M}^o\cdot\vec{Y}_o \qquad (5.73)$$

where

$$\vec{L} \equiv \frac{\partial}{\partial\theta}\Big|_\beta \vec{M}(\theta)\frac{\partial}{\partial\theta}\Big|_\beta = \vec{L}^o + \varepsilon\vec{L}^1 \quad . \qquad (5.74)$$

Again, as in Chapter 3, since $\vec{M}$ and $\vec{L}$ are hermitian operators, so are $\vec{M}^o$, $\vec{M}^1$, $\vec{L}^o$, and $\vec{L}^1$. Thus, formal perturbation techniques may be used to solve for λ, $\vec{Y}$ order by order.

The lowest order equations, Eq. (5.71), are equivalent to those describing an incompressible, cylindrically-symmetric screw pinch plasma. Following the developments in Chapter 2, the shear Alfvén and cusp continua are degenerate in this limit and are defined by

$$\lambda^o_{MN} = (M+Nq)^2 \quad , \qquad (5.75)$$

where M and N are the poloidal and toroidal mode numbers, respectively. On most surfaces and for most choices of M,N each eigenvalue, Eq. (5.75), is doubly degenerate with the following two linearly independent eigenvectors,

$$\vec{u}_M = \frac{1}{2\pi r}\begin{bmatrix}1\\0\end{bmatrix}e^{i(M+Nq)\theta}\,e^{-iN\beta} \quad ,$$

$$\vec{v}_M = \frac{1}{2\pi R_o}\begin{bmatrix}0\\1\end{bmatrix}e^{i(M+Nq)\theta}\,e^{-iN\beta} \qquad (5.76)$$

where the normalizations have been chosen so

$$\langle u_M|M^o|u_{M'}\rangle = \langle v_M|M^o|v_{M'}\rangle = \delta_{MM'} \qquad (5.77)$$

and where it follows

$$\langle u_M|M^o|v_{M'}\rangle = 0 \quad . \qquad (5.78)$$

The additional degeneracies which arise because the combination

$$e^{-i(M+Nq)\theta}\,e^{iN\beta}$$

yields two more linearly independent vectors of the form (5.76) have been ignored. This is justified because these additional solutions are never coupled to the solutions in Eqs. (5.76) by poloidal variations in the equilibrium. However, on certain rational q surfaces for particular choices of M and N, additional nonignorable degeneracies, of the type discussed extensively in Chapter 3, occur when

$$\lambda^{o}_{MN} = (M+Nq)^2 = \lambda^{o}_{M'N} = (M'+Nq)^2 \quad . \tag{5.79}$$

The conditions which M, M', N and q must satisfy are given in Eqs. (3.13) and (3.19). These modes, (M,N) and (M±1,N) are coupled in first order by the toroidicity-induced variations of the equilibrium. In addition to the two vectors given in Eq. (5.76), two more linearly independent vectors of the form Eq. (4.76), but with M replaced by M', also give rise to the zeroth order eigenvalue, Eq. (5.75). Hence, for these cases, the zeroth order solution is four-fold degenerate.

First order corrections to both the doubly degenerate and four-fold degenerate lowest order eigenvalues may be readily calculated by writing $\vec{Y}_o$ as an arbitrary linear combination of the degenerate eigenvectors, substituting in Eq. (5.72), and considering the set of equations which arise by subsequently taking the inner product of Eq. (5.72) with each of the linearly independent degenerate eigenvectors. Alternatively, the first order corrections may be determined by using the equivalent formulation developed in Chapter 2 in sections 1 and 3. The elements, $H_{\alpha\beta}$, which appear in the perturbation matrix, Eq. (3.6), are defined in Eq. (3.16). Using the vectors $\vec{u}_M$, $\vec{u}_{M'}$, $\vec{v}_M$, $\vec{v}_{M'}$, as defined in Eq. (5.76) and identifying $\vec{M}^1$ and $\vec{L}^1$ by expanding Eq. (5.69), the elements, $H_{\alpha\beta}$ of interest are given by

$$\langle u_M|H^1|u_{M'}\rangle = \frac{\Lambda}{qR_o^2}\, h_\pm$$

$$\langle u_M|H^1|v_{M'}\rangle = \frac{-h_\pm}{rR_o} = \langle v_M|H^1|u_{M'}\rangle \tag{5.80}$$

$$\langle v_M|H^1|v_{M'}\rangle = \frac{1}{qR_o^2}\, h_\pm$$

where

$$H^1 \equiv \lambda^{o}_{MN}\, \vec{M}^1 + \vec{L}^1 \tag{5.81}$$

and

$$h_\pm \equiv \varepsilon qR_o^2\,(r/a)\left[(M+Nq)^2 - (M'+Nq)^2 \pm (M'+Nq)\right]\delta_{M',M\pm1}\,\delta_{N',N} \quad . \tag{5.82}$$

In the case where the shear Alfvén and cusp modes are only doubly degenerate in the lowest order, then the two independent vectors are given in Eq. (5.76). Since M' = M for these modes, the first order terms, $H_{\alpha\beta}$, all vanish as can be seen by inspection of Eq. (5.80). As a consequence, the first order corrections to the eigenvalue all vanish and these modes remain degenerate after first order toroidal effects are included. It will be necessary to apply

second order degenerate perturbation methods, later on in this section, to demonstrate that toroidicity can remove the degeneracy in higher orders.

When the modes $\vec{u}_M$, $\vec{v}_M$, $\vec{u}_{M\pm1}$, $\vec{v}_{M\pm1}$, are all degenerate in lowest order (where the appropriate choice, $M' = M + 1$ or $M' = M - 1$, consistent with the conditions in Eqs. (3.13), (3.19), has been made), then, from Eq. (5.80), the off-diagonal elements in the fourth order perturbation matrix which determines λ^1 for these modes are nonzero. Four distinct solutions for λ^1 of the form

$$\lambda^1 = \pm \sqrt{W_1 \pm W_2} \tag{5.83}$$

are found, where W_1 and W_2 are functions of the equilibrium quantities such that $W_1 > W_2 > 0$ always. The first order toroidal coupling which occurs between these modes completely removes the degeneracy, resulting in two distinct shear Alfvén-type modes and two distinct cusp-type modes, which can be identified by their polarization.

Though first order toroidal coupling does not occur between the two modes, Eq. (5.76), corresponding to an eigenfrequency, λ^o_{MN}, which is doubly degenerate in the zeroth order approximation, it will now be shown that by including the second order toroidal couplings, which occur between the two degenerate modes and all other modes of the system, the degenerate solution is resolved into two distinct, nondegenerate waves. One could proceed by using

Eq. (5.80) and retaining, in the perturbation matrix, Eq. (3.6), all zeroth order elements, all first order elements on the main diagonal, and only those off-diagonal first order elements, $H_{\alpha\beta}$, which involve either of the two degenerate eigenvectors in Eq. (5.76). However, it is more expedient to proceed in the following manner[40], since the resulting equation for λ^1 is of a lower order than the one which would be obtained by utilizing Eq. (3.6).

The zeroth order solution for $\vec{Y}_o$ is written as linear combination of the independent vectors in Eq. (5.76),

$$\vec{Y}_o = a_M \vec{u}_M + b_M \vec{v}_M \quad . \tag{5.84}$$

Because the first order corrections to λ^o_{MN} vanish, a_M and b_M are not determined by the first order equations. The first order corrections, $\vec{Y}_1$, to the solution for $\vec{Y}$ may be expanded in terms of the complete set of eigenvectors, $\vec{\phi}_k$, which are defined by Eq. (5.71) with $\lambda^o = \lambda^o_{MN}$. [Equation (5.71) consist of two, uncoupled harmonic oscillator type equations, for which it is well known that the solutions form a complete set of orthornormal functions.] The expansion for $\vec{Y}_1$ is written as

$$\vec{Y}_1 = \sum_k{}' a^1_k \vec{\phi}_k \quad , \tag{5.85}$$

where the prime indicates that the terms involving $\vec{u}_M$ and $\vec{v}_M$ have

been deleted. This omission is permissible since, by Eq. (5.71), an arbitrary addition of $\vec{Y}_o$ to $\vec{Y}_1$ in Eq. (5.72) will not alter the solutions of Eq. (5.72). The arbitrary addition of $\vec{Y}_o$ is chosen so $\vec{Y}_1$ is orthogonal to $\vec{Y}_o$. Substitution of Eqs. (5.84)-(5.85) into Eq. (5.72) yields solutions for a_k^1 in terms of a_M and b_M:

$$a_k^1 = \frac{\langle \phi_k | H^1 | u_N \rangle a_M + \langle \phi_k | H^1 | v_N \rangle b_M}{\lambda_k^o - \lambda^o{}_{MN}} \quad , \tag{5.86}$$

when the inner product of Eq. (5.72) with $\vec{\phi}_k$ is taken. Finally, by substituting expansions (5.84)-(5.85) into Eq. (5.73) and again taking inner products with $\vec{u}_M$ and $\vec{v}_M$, the following pair of two coupled algebraic eigenvalue equations for a_M, b_M, and λ^2 is derived:

$$\begin{bmatrix} P_1 - \lambda^2 & P_2 \\ P_2 & P_3 - \lambda^2 \end{bmatrix} \cdot \begin{bmatrix} a_M \\ b_M \end{bmatrix} = 0 \tag{5.87}$$

where

$$P_1 \equiv \sum_k{}' \frac{|\langle \phi_k | H^1 | u_M \rangle|^2}{\lambda_{MN}{}^o - \lambda_k{}^o} \tag{5.89}$$

$$P_2 = \sum_k{}' \frac{\langle u_M | H^1 | \phi_k \rangle \langle \phi_k | H^1 | v_M \rangle}{\lambda_{MN}{}^o - \lambda_k{}^o} \tag{5.89}$$

$$P_3 = \sum_k{}' \frac{|\langle \phi_k | H^1 | v_M \rangle|^2}{\lambda_{MN}{}^o - \lambda_k{}^o} \quad . \tag{5.90}$$

From Eq. (5.87), it is easy to see that degeneracy will be removed by the second order corrections, λ^2, if there is at least one other vector, $\vec{\phi}_k$, belonging to a different zeroth order eigenvalue, $\lambda_k{}^o \neq \lambda_{MN}{}^o$, such that

$$\langle u_M | H^1 | \phi_K \rangle \neq 0 \quad \text{and} \quad \langle v_M | H^1 | \phi_k \rangle \neq 0 \quad . \tag{5.91}$$

According to Eq. (5.80), four vectors, $\vec{u}_{M\pm1}$ and $\vec{v}_{M\pm1}$, belonging to the eigenvalues $\lambda^o_{M\pm1,N}$, exist which satisfy Eq. (5.91), so the degeneracy is broken in this order.

To summarize, then, the spatial singularities associated with the continuum modes in an incompressible, axisymmetric tokamak plasma are the same as those associated with the continuum modes in a compressible, axisymmetric tokamak. This conclusion follows because in each instance, distinct solutions for the modes are found which may be analyzed as shown in sections 1-3 of this chapter. For

an up-down symmetric equilibrium the radial velocity perturbations exhibit logarithmic singularities about the resonant surfaces, where the wave frequency matches that of a mode in the continuous spectra. For an up-down asymmetric equilibrium, the radial velocity perturbations vary as $(\phi-\phi_o)^{i|\nu|}$ about the resonant surfaces, where ν is defined in Eq. (5.7). These results for the incompressible tokamak plasma differ from those of an incompressible, cylindrically symmetric screw pinch plasma primarily because the toroidal nature of the equilibrium precludes the occurence of the degeneracies present between the shear Alfvén and cusp waves in a straight cylindrical screw pinch equilibrium. The radial velocity perturbations in a cylindrically-symmetric, incompressible screw pinch plasma have been shown[22] to vary as $(r-r_o)^{i|\nu|}$ about the resonant surfaces, r_o. Based on the analysis in this chapter, one may infer that if an up-down symmetric poloidal perturbation (such as ellipticity) is present in a incompressible straight screw pinch plasma, then mode coupling will resolve the degeneracy between the shear Alfvén and cusp continua, thereby recovering the logarithmic behavior of the radial velocity perturbation, v_r, present if the plasma is compressible. However, if an asymmetric perturbation of the equilibrium is present, even though the shear Alfvén and cusp modes will be nondegenerate, the spatial behavior of v_r will, in general, be of the form $(r-r_o)^{i|\nu|}$, rather than logarithmic. In any case, for either the tokamak or screw pinch plasma, the spatial wavestructure is non-square-integrable because the velocity

perturbations within the flux surface vary as $1/(\phi-\phi_o)$ or else as $(\phi-\phi_o)^{i|\nu|-1}$, according to whether the radial perturbations are logarithmic or of the form $(\phi-\phi_o)^{i|\nu|}$, respectively.

The conclusions obtained thus far in this chapter will be compared in the next section with the results obtained in earlier studies. In Chapter 6, the spatial wavestructure of the continuum modes present in a low beta tokamak will be analyzed and also proven to be non-square-integrable.

Section 5. Comparison with Earlier Studies

The spatial structure of the continuum modes in the vicinity of the resonant surfaces has been previously examined for toroidal equilibria by several authors, including Pao[20], Tataronis, Talmadge, and Shohet[18], Tataronis and Salat[22], and Hameiri[35]. Different generalizations of the method of Frobenius were developed in each of these earlier studies. In this chapter, Eqs. (5.7)-(5.13) are based on the formalism developed by Tataronis and Salat[22] in their treatment of general toroidal equilibria. However, the formulation of the solvability conditions as an eigenvalue problem for the parameter, ν, in Eq. (5.14)-(5.17) of this thesis, clarifies the solution method given for ν in the work by Tataronis and Salat. In addition, in this chapter, the solvability conditions were evaluated and shown to always yield non-square-integrable singularities in the wavestructure of a continuum mode about a resonant surface in an axisymmetric toroidal equilibrium.

A somewhat different generalized method of Frobenius was employed by Pao[20] in his study of the continuum modes in an axisymmetric tokamak. He wrote the linearized ideal MHD equations in a form similar to that used in Eq. (5.1)-(5.2) but chose orthogonal flux coordinates (ϕ,χ,θ) and considered the set of four coupled first order differential equations which are equivalent to Eq. (5.2). By writing

$$v^1 \equiv \xi = \lambda(r)[\xi_o(\chi)+r\xi_1(\chi) + \cdots]$$

$$i\omega p^* \equiv \tau = \lambda(r)[\tau_o(\chi)+r\tau_1(\xi) + \cdots]$$

$$b_j = \lambda'(r)[b_{jo}(\chi)+rb_{j1}(\chi) + \cdots] \qquad j = \theta,\chi$$

$$u_j = \lambda'(r)[u_{jo}(\chi)+ru_{j1}(\chi) + \cdots] \qquad j = \theta,\chi$$

where $r \equiv \phi - \phi_o$, b_j and u_j are the j^{th} components of the perturbed magnetic field and fluid velocity respectively, λ' is the derivative of λ with respect to ϕ, and by assuming

$$\lambda/\lambda' \to 0 \quad \text{as} \quad r \to 0$$

he derived a solvability condition on the system of equations which determines the function $\lambda(r)$. This condition (Eq. 43 in Pao's paper), may be written in the form

$$[r\lambda'(r)]' = -\frac{A}{G}\lambda'$$

where A and G are integrals over the poloidal angle χ of products of equilibrium quantities and the functions ξ_i, τ_i, b_{ji}, and u_{ji} for $i = 0,1$. In this expression, A is analogous in form to the elements of $\vec{\vec{K}}$ and G to the elements of $\vec{\vec{S}}$, defined in Eq. (5.15)-(5.16) of this chapter. Using Pao's equations and stated assumptions, the integral G may be shown to be real and, for cases of experimental interest, nonnegative. The integral A may be shown to be equal to

$$A = \oint \frac{d\ell_p}{B_p}\,[\tau_o\xi_o^* - \xi_o\tau_o^*] \quad ,$$

instead of zero, as Pao stated. Clearly, A is either zero or purely imaginary. It is definitely equal to zero only if the equilibrium is up-down symmetric. Hence, though Pao concludes in his work that the singularities associated with the continuum modes are logarithmic, in fact they may be of the form

$$\lambda \sim c_1 r^{-i\alpha} + c_2$$

where $i\alpha$ is the value of the integral A. This is consistent with the analysis completed in this chapter.

Hameiri[35] also has considered the nature of the singularities associated with the continuum modes in a compressible plasma in a general, nonsymmetric, static equilibrium. Though he states that it can be shown that the singularities are always logarithmic, he does

not provide the details of his analysis. His statement, however, appears to be contradicted by the analysis presented in this chapter for an axisymmetric but otherwise nonsymmetric compressible tokamak plasma. It is possible that his result is valid only if the equilibrium lacks any sort of symmetry.

In summary, the result that the wavestructure associated with a mode in the continuum of an axisymmetric but otherwise arbitrary toroidal equilibrium is always non-square-integrable is consistent with earlier analyses. In addition, because the modes have been shown to be non-square-integrable, it may be possible to heat the plasma via the resonant excitation of these modes, in accordance with the ideal MHD model of shear Alfvén wave heating.

FIGURE 5.1 Solutions for the Floquet Parameter in the Complex Plane

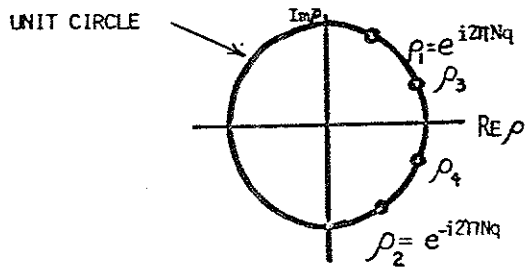

FIGURE 5.1 a

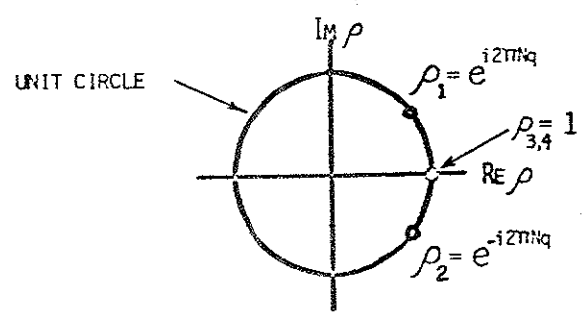

FIGURE 5.1 b

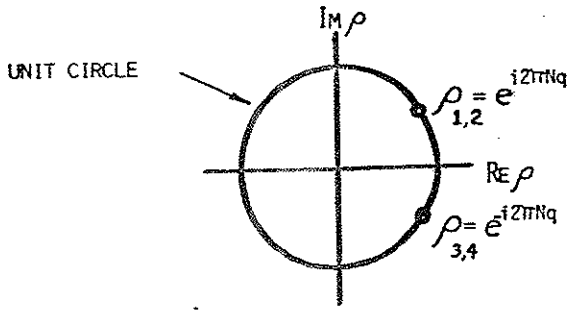

FIGURE 5.1 c

CHAPTER 6

THE LOW BETA MODEL

The equations which describe the continua in an axisymmetric toroidal geometry are a complicated set of two coupled second order differential equations which involve only the operator $\vec{B} \cdot \nabla$ and which are solved in each flux surface[18,20,22]. These equations have been solved, in the preceding chapters for tokamak geometry analytically in the large aspect ratio limit and numerically for a finite aspect ratio, noncircular cross section tokamak. The purpose of this chapter is to demonstrate how this complicated set of equations, together with the equations which determine the linearized plasma velocity and magnetic field, may be considerably simplified in the limit of very low plasma beta. In particular, if the equilibrium pressure, P_o, is set equal to zero in the ideal MHD equations, then the cusp continuum, which describes modes with $\omega^2 \sim \gamma P_o \omega_A^2$, where ω_A^2 is the square of shear Alfvén continuum frequency, is reduced to a single point $\omega = 0$ in the spectrum and hence is effectively eliminated from the set of equations which describes the continua. A single second order differential equation, which describes the shear Alfvén continuum, survives in the limit $P_o = 0$. A second advantage of this model is the matrix elements, which appear in Eqs. (2.17)-(2.19) in the analysis of the radial structure of the waves about the resonant surfaces, also simplify considerably. Since the current experiments are expected

to operate with very low beta plasmas, this single equation may provide a good representation of the continuum modes for these experiments.

In this chapter, the equations which determine the shear Alfvén continuum and the associated magnetic field and fluid velocity perturbations in the limit of zero plasma beta are derived, and the solutions for the wave structure about the resonant surfaces are discussed. The linearized equations of ideal MHD theory, Eqs. (2.3) to (2.5), form the basis for the analysis. The equilibrium pressure, P_o, and magnetic field, $\vec{B}$, are related through the MHD equilibrium condition,

$$\nabla P_o = \vec{J} \times \vec{B} \tag{6.1}$$

where $\vec{J}$, the equilibrium current density, is related to $\vec{B}$ by $\nabla \times \vec{B} = \mu_o \vec{J}$. When the plasma beta, $\beta \equiv P_o/(|\vec{B}|^2/2\mu_o)$, is sufficiently small, Eqs. (2.3)-(2.5), (6.1) may be simplified by neglecting effects due to the equilibrium pressure, P_o. In the limit $P_o = 0$, the equation of state, Eq. (2.5), reduces to

$$p = 0 \tag{6.2}$$

and, hence, the total perturbed pressure, p^*, becomes simply

$$p^* = \vec{B} \cdot \vec{b}/\mu_o. \tag{6.3}$$

The MHD equilibrium condition reduces to

$$\vec{J} \times \vec{B} = 0 \tag{6.4}$$

so the equilibrium current is everywhere parallel to the equilibrium magnetic field. Using this feature and the dot product of $\vec{B}$ with the momentum balance equation, Eq. (2.3), it is easy to show that the perturbed fluid velocity is everywhere perpendicular to the equilibrium magnetic field,

$$\vec{v} \cdot \vec{B} = 0 \quad . \tag{6.5}$$

Similarly, from the dot product of $\vec{B}$ with the Maxwell equation, Eq. (2.4), a relationship between p^* and $\vec{v}$, which will be used further on, can be derived,

$$i\omega\mu_o p^* = - \nabla \cdot (|\vec{B}|^2 \vec{v}), \tag{6.6}$$

where $|\vec{B}|$ is the magnitude of the equilibrium magnetic field. This condition relates the divergence of the perturbed velocity to the total perturbed pressure and essentially replaces information lost when P_o was set equal to zero in Eq. (2.5).

The equilibria considered here consist of closed, simply nested flux surfaces in an axisymmetric, toroidal configuration with both poloidal and toroidal magnetic fields. For coordinates, a

convenient choice is orthogonal flux coordinates, (ϕ, χ, ϕ) where ϕ is the poloidal flux divided by 2π, ϕ is the toroidal angle which varies uniformly from 0 to 2π in one circuit about the major axis of symmetry, and χ is a poloidal angle which varies from 0 to 2π in one circuit about the minor axis of symmetry. The angle χ is chosen so ϕ, χ, ϕ form a right-handed orthogonal coordinate system. (See Appendix A.) In this system, the Jacobian, j_o is given by

$$\frac{\partial \ell n j_o}{\partial \phi} = -2\frac{\partial}{\partial \phi} \ell n\, B_P - \left(\frac{B_T}{B_P}\right)^2 \frac{\partial \ell n f}{\partial \phi} - \frac{1}{B_P{}^2}\, \mu_o \frac{\partial P_o}{\partial \phi} \quad , \tag{6.7}$$

where the last term involving P_o is negligible in the limit $P_o = 0$. The gradient operator is given by

$$\nabla = \nabla\phi \frac{\partial}{\partial \phi} + \nabla\chi \frac{\partial}{\partial \chi} + \nabla\phi \frac{\partial}{\partial \phi} = RB_P\hat{\phi} \frac{\partial}{\partial \ell_p} + \hat{\chi} \frac{\partial}{\partial \ell_p} + \frac{\hat{\phi}}{R} \frac{\partial}{\partial \phi} \quad , \tag{6.8}$$

where R is the distance to a point on the flux surface as measured radially from the major axis of symmetry, $d\ell_p = j_o B_P\, d\chi$ is a differential length element along the poloidal magnetic field, and $\hat{\phi}$, $\hat{\chi}$, $\hat{\phi}$ are unit vectors. Derivatives of the unit vectors with respect to the coordinates, which are needed to complete the derivation outlined in this section, are listed in Appendix C. Because $\vec{B} \cdot \nabla\phi = 0$, the operator $\vec{B} \cdot \nabla$, which appears in Eqs. (2.3) and (2.4), involves only derivatives within a flux surface,

$$\vec{B} \cdot \nabla = B_P \frac{\partial}{\partial \ell_p} + \frac{B_T}{R} \frac{\partial}{\partial \phi} \quad . \tag{6.9}$$

Axisymmetry of the system leads to the fact that the quantity $f \equiv RB_T$ is a flux function. In the following paragraphs, it will be convenient to use the variables $v^1 \equiv RB_P v_\phi$, which is the ϕ-contravariant component of $\vec{v}$, and $v_3 \equiv Rv_\phi$, which is the ϕ-covariant component of $\vec{v}$, instead of v_ϕ and v_ϕ.

To proceed further with the reduction of Eqs. (2.3)-(2.5), (6.1) to a system in which the continuum is clearly evident, it is particularly advantageous to use Eqs. (6.5) and (6.3), which resulted from the zero beta approximation, in place of the $\hat{\chi}$ components of the Maxwell equation, Eq. (2.4), and the momentum balance equation, Eq. (2.3). In this way, a differential equation for v_χ is replaced by

$$v_\chi = \frac{-B_T}{RB_P} v_3 \tag{6.10}$$

and a differential equation for b_χ is replaced by

$$b_\chi = (\mu_o p^* - B_T b_\phi)/B_P \quad . \tag{6.11}$$

It is at this point, when the zero beta aproximations are used to

eliminate two derivatives from the set of equations, thereby reducing the order of the system by two, that a mode, namely, the cusp continuum, is excluded from consideration. This is not surprising, since, according to the theory for equilibria which are inhomogeneous in only one direction, the cusp continuum is given by $\omega_c^2 = \frac{\gamma\beta}{1+\gamma\beta}\,\omega_A^2$, where ω_A is the shear Alfvén continuum. Clearly, when, $P_o = 0$, i.e., $\beta = 0$, the cusp continuum collapses to a single point, $\omega_c^2 = 0$.

The ϕ component of the Maxwell equation can be written as

$$i\omega R B_P b_\phi = \vec{B} \cdot \nabla v^1 \quad , \tag{6.12}$$

yielding b_ϕ in terms of v^1. The only derivatives of perturbed quantities with respect to ϕ that appear in the system are in the ϕ component of the momentum balance equation, Eq. (2.3),

$$\mu_o \frac{\partial p^*}{\partial \psi} = \frac{-i}{\omega}\left[\mu_o \rho \omega^2 v^1/(R^2 B_P{}^2) + \vec{B} \cdot \nabla \frac{1}{R^2 B_P{}^2}\, \vec{B} \cdot \nabla v^1\right] \tag{6.13}$$

$$+ 2\,\frac{\partial \ell n(j_o B_P)}{\partial \psi}\,\mu_o p^* + 2\,B_T b_\phi \frac{\partial \ell n(\mu_o B_P/R)}{\partial \psi}$$

and, from Eq. (6.6),

$$\frac{\partial v^1}{\partial \psi} = -v^1 \frac{\partial \ell n(j_o |B|^2)}{\partial \psi} - \frac{i\omega\mu_o p^*}{|B|^2}$$

$$+ \frac{B_P}{|B|^2}\frac{\partial}{\partial \ell p}\left(v_3 \frac{f|B|^2}{R^2 B_P{}^2}\right) - \frac{1}{R^2}\frac{\partial v_3}{\partial \phi} \quad . \tag{6.14}$$

To arrive at Eqs. (6.13) and (6.14), Eqs. (6.10)-(6.12) and the following expression for $\nabla \cdot \vec{v}$ in this coordinate system have been used:

$$\nabla \cdot \vec{v} = \frac{1}{j_o}\frac{\partial}{\partial \psi}(j_o v^1) + B_P \frac{\partial}{\partial \ell p}\left(\frac{v_\chi}{B_P}\right) + \frac{1}{R}\frac{\partial v_\phi}{\partial \phi} \quad . \tag{6.15}$$

An equation for b_ϕ in terms of v^1, p^*, and v_3 is obtained from the ϕ component of the Maxwell equation, where, again, use is made of Eqs. (6.6), (6.10)-(6.12),

$$R b_\phi = \frac{-i}{\omega}\frac{R^2 B_P{}^2}{|B|^2}\,\vec{B}\cdot\nabla\left(\frac{|B|^2}{R^2 B_P{}^2}\, v_3\right) + \frac{i}{\omega}\, v^1 \frac{\partial}{\partial \psi}\, \ell n\left(\frac{B_T f}{R|B|^2}\right) + \frac{\mu_o f}{|B|^2}\, p^* \quad . \tag{6.16}$$

Finally, an equation for v_3 in terms of v^1, p^* is found from the ϕ-component of Eq. (2.3), with v_χ, b_ϕ, b_ϕ eliminated in favor of v_3, v^1, p^* as before:

$$\mu_o \rho \omega^2 v_3 + \vec{B} \cdot \nabla\left\{\frac{R^2 B_p^2}{B^2} B \cdot \nabla\left[\frac{|B|^2}{R^2 B_p^2} v_3\right]\right\} = i\omega\mu_o \frac{\partial p^*}{\partial \phi}$$

$$-i\omega f \vec{B} \cdot \nabla\left(\frac{\mu_o p^*}{|B|^2}\right) - f \vec{B} \cdot \nabla\left[\frac{\partial \ln(R^2|B|^2)}{\partial \phi} v^1\right] \quad . \tag{6.17}$$

This equation contains the shear Alfvén continuum and may be written conveniently as

$$L\, v_3 = g(p^*, v^1) \tag{6.18}$$

where the definitions of L and g follow readily by comparison with Eq. (6.17).

The structure of the system of equations in the zero beta limit has now been established. The fundamental variables are v^1 and p^*. Their spatial structure is obtained for a given ω by specifying appropriate boundary values for them on the magnetic axis and then integrating Eqs. (6.13) and (6.14) across flux surfaces. To perform the integration over ϕ one must first eliminate b_ϕ and v_3 in favor of v^1, p^* by inverting Eq. (6.18) to obtain

$$v_3 = L^{-1} g(p^*, v^1) \quad , \tag{6.19}$$

where L^{-1} is the inverse operator of L, and then solving Eq. (6.16) for $b_\phi = b_\phi(v^1, p^*)$. Once v^1, p^* have been obtained on a flux

surface, the remaining perturbed quantities, v_3, b_ϕ, v_χ b_χ, and b_ϕ are obtained from Eqs. (6.19), (6.16), (6.10), (6.11), and (6.12) respectively. However, if a nontrivial solution exists for the equation,

$$Lv_3 \equiv \mu_o \rho \omega^2 v_3 + \vec{B} \cdot \nabla\left\{\frac{R^2 B_p^2}{|B|^2} \vec{B} \cdot \nabla\left[\frac{|B|^2}{R^2 B_p^2} v_3\right]\right\} = 0 \quad , \tag{6.20}$$

subject to the boundary condition that v_3 be periodic in χ and ϕ, then the inverse operator, L^{-1}, does not exist. The set of frequencies which satisfies Eq. (6.20) defines the shear Alfvén continuum for the system. Though the values are discrete on any particular flux surface, they sweep out a continuous range of frequencies as the flux surface is varied. For frequencies which lie in the continuum, the system of equations may be solved everywhere only if the inhomogeneous term in Eq. (6.18) satisfies certain conditions analogous to the ones discussed in Chapter 5 for the more general, finite pressure system.

The system of reduced MHD equations which have been derived in this section may be readily written in a form analogous to that developed in Chapter 2 for the more general, finite pressure system, Eqs. (2.6)-(2.8), (2.11), and (2.16)-(2.19). In particular, Eqs. (6.14) and (6.13), which involve the derivative across flux surfaces and are analogous to Eq. (2.6) may be written as

$$\frac{\partial v^1}{\partial \phi} = \alpha_{11}(\phi,\chi)v^1 + \alpha_{12}(\phi,\chi)p^* + c_1(\phi,\chi)v_3 \qquad (6.21)$$

and

$$\frac{\partial p^*}{\partial \phi} = \alpha_{21}(\phi,\chi)v^1 + \alpha_{22}(\phi,\chi)p^* + c_2(\phi,\chi)v_3 \qquad (6.22)$$

respectively. Equation (6.12) for b_ϕ is identical to Eq. (2.8). The inhomogeneous set of coupled differential equations which relate the perturbed velocities and magnetic fields in the surface to those perpendicular to the flux surface, Eq. (2.7), is replaced by a single, second order inhomogeneous differential equation, Eq. (6.18), for v_3

$$Lv_3 = g(p^*,v^1) \quad , \qquad (6.18)$$

two algebraic equations for v_ϕ and b_ϕ, Eqs. (6.10) and (6.11), and a differential equation for b_ϕ, Eq. (6.16), which is trivially solved once v_3, v^1, and p^* are known on the flux surface. The corresponding set of coupled differential equations which comprise the eigenvalue problem for the continua in a finite pressure axisymmetric tokamak, Eqs. (2.11) and (2.27), are now replaced by a single second order differential equation for the shear Alfvén continuum, Eq. (6.20),.

$$L(\omega^2,\phi)v_3 = 0 \qquad (6.20)$$

This equation is of the Sturm-Liouville form and is self-adjoint with periodic boundary conditions. It may therefore be readily analyzed using the techniques developed in the previous chapters for the more general system. In particular, a large aspect ratio expansion solution of the continuum equation in the zero pressure limit yields the same solutions for the shear Alfvén continuum as were derived for the finite pressure case in Chapter 3.

The behavior of the mode structure about the resonant surface, ϕ_o, where Eq. (6.20), is satisfied, may be studied by assuming series expansions in $(\phi-\phi_o)$, analogous to Eq. (2.12). Expanding v^1, p^*, v_3 in this manner and using Eqs. (6.18), (6.21), (6.22) yields

$$L_o v_o^1 = 0 \qquad (6.23)$$

$$L_o v_1^1 = \frac{G}{\nu}\frac{\partial}{\partial\phi}v_o^1 + Hv_o^1 \quad , \qquad (6.24)$$

where G and H, which depend only on the equilibrium magnetic field and contain no derivatives, are given by

$$G = \frac{|B|^2}{R^2 B_p^2} f\left[B_p \frac{\partial}{\partial \ell_p}\frac{\partial \ell_n R^2|B|^2}{\partial\psi}\right]\frac{\partial}{\partial\phi} \equiv G(\ell_p)\frac{\partial}{\partial\phi} \qquad (6.25)$$

and

$$H = \frac{\partial}{\partial\phi}\left[\mu_o\rho\omega^2+\vec{B}\cdot\nabla\frac{R^2B_p^2}{|B|^2}\vec{B}\cdot\nabla\frac{|B|^2}{R^2B_p^2}\right] \quad . \tag{6.26}$$

Because of Eq. (6.23), Eq. (6.24) is singular and hence may be solved if and only if

$$\langle u_i|\frac{G}{\nu}\frac{\partial}{\partial\phi} + H|v_o^1\rangle = 0 \quad i = 1, \ldots n \quad , \tag{6.27}$$

where the u_i are the independent basis functions of the null space of L_o. In the zero pressure limit, in the complex representation, $i = 1$, and the basis function is given as

$$u = a(\chi)e^{in\phi} \tag{6.28}$$

where n is the toroidal mode number. This form follows from the discussions in Chapter 4. The parameter, ν, is thus given by

$$\nu = -\frac{\langle u|G(\hat{x}p)\frac{\partial}{\partial\phi}|u\rangle}{\langle u|H|u\rangle} \tag{6.29}$$

Again, as in Chapter 4, the denominator can be shown to be purely real, while numerator is given by

$$in\oint d\chi|u|^2G(\chi) \quad . \tag{6.30}$$

In an up-down symmetric equilibrium, the function G is odd and, clearly, $|u|^2$ is even, so $\nu = 0$ and the logarithmic singularity is recovered. This is not surprising since the logarithmic singularity is present in an up-down symmetric, finite pressure, compressible tokamak plasma and the main effect of taking the zero pressure limit is to eliminate any possible coupling between a shear Alfvén wave and a cusp wave. If the equilibrium is not up-down symmetric, the parameter ν is, in general, imaginary, so again, non-square-integrable spatial singularities are present in the solutions.

In conclusion, a system of reduced MHD equations which may be useful for predicting the dynamics of low beta axisymmetric toroidal configurations has been derived by formally allowing the plasma pressure to approach zero. In this limit, the order of the system of linearized partial differential equations is lowered, and the shear Alfvén continuum is specified by a single second-order ordinary differential equation involving the operator, $\vec{B}\cdot\nabla$. Moreover, the cusp continuum is reduced to a single point, $\omega_c^2 = 0$. The continuum equation obtained in the zero beta limit is formally equivalent to Eq. (40) in Ref. 12 when γ is set equal to zero in that equation. In Ref. 13 , the equations which describe the continuous spectra of a cylindrical equilibrium with axial and azimuthal symmetry have been derived by an approach similar to the

one used in this chapter. In either the present study or Ref. 13, differential equations are replaced by algebraic expressions, thereby reducing the order of the system. However, in the case of the cylinder, the algebraic expressions are the result of a Fourier analysis in the directions of symmetry, while in the toroidal case, the algebraic expressions are the result of allowing the plasma beta to formally approach zero. Because of the additional degree of symmetry afforded by the circular cross section of the cylindrical equilibrium, the differential equation, which corresponds to the shear Alfvén continuum equation in a low beta tokamak, is replaced by an algebraic dispersion relation. The shear Alfvén continuum of a low beta cylindrical equilibrium with an arbitrary noncircular cross section may be studied using Eq. (6.20) of this chapter by setting R equal to a constant and identifying ϕ with an axial coordinate z. A similar equation has been derived for the special case of a low-pressure cylindrical plasma column with an elliptical cross section by Dewar et al.[42]

CHAPTER 7

CONCLUSIONS

Shear Alfvén waves in an axisymmetric toroidal equilibrium, such as a tokamak or compact torus, have been examined in this thesis, within the framework of the linearized ideal MHD equations, to determine their suitability for use in the low frequency RF heating scheme suggested first by Tataronis and Grossmann[3,4]. The shear Alfvén and cusp continua of ideal MHD theory have been analyzed in an axisymmetric equilibrium using the formalism of Tataronis, et al.[18]. By solving a set of coupled differential equations for the eigenvalues on each flux surface, the continuous spectra are obtained as a function of radius for particular mode numbers. Analytic expressions for the continua have been obtained by solving the eigenvalue equations in an expansion scheme in powers of small inverse aspect ratio $\varepsilon \equiv a/R_o$.

To lowest order in ε, the continua are given by the appropriate generalization of their counterparts in a periodic, infinitely long screw pinch. In the screw pinch, the shear Alfvén continuum is given by Eq. (2.2), while in the tokamak, to the lowest order, the corresponding expression is

$$\omega_A^2 = \frac{(MB^2+NB^3)^2}{\mu_o \rho} \tag{7.1}$$

Correspondence between the two is established when $k \to \frac{N}{R_o}$ and in the limit $\epsilon = 0$, $B^2 \to B_p/r$ and $B^3 \to B_{To}/R_o$. Similar expressions may be written for the cusp continuum. The eigenvalues for each spectra on a flux surface are at least two-fold degenerate with multiple degeneracy possible on rational surfaces.

First order corrections due to toroidicity have been calculated explicitly and are given in Eqs. (3.27)-(3.28) for the Alfvén continuum. The effect of toroidicity is to couple different poloidal modes on and very close to rational surfaces for which the unperturbed modes are degenerate. If perturbations due to noncircularity of the flux surfaces had been treated explicitly, then additional coupling of modes on the rational surfaces would have been found. The criterion which determines whether modes M,N and $M' = M \pm 1$,N will couple on the rational surface, q_r, is given in Eqs. (3.13), (3.19). The effect of the perturbation is important over a range in radius corresponding to range in q of $q_r - \frac{\Delta}{2} < q < q_r + \frac{\Delta}{2}$, where Δ is given in Eqs. (3.22)-(3.23). The behavior of the spectrum in the vicinity of q_r is displayed in Fig. 3.1 and specified analytically in Eqs. (3.22)-(3.24). Further away from the surface, q_r, the corrections to the spectra are second order in ϵ, so Eq. (3.9) is a good approximation to the spectra. These results apply to the coupling of different Alfvén modes or to the coupling of different cusp modes.

An analogy may be drawn between the effect on the continuous spectra by the periodic variations in the equilibrium field structure due to toroidicity and/or non-circularity, and the effect on the energy spectrum of an electron in a one-dimensional crystal by the periodic modulation of the potential by the ions in the crystal lattice[41]. The allowed wave numbers, k, for an electron in a crystal consisting of N identical cells of length a, are

$$k = \frac{2\pi}{L} n = \frac{2\pi}{Na} n \qquad n = 0, \pm 1, \pm 2, \cdots \qquad . \qquad (7.2)$$

Gaps appear in the electron energy spectrum for wave numbers equal to $\pm p \frac{\pi}{a}$, where p is an integer. For these wave numbers, the travelling electron waves Bragg reflect off the crystal planes and interfere to form standing waves localized either in the potential well between the ions or at the top of the potential well near the ions. In the case of the shear Alfvén continuum, gaps appear in the spectrum on rational surfaces when the periodic variation of the equilibrium fields induces coupling of the modes M,N to M±p,N. Since the field lines are closed on rational surfaces, an integral number of wavelengths must be equal to the total length of the field line. On a rational surface, $q_r = i/j$, where i and j are integers, and the total poloidal angle covered by a field line before it closes on itself once is equal to $2\pi j$. This closure of the field line implies that the mode numbers M,N must satisfy

$$M+Nq_r = \frac{n}{j} \quad \text{for} \quad n = 0, \pm 1, \cdots \quad . \tag{7.3}$$

Note that the combination M+Nq is analogous to the electron wavevector, k, while the total length of the field line and the number of poloidal turns it completes are analogous to the crystal length, L, consisting of N cells of length a. When the equilibrium fields vary as cos pθ, coupling occurs on and near the surface, q_r, between modes which satisfy the condition $M+Nq_r = \pm p/2$. The modes M, N and M±p,N have the same frequency, $\omega^2 \sim \lambda \sim (M+Nq_r)^2$, but equal and opposite poloidal phases,

$$\exp[i(M+Nq_r)\theta] = \exp[i(M\pm p+Nq_r)\theta] \quad . \tag{7.4}$$

Hence, these modes interfere to form standing waves which are localized either in regions of increased field strength, on the inside of the torus for p = 1, or in regions of decreased field strength, on the outside of the torus for p = 1. Similar analogies have been noted by others[42-45] in related problems involving periodic perturbations of the equilibrium fields. The presence of gaps in the spectrum could have important implications in heating fusion plasmas with shear Alfvén waves. Depending on the structure of the unperturbed continua near the location of coupling, the formation of the gaps may either recove the possibility of heating with particular frequency and mode numbers, or else may result in

the existence of two resonant surfaces separated from each other by distances on the order of 1 cm.

Though this effect of gap formation in the continuous spectra has been derived explicitly in a small inverse aspect ratio expansion scheme, the results of the numerical solutions for the shear Alfvén continuum in the tokamak region of the Tokapole II device are in qualitative agreement with the predictions of the analytic model. However, additional effects due to finite aspect ratio, noncircular flux surfaces and regions of high shear near the separatrices are evident in the numerical results in Fig. 4.4-4.24. Strong mode coupling induced by extreme shear and noncircularity of the plasma cross section in the region near the separatrix alters the magnitude and behavior of the continuum eigenvalues in the region, as can be seen by comparing Fig. 4.4 to Fig. 4.5 and Fig. 4.14 to Fig. 4.15. For flux surfaces which are located closer to the separatrix than to the magnetic axis, i.e., for $r \gtrsim 4$ cm, additional shifts in the magnitudes of the eigenvalues occur due to finite aspect ratio and noncircularity of the plasma cross sections. Because of these differences, the numerical solutions provide a more quantitatively accurate framework for correlation of theory with experiment than do the screw pinch model solutions.

The ideal MHD theory of plasma heating via the resonant excitation of shear Alfvén continuum waves is based on the idea that these waves are characterized by non-square-integrable spatial singularities at particular locations in the plasma. As a result of

these singularities, the physical amplitude of excited waves grows in time, leading to a growth of the total plasma energy[4,14] at the resonant surface. In Chapter 5, the spatial structure of the ideal MHD shear Alfvén wave in an axisymmetric but otherwise arbitrary tokamak equilibrium has been shown to be always non-square-integrable, thereby lending support to the ideal MHD model for low frequency RF heating of tokamaks. The spatial structure was analyzed using a generalized method of Frobenius in which the perturbed velocity and magnetic field components, along with the equilibrium quantities, were expanded in power series about $\phi=\phi_o$, where ϕ_o is the resonant surface at which $\omega^2 = \omega_A^2(\phi_o)$. The expansions, given in Eq. (5.7), involve an arbitrary exponent, ν, which is determined by requiring that the resulting hierarchy of equations, Eqs. (5.8)-(5.10), be self-consistent and completely solvable to all orders in $(\phi-\phi_o)$. These consistency conditions are described in Eqs. (5.13)-(5.20).

For an axisymmetric tokamak, the exponent, ν, was shown to be either purely imaginary or zero. If the equilibrium is up-down symmetric with respect to reflection about the midplane, then ν has been shown to be equal to zero, using parity arguments. When $\nu = 0$, it is necessary to assume alternate expansions for the perturbed fields which involve the $\ln(\phi-\phi_o)$, as given explicitly in Eqs. (5.23)-(5.24). This result is independent of the plasma pressure or compressibility; it depends solely on the reflection symmetry about the midplane exhibited by the equilibrium. In

contrast, previous analyses for a cylindrically symmetric screw pinch[22] have indicated that the singularities of the perturbed radial velocity are logarithmic if the plasma is compressible but are of the form $(\phi-\phi_o)^{i|\nu|}$ if the plasma is incompressible. The change in the spatial character of the singularities in the screw pinch as the plasma is changed from compressible to incompressible is due directly to the degeneracy which occurs between the shear Alfvén and cusp continua in this limit. In the tokamak, however, even in the incompressible limit, the shear Alfvén and cusp continua remain distinct due to toroidal effects and the spatial singularities of the perturbed radial velocity remain logarithmic as long as the equilibrium is up-down symmetric. When the equilibrium is allowed to possess some degree of up-down asymmetry, the integrals which determine ν must be evaluated for the particular equilibrium in question. In general, ν will be purely imaginary for a reflection asymmetric equilibrium, though it may be possible to find particular examples in which ν is once again equal to zero.

These results generalize and are consistent with the earlier conclusions of Pao[20]. In addition, these results may be used to infer that if an up-down symmetric poloidal variation is applied to a cylindrical screw pinch then the singularities in the perturbed radial velocity will be logarithmic for both a compressible and incompressible plasma. This follows because the poloidal variations will remove the degeneracy between the shear Alfvén and cusp continua which occurs for an incompressible plasma when the

equilibrium is cylindrically symmetric. If an up-down asymmetric poloidal variation is applied to the cylindrical screw pinch, then the spatial structure will, in general, be altered from logarithmic to $(\phi-\phi_o)^{i|v|}$, as in the tokamak.

Numerical solutions for the shear Alfvén continuum of a typical Tokapole II equilibrium are being used in the interpretation of the shear Alfvén wave excitation and heating studies currently underway on the device[11]. Though a detailed comparison between the experimentally observed and theoretically determined resonance locations has not yet been completed due to the difficult nature of the experimental procedures, there exists a good qualitative agreement between the observations and the predictions of the model. In particular, resonances in the perturbed poloidal magnetic field have been observed at the locations where the frequency of the external oscillator is approximately equal to the local shear Alfvén continuum frequency, as determined numerically. A more detailed comparison will be possible when a complete set of measurements of the resonance locations and poloidal and toroidal mode numbers is obtained.

Currently, all of the ongoing shear Alfvén wave heating experiments on tokamaks are conducted with very low beta plasmas. With this in mind, a reduced set of ideal MHD equations has been derived in Chapter 6 by taking the limit where the equilibrium pressure, P_o, is set equal to zero. In this limit, the cusp continuum, which scales as $P_o\omega_A^2$, is reduced to a single point,

$\omega_c = 0$, in the spectrum. As a result, a single second order ordinary differential equation, Eq. (6.20), which describes the shear Alfvén continuum replaces the two coupled second order differential equations, Eq. (2.11), which describe the shear Alfvén and cusp continua in a finite pressure plasma. An added benefit is that the coefficient matrices, $\vec{A}$, $\vec{C}$, and $\vec{K}$ in Eqs. (2.6)-(2.7), also simplify considerably to the forms given in Eqs. (6.13)-(6.17). This reduced set of equations, valid in the limit $P_o \to 0$, is easier to analyze than the more general set, valid for finite P_o plasmas. It should also provide a good representation of the shear Alfvén waves in the current experiments.

A number of important questions concerning the effectiveness of shear Alfvén wave resonance heating schemes in toroidal devices remain to be answered. One such question concerns the effects of nonaxisymmetry on the existence of continuum modes and on the possibility of heating a plasma via the resonant excitation of these modes. Since all tokamaks are nonaxisymmetric to some extent, due to the finite size of the toroidal field coils, etc., and since advanced concepts devices may include the use of helical windings which destroy axisymmetry, the theory of the shear Alfvén wave heating in a nonaxisymmetric toroidal device must be developed more fully before the effectiveness of this particular heating for these devices can be established.

A calculation of the heating rates (or, alternately, of the plasma impedances) in toroidal devices is needed to evaluate the efficiency of this heating scheme in comparison to that of other methods such as electron cyclotron resonance heating, ion cyclotron resonance heating, lower hybrid wave heating, etc. In the context of the ideal MHD model, this can be accomplished for an axisymmetric toroidal geometry by using the results contained in this thesis and by generalizing the methods used by Tataronis and Grossman in their analysis for a cylindrical screw pinch plasma[4,14]. However, kinetic effects are likely to be significant in the regions about the resonant surfaces, where scale lengths of the perturbations approach the size of the ion Larmor radius. Early studies by Hasegawa and Chen[46,47] indicate that the inclusion of kinetic effects allows for a more complete description of the thermalizations mechanisms involved in the process. More recently, Ross, Chen, and Mahajan[48] have included numerous kinetic effects in their estimations of plasma impedances in a cylindrical plasma equilibrium. A fully kinetic treatment of the shear Alfvén wave in an axisymmetric toroidal geometry has yet to be developed.

A final, more encompassing, question concerns the effects that the excitation of these modes might have on the energy confinement times of the discharge. Measurements of the confinement times during these experiments have yielded mixed results, with some experiments indicating a degradation of confinement[5] and others indicating an enhancement of confinement[6,7]. The bulk of the

theoretical analyses thus far has been based on linearized ideal MHD and kinetic theories. An example of how a linear kinetic interaction between a shear Alfvén wave and another mode of the plasma can lead to a degradation of confinement has been studied by Tsang, Sigmar and Whitson[49]. However, it is possible that nonlinear interaction of the shear Alfvén wave with other waves in the system may cause more serious problems with the stability of the discharge or may lead to very poor heating efficiencies. More effort is needed in all these areas before the advantages and disadvantages of a heating scheme based on the resonant excitation of the shear Alfvén wave may be accurately assessed.

APPENDIX A

COORDINATE SYSTEMS FOR AXISYMMETRIC TOKAMAK EQUILIBRIA

Three coordinate systems which are particularly well-suited for problems dealing with axisymmetric tokamak equilibria will be described in this appendix. The methods presented are informal, with an emphasis on the construction of such coordinate systems. After a brief review of general non-orthogonal curvilinear coordinates, a sequence of two coordinate transformations will be applied to the familiar orthogonal flux coordinate system. The first transformation will result in a system in which the magnetic lines of force appear as straight lines in two of the coordinates. The second transformation will yield one possible set of Hamada coordinates for a tokamak-like equilibrium.

INTRODUCTION

The study of physical processes in various magnetic field configurations is often simplified if the governing equations are expressed in coordinates which are, in some sense, the "natural" choice for the configuration. One common set for axisymmetric toroidal systems is orthogonal flux coordinates[53,58,61]. In this system, the poloidal magnetic field flux, ϕ, contained between the magnetic axis and a particular magnetic surface, serves as a radial-type coordinate. Poloidal and toroidal angles on each surface are then denoted typically by χ and ϕ, respectively, and can

range from 0 to 1 or 2π, depending on one's preference. The angle θ is identical to the usual azimuthal angle θ of cylindrical coordinates if the z-axis of the cylindrical system lies along the major axis of symmetry of the torus. The angle χ is chosen so that ϕ, χ, ϕ form a right-handed orthogonal coordinate system.

A second option is a modified version of orthogonal flux coordinates in which the magnetic lines of force appear as straight lines in the two coordinates which span a magnetic surface[58]. In these coordinates the magnetic field is given simply in the form

$$\vec{B} = \nabla\alpha \times \nabla\beta \quad , \tag{A.1}$$

where β can be a function of ϕ, χ and ϕ.

An Hamada coordinate system[50-57] is a viable, albeit somewhat complicated, option in which both the magnetic field and current density lines of force appear as straight lines. The Jacobian for these coordinates is then either a constant or else a function only of ϕ, depending on the particular choice for these coordinates. Equations written in Hamada coordinates often have the most simple appearance, since all geometrical effects are contained in the metric tensor elements, g_{ij}, instead of appearing explicitly in the equations.

Section A.1 Review of Non-orthogonal Curvilinear Coordinate Systems

Though non-orthogonal curvilinear coordinate systems are significantly more complicated than cartesian coordinate systems, there are some similarities between the two[53,59-62]. Let u^1, u^2, u^3 be the three coordinates in the non-orthogonal system corresponding to x, y, z in cartesian coordinates. The basis vectors for cartesian coordinates are given in terms of the differential position vector,

$$d\vec{R} = \frac{\partial \vec{R}}{\partial x}dx + \frac{\partial \vec{R}}{\partial y}dy + \frac{\partial \vec{R}}{\partial z}dz = \mathbf{i}dx + \mathbf{j}dy + \mathbf{k}dz \quad . \tag{A.1.1}$$

Similarly, the basis vectors $\hat{e}_i$ for the general system may also be defined in terms of $d\vec{R}$:

$$d\vec{R} = \frac{\partial \vec{R}}{\partial u^i}du^i = \hat{e}_i du^i \quad . \tag{A.1.2}$$

In cartesian coordinates, the basis vectors are also unit vectors. In the general system, this is not the case. Although the basis vectors in a cartesian system are mutually orthogonal, in a general system they generally are not. However, a set of vectors, called the reciprocal basis vectors, may be constructed in the general system to be orthogonal to the set of basis vectors. Reciprocal

basis vectors are denoted by $\hat{e}^i$ and are defined through the following relation:

$$\hat{e}^i \cdot \hat{e}_j = \delta^i{}_j \quad . \tag{A.1.3}$$

This relation fixes the normalization of the reciprocal basis vectors and requires $\hat{e}^i$ to be perpendicular to the plane formed by $\hat{e}_j$ and $\hat{e}_k$. It follows that the reciprocal basis vectors may be expressed in terms of the basis vectors as

$$\hat{e}^i = \frac{1}{j}\hat{e}_j \times \hat{e}_k \quad \text{and/or} \quad \hat{e}_i = j\hat{e}^j \times \hat{e}^k \tag{A.1.4}$$

where j is the Jacobian for the system,

$$j = \hat{e}_i \cdot (\hat{e}_j \times \hat{e}_k) \tag{A.1.5}$$

and is the appropriate normalization factor, in accordance with Eq. (A.1.3).

Recall that the Jacobian is the volume contained by the parallelepiped formed by the set of basis vectors. It is thus the appropriate factor to appear in the differential volume element of the system:

$$d\tau = d\vec{R}_1 \cdot (d\vec{R}_2 \times d\vec{R}_3) = j du^1 du^2 du^3 \quad . \tag{A.1.6}$$

An expression which may be used to define the gradient of a scalar quantity, Φ, in a general curvilinear system,

$$d\Phi = d\vec{R} \cdot \nabla\Phi \qquad \text{(A.1.7)}$$

may also be used to derive a more useful expression for the reciprocal basis vectors, $\hat{e}^i$. If, as the scalar Φ, one of the general coordinates, u^i is taken, then,

$$du^j = d\vec{R} \cdot \nabla u^j = (\hat{e}_i du^i) \cdot \nabla u^j \quad . \qquad \text{(A.1.8)}$$

Hence,

$$\hat{e}_i \cdot \nabla u^j = \delta^j_i \qquad \text{(A.1.9)}$$

so ∇u^j may be identified with the j^{th} reciprocal basis vector:

$$\hat{e}^j = \nabla u^j \quad . \qquad \text{(A.1.10)}$$

Geometrical effects arising from the nature of the coordinate system are contained neatly in the elements of the metric tensor, g_{ij}, for the system. The metric tensor elements may be introduced by considering the square of a differential arc length in the system:

$$ds^2 = d\vec{R}_1 \cdot d\vec{R}_2 = (\hat{e}_i du^i) \cdot (\hat{e}_j du^j) = g_{ij} du^i du^j \quad . \qquad \text{(A.1.11)}$$

From its definition, the metric tensor is obviously symmetric. For cartesian coordinates, the metric tensor is the identity tensor. The determinant of the metric tensor, denoted by g, may be shown to be equal to the square of the Jacobian for the system. This follows by combining the definition of the Jacobian, Eq. (A.1.5), with the definition of the basis vectors, Eq. (A.1.2), and a bit of algebra:

$$g = \det(g_{ij}) = j^2 \quad . \qquad \text{(A.1.12)}$$

A reciprocal metric tensor, g^{ij}, may be similarly defined from the reciprocal basis vectors, $\hat{e}^i$:

$$g^{ij} = \hat{e}^i \cdot \hat{e}^j \quad . \qquad \text{(A.1.13)}$$

By inserting Eq. (A.1.4) into the definition for g^{ij}, the elements of the reciprocal metric tensor may be expressed in terms of the elements for the metric tensor;

$$g^{ij} = \frac{1}{g} G_{ij} \quad , \qquad \text{(A.1.14)}$$

where G_{ij} is the i^{th}, j^{th} minor of g_{ij}.

Vectors in the general coordinate system may be written in terms of either the basis or reciprocal basis vectors:

$$\vec{A} = A^i \hat{e}_i = A_i \hat{e}^i \quad . \qquad \text{(A.1.15)}$$

The contravariant components of $\vec{A}$, namely A^i, are found by taking the dot product of $\vec{A}$ with reciprocal basis vector, $\hat{e}^i$. Similarly, the covariant components of $\vec{A}$, i.e., A_i, are found by taking the dot product of $\vec{A}$ with the basis vector, $\hat{e}_i$. The contravariant components are related to the covariant components via the metric tensor or reciprocal metric tensor:

$$A_i = g_{ij}A^j \quad , \quad A^i = g^{ij}A_j \quad . \tag{A.1.16}$$

These relations are easily verified by taking the dot product of Eq. (A.1.15) with $\hat{e}_j$ and $\hat{e}^j$, respectively.

A variety of vector operations and identities may be written in covariant and/or contravariant components in a general system. This review of general non-orthogonal curvilinear coordinate systems ends with a partial summary of them:

$$\vec{A} \cdot \vec{B} = A^iB_i = A_iB^i \tag{A.1.17}$$

$$[\vec{A}\times\vec{B}]^i = \frac{1}{\sqrt{g}}\,\varepsilon^{ijk}A_jB_k \tag{A.1.18}$$

$$[\vec{A}\times\vec{B}]^i = \sqrt{g}\,\varepsilon_{ijk}A^jB^k \tag{A.1.19}$$

$$(\nabla\Phi)_i = \frac{\partial\Phi}{\partial u^i} \tag{A.1.20}$$

$$\nabla \cdot \vec{A} = \frac{1}{\sqrt{g}}\,\frac{\partial}{\partial u^i}(\sqrt{g}A^i) \tag{A.1.21}$$

$$(\nabla\times\vec{A})^i = \frac{1}{\sqrt{g}}\,\varepsilon^{ijk}\,\frac{\partial}{\partial u^j}A_k \tag{A.1.22}$$

$$\nabla^2\Phi = \frac{1}{\sqrt{g}}\,\frac{\partial}{\partial u^i}\,(\sqrt{g}\,g^{ij}\,\frac{\partial\Phi}{\partial u^j}) \tag{A.1.23}$$

$$[\nabla\times(\vec{A}\times\vec{B})]^i = A^i\nabla\cdot\vec{B} + \vec{B}\cdot\nabla A^i - B^i\nabla\cdot\vec{A} - \vec{A}\cdot\nabla B^i \tag{A.1.24}$$

$$\vec{A}\cdot\nabla = A^i\,\frac{\partial}{\partial u^i} \quad . \tag{A.1.25}$$

Recall that $\sqrt{g} = j$ = Jacobian, and ε^{ijk} is the permutation tensor.

Section A.2 Orthogonal Flux Coordinates

An axisymmetric tokamak equilibrium is most frequently described by orthogonal flux coordinates ϕ, χ, ϕ[53,58,61] (see Figure A.1). Each magnetic surface is labelled by a radial-like coordinate, ϕ, which is generally taken to be proportional to the total poloidal magnetic flux, ϕ_{pol}, contained between it and the magnetic axis:

$$\phi = \frac{1}{2\pi}\phi_{pol} = \frac{1}{2\pi}\int_{S_{pol}} d\vec{s} \cdot \vec{B} = \frac{1}{(2\pi)^2}\int d\tau \vec{B} \cdot \nabla\chi \qquad (A.2.1)$$

On each flux surface, the distance around toroidally is measured by the angle ϕ, which varies uniformly from 0 to 2π in one complete circuit around the major axis. The toroidal angle, ϕ, corresponds to the angle coordinate θ of cylindrical coordinates, R, θ, z, if the z axis lies along the major axis of symmetry. All equilibrium quantities are independent of the angle ϕ.

A poloidal angle, χ, is chosen on each flux surface such that ϕ, χ, ϕ form a right-handed orthogonal system. In one complete circuit around the minor axis, χ varies from 0 to 2π.

We will assume that the equilibrium has been found by solving the Grad-Shafranov equation in cylindrical coordinates. By considering the amount of poloidal flux, $d\phi_p$, contained between two flux surfaces separated by a differential amount, dr, we find that

$$\nabla\phi = e^1 = RB_p\hat{\phi} \qquad (A.2.2)$$

In cylindrical coordinates it is well known that

$$\nabla\phi = \frac{\hat{\phi}}{R} = e^3 \quad . \qquad (A.2.3)$$

From the relations in Sections A.1, one can show that the Jacobian for this system, j_o, is given by

$$j_o^{-1} = \nabla\phi \cdot (\nabla\chi\times\nabla\phi) \quad . \qquad (A.2.4)$$

This may be solved for $\nabla\chi$, the remaining reciprocal basis vector:

$$e^2 = \nabla\chi = (j_o B_p)^{-1}\hat{\chi} \quad . \qquad (A.2.5)$$

All metric tensor elements may now be readily computed.

In principle, the Jacobian may be found by solving the following differential equation, derived from the equilibrium condition:

$$\frac{\partial}{\partial\phi}\ln j_o = -2\frac{\partial}{\partial\phi}\ln B_p - 2\beta_p\frac{\partial}{\partial\phi}\ln(\mu_o p) - \left(\frac{B_T}{B_p}\right)^2\frac{\partial}{\partial\phi}\ln f \quad . \qquad (A.2.6)$$

where $f = RB_T$ and $\beta_p = p/(B_p^2/2\mu_o)$. In practice it is almost never

necessary to solve explicitly for j_o, since most operations involving $d\chi$ and j_o may be treated in terms of $d\mathcal{L}p$ instead:

$$d\mathcal{L}_p = j_o B_p d\chi \quad . \tag{A.2.7}$$

There are four more flux surface quantities, in addition to the poloidal flux and pressure, which will be of use in the following sections. The toroidal magnetic flux, ϕ_T, is one quantity:

$$\phi_T = \int_{S_{tor}} d\vec{s} \cdot \vec{B} = \left(\frac{1}{2\pi}\right) \int d\tau \vec{B} \cdot \nabla u^3 \quad . \tag{A.2.8}$$

The two current fluxes, toroidal current flux, I_T, and poloidal current flux, I_p, are each flux surface functions:

$$I_p(\phi) = \int_{S_{pol}} d\vec{s} \cdot \vec{J} = \frac{1}{2\pi} \int d\tau \vec{J} \cdot \nabla u^2 \quad , \tag{A.2.9}$$

$$I_T(\phi) = \int_{S_{tor}} d\vec{s} \cdot \vec{J} = \frac{1}{2\pi} \int d\tau \vec{J} \cdot \nabla u^3 \quad , \tag{A.2.10}$$

where u^2, u^3 are poloidal and toroidal angles. A final flux quantity is the volume, V, contained within a flux surface:

$$V = \int d\tau \quad . \tag{A.2.11}$$

In this system, the contravariant components of B and J are not flux surface quantities:

$$B^1 = \vec{B} \cdot \nabla\phi = 0 \qquad B^2 = \vec{B} \cdot \nabla\psi = \frac{1}{j_o} \qquad B^3 = \vec{B} \cdot \nabla\phi = \frac{B_T}{R} \quad , \tag{A.2.12}$$

$$J^1 = 0 \qquad J^2 = \frac{J_p}{j_o B_p} \qquad J^3 = \frac{J_T}{R} \quad . \tag{A.2.13}$$

Using the contravariant components of $\vec{B}$, the magnetic field may be conveniently written as

$$B = -\nabla\psi \times \nabla\phi + f\nabla\phi \quad . \tag{A.2.14}$$

Recall that in a true flux coordinate system, the magnetic field is given in the form

$$\vec{B} = \nabla\alpha \times \nabla\beta \quad . \tag{A.2.15}$$

Comparison of (A.2.15) with (A.2.14) indicates that orthogonal flux coordinates are not true flux coordinates. The coordinate transformation of the next section will result in a true flux coordinate system.

Section A.3 True Flux Coordinates

Consider the form for the magnetic field given in Eq. (A.2.15). If the function, α, is taken to be the coordinate, ϕ, then field lines on a ϕ = constant surface are described by β = constant. The function, β, corresponds to a particular combination of the χ, ϕ coordinates. This particular combination may be used to define two new angle coordinates on a surface in which the magnetic field lines appear straight.

From the divergence of $\vec{B}$ in orthogonal flux coordinates,

$$\nabla \cdot \vec{B} = \frac{\partial}{\partial \chi}(j_o B^2) + \frac{\partial}{\partial \phi}(j_o B^3) \quad ,$$

if

$$j_o B^2 = -\frac{\partial \beta}{\partial \phi} \quad \text{and} \quad j_o B^3 = \frac{\partial \beta}{\partial \chi} \quad , \tag{A.3.2}$$

then, since B^2 and B^3 are periodic in χ, ϕ, the general form for β is

$$\beta = A(\phi)\chi + C(\phi)\phi + \lambda(\phi,\chi,\phi) \quad , \tag{A.3.3}$$

where λ is an arbitrary periodic function of χ, ϕ. The functions $A(\phi)$ and $C(\phi)$ may be determined from equilibrium quantities.

Consider the amount of flux, $d\phi_T$, contained between flux surfaces ϕ and $\phi + d\phi$:

$$d\phi_{tor} = \frac{1}{2\pi}\int_{\phi}^{\phi+d\phi} d\phi \int_o^{2\pi} d\chi \int_o^{2\pi} d\phi\, j_o B^3 = d\phi_{pol}\, A(\phi) \quad . \tag{A.3.4}$$

The coefficient, $A(\phi)$, is seen to be equal to the safety factor, $q(\phi) = \frac{d\phi_T}{d\phi_p}$. In a similar way, by considering the amount of poloidal flux contained between the surfaces ϕ and $\phi+d\phi$, the coefficient, $C(\phi)$, is found to be equal to -1:

$$d\phi_{pol} = \frac{1}{2\pi}\int_{\phi}^{\phi+d\phi} d\phi \int_o^{2\pi} d\chi \int_o^{2\pi} d\phi\, j_o B^2 = -d\phi_{pol}\, C(\phi) \quad . \tag{A.3.5}$$

Thus far, the function β has been determined up to an arbitrary periodic function of χ, ϕ and ϕ. The arbitrary function will now be absorbed into the coordinate, χ, resulting in a new poloidal coordinate, θ_1. Let

$$\theta_1 = \chi + \frac{\Lambda}{q} \quad \text{and} \quad \phi_1 = \phi \quad . \tag{A.3.6}$$

In the new coordinates θ_1, ϕ_1, the function β becomes

$$\beta = q\theta_1 - \phi \tag{A.3.7}$$

and the magnetic field is seen to be given by Eq. (A.2.15). Note

that the field lines on a given flux surface are given by β = constant and appear as straight lines in the coordinates θ_1, ϕ.

Some more understanding of the new coordinates is gained by calculating the function Λ. To accomplish this, combine Eq. (A.2.12) with Eq. (A.3.2):

$$j_o B^2 = 1 = -\frac{\partial\theta}{\partial\phi} \quad \text{and} \quad J_0 B^3 = j_o \frac{B_T}{R} = \frac{\partial\theta}{\partial\chi} \quad . \tag{A.3.8}$$

By now inserting Eq. (A.3.3) for β, we find

$$\frac{\partial\Lambda}{\partial\phi} = 0 \quad \text{and} \quad \frac{\partial\Lambda}{\partial\chi} = j_o \frac{B_T}{R} - q \quad . \tag{A.3.9}$$

Integration of these results then yields

$$\Lambda(\phi,\chi,\phi) = f\int^{\ell} \frac{d\ell_p}{B_p}\frac{1}{R^2} - q\chi \quad . \tag{A.3.10}$$

Returning now to Eq. (A.3.6), the new poloidal angle, ϕ_1, is given by

$$\theta_1 = \frac{f}{q}\int \frac{d\ell_p}{B_p}\frac{1}{R^2} \tag{A.3.11}$$

and is related to the safety factor, q, since an alternate definition of q is

$$q = \frac{f}{2\pi}\oint \frac{d\ell_p}{B_p}\frac{1}{R^2} \quad . \tag{A.3.12}$$

In transforming from χ to θ_1, the poloidal coordinate has been modified in such a way that the magnetic field lines in a flux surface appear as straight lines in the two coordinates which span the surface. Similar modification of ϕ could have been performed instead.

Surprisingly, the Jacobian, j_1, for this new system is more readily calculated than the Jacobian for the previous system. From an expression analagous to Eq. (A.2.4),

$$j_1^{-1} = \nabla\phi \cdot (\nabla\theta\times\nabla\phi) \tag{A.3.13}$$

combined with Eq. (3.11), the new Jacobian is found to be:

$$j_1 = R^2 q/f \quad . \tag{A.3.14}$$

Since two of the coordinates have been unchanged by the transformation, namely, ϕ and ϕ, the reciprocal basis vectors corresponding to them also remained unchanged. Hence, we have:

$$e^1 = \nabla\phi = RB_p\phi \tag{A.3.15}$$

$$\epsilon^3 = \nabla\phi = \frac{1}{R}\hat{\phi} \quad . \tag{A.3.16}$$

The remaining reciprocal basis vector may be found by taking the gradient of Eq. (A.3.11):

$$\nabla\theta_1 = \frac{\partial\theta_1}{\partial\psi}\nabla\psi + \frac{\partial\theta_1}{\partial\chi}\nabla\chi \quad . \tag{A.3.17}$$

By taking appropriate dot products, the reciprocal metric tensor elements may be formed:

$$g^{11} = (RB_p)^2 \qquad g^{12} = \left(\frac{\partial\theta_1}{\partial\psi}\right)(RB_p)^2 \qquad g^{13} = 0 \tag{A.3.18}$$

$$g^{22} = \left(\frac{\partial\theta_1}{\partial\psi}\right)^2(RB_p)^2 + \left(\frac{\partial\theta_1}{\partial\ell_p}\right)^2 \qquad g^{23} = 0 \qquad g^{33} = \frac{1}{R^2} \quad .$$

Two derivatives of θ_1 must next be calculated. One of them follows easily from Eq. (A.3.11):

$$\frac{\partial\theta_1}{\partial\ell_p} = \frac{f}{q}\frac{1}{B_p}\frac{1}{R^2} \quad . \tag{A.3.19}$$

The other one, it seems, must be evaluated numerically, using the following complicated expression

$$\frac{\partial\theta_1}{\partial\psi} = \frac{\partial}{\partial\psi}\left(\frac{f}{q}\right)\int\frac{d\ell_p}{B_p}\frac{1}{R^2} + \frac{f}{q}\int\frac{d\ell_p}{B_p}\frac{1}{R^2}\left[\frac{\partial\ell n j_o}{\partial\psi} - 2\frac{\partial\ell nR}{\partial\psi}\right] \tag{A.3.20}$$

where, from section A.2,

$$\frac{\partial\ell n j_o}{\partial\psi} = -2\frac{\partial\ell nB_p}{\partial\psi} - 2\beta_p\frac{\partial}{\partial\psi}\ell n(\mu_o p) - \left(\frac{B_T}{B_p}\right)^2\frac{\partial\ell nf}{\partial\psi} \quad . \tag{A.3.21}$$

Though one could now calculate the metric tensor elements using the preceding expressions for g^{ij} and the analogue of Eq. (A.1.14), it is instructive to take an alternate approach. From section A.2 and the results thus far of this section, the magnetic field B and current J are given by:

$$\vec{B} = \frac{1}{j_o}f_2 + \frac{B_T}{R}f_3 = \frac{1}{j_1}\hat{e}_2 + \frac{q}{j_1}\hat{e}_3 \quad , \tag{A.3.22}$$

$$\vec{J} = \left(\frac{J_p}{j_o B_p}\right)f_2 + \frac{J_T}{R}f_3 = \frac{f}{q}\frac{J_p}{B_p}\frac{1}{R^2}\hat{e}_2 + \frac{J_T}{R}\hat{e}_3 \quad , \tag{A.3.23}$$

where f_2 and f_3 are basis vectors in the orthogonal flux coordinate system. These two equations may be solved for $\hat{e}_2$ and $\hat{e}_3$ in terms of known quantities:

$$\hat{e} = \frac{q}{J_o}\frac{R}{B_T} f_2 \quad , \tag{A.3.24}$$

$$\hat{e}_3 = f_3 \quad . \tag{A.3.25}$$

Note that the third basis vector has remained unchanged by the coordinate transformation. However, the second basis vector is now multiplied by a factor depending on ϕ and χ. These two equations now yield three metric tensor elements, using Eq. (A.1.14):

$$g_{22} = \frac{q^2 R^2 B_p^2}{B_T^2} \qquad g_{23} = 0 \qquad g_{33} = R^2 \quad . \tag{A.3.26}$$

The three remaining metric tensor elements are now most readily calculated from the reciprocal metric tensor elements:

$$g_{11} = \frac{q^2}{B_T^2} g^{22} \qquad g_{12} = \frac{-q^2}{B_T^2} g^{12} \qquad g_{13} = 0 \quad . \tag{A.3.27}$$

In closing, note that in transforming to true flux coordinates, we have transformed from an orthogonal coordinate system to one which has two basis vectors which are not orthogonal, i.e.,

$$\hat{e}_1 \cdot \hat{e}_2 \neq 0 \quad \text{but} \quad \hat{e}_1 \cdot \hat{e}_3 = \hat{e}_2 \cdot \hat{e}_3 = 0 \quad . \tag{A.3.28}$$

The transformation to Hamada coordinates, in the next section, will leave us with a completely non-orthogonal coordinate system.

Section A.4 Hamada Coordinates

There is still a bit of arbitrariness remaining in the transformation described in the preceding section. In particular, if G is an arbitrary function of ϕ which is also periodic in θ_1, ϕ then the coordinate transformation

$$\theta = \theta_1 + G(\phi, \theta_1, \phi)$$

$$\xi = \phi + qG(\phi, \theta_1, \phi) \tag{A.4.1}$$

results in a new coordinate system in which the magnetic field lines still appear as straight lines in the two coordinates which span the flux surface. This is verified by inserting Eq. (A.4.1) into the following expression for B from section A.3 (see Eqs. A.2.14 and A.3.7)

$$\vec{B} = \nabla\phi \times \nabla(q\theta_1 - \phi) = \nabla\phi \times \nabla(q\theta - \xi) \quad . \tag{A.4.2}$$

The arbitrariness represented by the function G may be utilized to transform to a system in which the Jacobian is, at most, a function of ϕ and the current lines, in addition to the magnetic field lines, appear as straight lines in the two coordinates, θ, ξ,

which span a flux surface. This is accomplished by using the definition of the Jacobian in terms of reciprocal basis vectors:

$$\frac{1}{J} = \nabla\phi \cdot (\nabla\theta \times \nabla\xi) = \frac{1}{J_1} + \vec{B} \cdot \nabla G \quad . \tag{A.4.3}$$

Solving for G, we find that it is determined by a magnetic differential equation:

$$\vec{B} \cdot \nabla G = \frac{1}{J} - \frac{1}{J_1} \quad . \tag{A.4.4}$$

Newcomb[63] and others[51] have derived two necessary and sufficient conditions that equations of the form:

$$\vec{B} \cdot \nabla = S \tag{A.4.5}$$

have solutions for G which are single-valued. The two conditions are

$$\int_{\phi}^{\phi+d\phi} S\, d\tau = 0 \tag{A.4.6}$$

and

$$\oint \frac{S\, d\ell}{B} = 0 \quad . \tag{A.4.7}$$

The first condition is trivially satisfied for Eq. (A.4.4)

$$\int \left[\frac{1}{J} - \frac{1}{J^1}\right] d\tau = \int_{\phi}^{\phi+d\phi} \frac{1}{J} J\, d\phi d\theta d\xi - \int_{\phi}^{\phi+d\phi} \frac{1}{J_1} d\phi d\theta_1 d\phi = 0 \quad . \tag{A.4.8}$$

Application of the second condition results in the specification of the Jacobian for this Hamada coordinate system, as shown in the following:

$$\oint \frac{d\ell}{B} \frac{1}{J} = \frac{1}{J} \oint \frac{d\ell}{B} \frac{1}{J_1} = \oint \frac{d\phi}{\vec{B}\cdot\nabla\phi} \frac{1}{J_1} = \frac{1}{q} \oint d\phi = \frac{2\pi N}{q} \quad . \tag{A.4.9}$$

Note that we are considering a field line which closes on itself after N circuits around toroidally. From the requirement of current closure, which is known to be satisfied in axisymmetric toroidal devices with a longitudinal current and $p' = \frac{dp}{d\phi}$, recall[51] that

$$\frac{1}{N} \oint \frac{d\ell}{B} = \frac{dV}{d\phi_T} \quad . \tag{A.4.10}$$

Upon combining Eqs. (A.4.9) and (A.4.10), the Jacobian is found to be

$$J = \frac{1}{2\pi} \frac{dV}{d\phi_p} = \frac{1}{(2\pi)^2} \frac{dV}{d\psi} \quad . \tag{A.4.11}$$

It is indeed a function only of ϕ, as was assumed in Eq. (A.4.9).

Since this construction depends on $p' \neq 0$, these coordinates may be constructed in any simply nested configuration, up to but not including the separatrix. Ideal MHD theory requires that $p' = 0$ on the separatrix. Presumably, these coordinates may be constructed in each such area of a device like Tokapole II.

The function G is found by solving the equation

$$\vec{B} \cdot \nabla G = \frac{1}{J_1} \frac{\partial G}{\partial \theta_1} + \frac{q}{J_1} \frac{\partial G}{\partial \phi} = 2\pi \frac{d\phi_{pol}}{dV} - \frac{f}{q} \frac{1}{R^2} \quad . \tag{A.4.12}$$

Because the right hand side is independent of ϕ and because G must be periodic in θ_1 and ϕ, then G can be a function only of ϕ and θ_1. Though Eq. (A.4.12) could now be integrated to find $G(\phi,\theta_1)$, it is more convenient to first recognize that $\theta_1 = \theta_1(\phi,\chi)$ and hence to find $G(\phi,\chi)$ from the following equation:

$$\vec{B} \cdot \nabla G(\phi,\chi) = B_p \frac{\partial}{\partial \ell_p} G(\phi,\ell_p) = 2\pi \frac{d\phi_{pol}}{dv} - \frac{f}{q} \frac{1}{R^2} \quad . \tag{A.4.13}$$

The resulting expression for G, using Eq. (A.3.11), is

$$G(\phi,\ell_p) = \frac{1}{J} \int \frac{d\ell_p}{B_p} - \theta_1 \quad . \tag{A.4.14}$$

Explicit definitions of the Hamada coordinates θ, ξ in terms of

orthogonal flux coordinates ϕ, χ, ϕ are readily obtained from Eqs. (A.4.1) and (A.4.14):

$$\theta = \frac{1}{J} \int \frac{d\ell_p}{B_p} \quad , \tag{A.4.15}$$

$$\xi = \phi + q\theta - f \int \frac{d\ell_p}{B_p} \frac{1}{R^2} \quad . \tag{A.4.16}$$

These expressions for θ and ξ will be used later on to calculate metric tensor elements.

Comparing Eq. (A.4.2) for $\vec{B}$ to Eq. (A.2.15), it is clear that Hamada coordinates are a variety of true flux coordinates. Next, we note that the contravariant components of $\vec{B}$ are now all flux surface quantities:

$$\vec{B} = 2\pi\left(0, \frac{d\phi_{pol}}{dV}, \frac{d\phi_{tor}}{dV}\right) \quad . \tag{4.17}$$

The current densities may now be shown to be similar in form to the magnetic field. In particular, the currents may be written in the form

$$\vec{J} = 2\pi \nabla\phi \times \nabla\left[\left(J\frac{dI_{tor}}{dV}\right)\theta - \left(J\frac{dI_{pol}}{dV}\right)\xi\right] \quad . \tag{A.4.18}$$

with contravariant components

$$\mathcal{J} = 2\pi(0, \frac{dI_{pol}}{dV}, \frac{dI_{tor}}{dV}) \quad . \tag{A.4.19}$$

To prove this, we will proceed by analogy with section A.3. First, from the fact that the current is divergenceless, we may define a function ω such that

$$\nabla \cdot \mathcal{J} = \frac{\partial}{\partial\theta}(j\mathcal{J}^2) + \frac{\partial}{\partial\xi}(j\mathcal{J}^3) = \frac{\partial}{\partial\theta}(-\frac{\partial\omega}{\partial\theta}) + \frac{\partial}{\partial\xi}(\frac{\partial\omega}{\partial\theta}) = 0 \tag{A.4.20}$$

where, in general,

$$\omega = a_1(\phi)\theta + b_1(\phi)\xi + \tilde{\omega}(\phi,\theta,\xi) \tag{A.4.21}$$

with $\tilde{\omega}$, a function of ϕ which is periodic in θ, ξ, to be determined consistently with the remainder of the coordinate system. Following the development of Eqs. (A.3.4) and (A.3.5), but using instead the toroidal and poloidal current fluxes, we find:

$$a_1(\phi) = \frac{dI_{tor}}{d\Phi_{pol}} \tag{A.4.22}$$

$$b_1(\phi) = -\frac{dI_{pol}}{d\Phi_{pol}} \quad . \tag{A.4.23}$$

Hence, J^2 and J^3 are given by

$$J^2 = 2\pi \frac{dI_{pol}}{dV} - \frac{\partial\tilde{\omega}}{\partial\xi}\frac{d\phi_{pol}}{dV} \tag{A.24}$$

$$J^3 = 2\pi \frac{dI_{tor}}{dV} + \frac{\partial\tilde{\omega}}{\partial\theta}\frac{d\phi_{pol}}{dV} \quad . \tag{A.4.25}$$

The equilibrium condition on ∇p demands that

$$\mu_o p'(\phi) = j(J^2B^3 - J^3B^2) = 2\pi[q\frac{dI_{pol}}{dV} - \frac{dI_{tor}}{dV}] - \vec{B} \cdot \nabla\tilde{\omega} \quad . \tag{A.4.26}$$

The function ω is thus determined by another magnetic differential equation. From the conditions on its solution we find that

$$\mu_o p'(\phi) = 2\pi q(\frac{dI_{pol}}{dV} - \frac{dI_{tor}}{dV}) \tag{A.4.27}$$

and hence

$$\vec{B} \cdot \nabla\tilde{\omega} = 0 \quad . \tag{A.4.28}$$

It is therefore permissible and convenient to choose $\tilde{\omega} = 0$, thus completing the proof.

Using the methods developed in the previous sections, the basis and reciprocal basis vectors and metric and reciprocal metric tensor elements can be readily expressed in terms of the orthogonal flux coordinate system, ϕ, χ, ϕ. Reciprocal basis vectors are obtained from Eqs. (A.2.2), (A.4.15), (A.4.16):

$$e^1 = \nabla\phi = RB_p\hat{\phi} \tag{A.4.29}$$

$$e^2 = RB_p \frac{\partial\theta}{\partial\psi}\hat{\phi} + \frac{1}{jB_p}\hat{\chi} \tag{A.4.30}$$

$$e^3 = RB_p \frac{\partial\xi}{\partial\phi}\hat{\phi} + \frac{1}{R^2 jB_p}(R^2 q - jf)\hat{\chi} + \frac{1}{R}\hat{\phi} \quad , \tag{A.4.31}$$

where $\hat{\phi}$, $\hat{\chi}$, and $\hat{\phi}$ are the appropriate unit vectors. Derivatives with respect to ϕ must be evaluated numerically. Appropriate dot products among Eqs. (A.4.19)- (A.4.31) then yield all the reciprocal metric tensor elements. Elements of the metric tensor may be formed using the reciprocal metric tensor and the analogue of Eq. (A.1.14):

$$g_{ij} = gG^{ij} \quad . \tag{A.4.32}$$

Alternately, they may be found by first constructing the basis vectors from the reciprocal basis vectors and then applying Eq. (A.1.11). The basis vectors are listed below:

$$e_1 = \frac{1}{RB_p}\hat{\phi} - \left(\frac{\partial\theta}{\partial\psi} jB_p\right)\hat{\chi} + \left[\frac{jf}{R}\frac{\partial\theta}{\partial\psi}\left(R^2\left\langle\frac{1}{R^2}\right\rangle - 1\right) - R\frac{\partial\xi}{\partial\phi}\right]\hat{\phi} \tag{A.4.33}$$

$$\hat{\chi} = jB_p\hat{\chi} + \frac{jf}{R}\left(1 - R^2\left\langle\frac{1}{R^2}\right\rangle\right)\hat{\phi} \tag{A.4.34}$$

$$e_3 = R\hat{\phi} \tag{A.4.35}$$

$$\left\langle\frac{1}{R^2}\right\rangle \equiv \frac{q}{fj} = \frac{\oint \frac{d\ell_p}{B_p}\frac{1}{R^2}}{\oint \frac{d\ell_p}{B_p}} \quad . \tag{A.4.36}$$

Finally, by taking the dot product of the magnetic field with Eq. (A.4.35), it is easy to see that the resulting covariant component of the magnetic field, B_3, is also a flux surface quantity:

$$B_3 = \vec{B} \cdot e_3 = RB_T\hat{\phi} = F(\phi)\hat{\phi} \quad . \tag{A.4.37}$$

permeability, and γ is the ratio of specific heats. After much algebra, the preceding set of equations may be written as follows, using general flux coordinates (u^1,u^2,u^3), such that $\vec{B}\cdot\nabla u^1=0$, covariant and contravariant tensor notation, and assuming a time dependence of $e^{i\omega t}$:

$$\frac{\partial \vec{X}}{\partial \phi} = \ddot{A}\cdot\vec{X} + \ddot{C}\cdot\vec{Y} \tag{B.5}$$

$$\ddot{\chi}\cdot\vec{Y} = \ddot{K}\cdot\vec{X} \tag{B.6}$$

$$i\omega b^1 = Dv^1 \tag{B.7}$$

In Eqs.(B.5)-(B.7), the operator D is defined as

$$D = \vec{B}\cdot\nabla \quad , \tag{B.8}$$

the vectors $\vec{X}$ and $\vec{Y}$ are defined as

$$\vec{X} = \begin{bmatrix} v^1 \\ i\omega p^* \end{bmatrix} \tag{B.9}$$

and

$$\vec{Y} = \begin{bmatrix} v^2 \\ v^3 \\ i\omega b^2 \\ i\omega b^3 \end{bmatrix} \quad , \tag{B.10}$$

and the matrices $\ddot{A}$, $\ddot{C}$, $\ddot{\chi}$ and $\ddot{K}$ contain differential operators with respect to the coordinates (u^2,u^3) which span the flux surface. The components of these matrices are listed below. The notation chosen defines J as the Jacobian, β_M as the total plasma beta,

$$\beta_M \equiv \frac{p_o}{|B^2|/2\mu_o} \quad , \tag{B.11}$$

$B_\star$ as

$$B_\star = |B|^2(1+\tfrac{1}{2}\gamma\beta_M) \quad , \tag{B.12}$$

and uses the convention that a differential operator such as D, $\partial/\partial u^2$ or $\partial/\partial u^3$ acts on all terms to its right that it multiplies, unless it is enclosed in parentheses. Hence, for example, in Eq.(B.14) for A_{11}, the term DB_1 means

$$DB_1 = B_1 D + (DB_1) \tag{B.13}$$

while the term (DB_1) means that D acts only on B_1. In addition, when a differential operator acting on a variable is written in fractional form, for example,

$$\frac{\partial g_{km}}{\partial u^2}$$

then the differentiation is understood to apply only to the term in the numerator, i.e., g_{km} in the above example. The Einstein summation convention on repeated indices is also understood.

$$A_{11} = \frac{1}{B_*}\left[B^k B^m \frac{\partial g_{km}}{\partial u^1} - (DB_1) + B_1 D \right] - \frac{\partial \ell n J}{\partial u^1} \tag{B.14}$$

$$A_{12} = \frac{-1}{B_*} \tag{B.15}$$

$$A_{21} = \rho\omega^2 g_{11} + D g_{11} D + \left[\frac{\partial B_1}{\partial u^1} - B^j \frac{\partial g_{1j}}{\partial u^1}\right] D \tag{B.16}$$

$$A_{22} = 0$$

$$C_{11} = \frac{1}{B_*}\left[B^k B^m \frac{\partial g_{km}}{\partial u^2} - (DB_2) + B_2 D \right] - \frac{\partial \ell n J}{\partial u^2} - \frac{\partial}{\partial u^2} \tag{B.18}$$

$$C_{12} = \frac{B_3}{B_*} D - \frac{\partial}{\partial u^3} \tag{B.19}$$

$$C_{21} = \rho\omega^2 g_{12} \tag{B.20}$$

$$C_{22} = \rho\omega^2 g_{13} \tag{B.21}$$

$$\chi_{11} = D - \frac{\partial B^2}{\partial u^2} - \frac{B^2}{B_*}\left[B^k B^m \frac{\partial g_{km}}{\partial u^2} - (DB_2) + B_2 D \right] \tag{B.22}$$

$$\chi_{12} = \frac{-B^2 B_3}{B_*} D \tag{B.23}$$

$$\chi_{13} = -1 \tag{B.24}$$

$$\chi_{14} = 0 \tag{B.25}$$

$$\chi_{21} = -\frac{\partial B^3}{\partial u^2} - \frac{B^3}{B_*}\left[B^k B^m \frac{\partial g_{km}}{\partial u^2} - (DB_2) + B_2 D \right] \tag{B.26}$$

$$X_{22} = \left(1 - \frac{B^3 B_3}{B_*} \right) D \qquad \text{(B.27)}$$

$$X_{23} = 0 \qquad \text{(B.28)}$$

$$X_{24} = -1 \qquad \text{(B.29)}$$

$$X_{31} = \rho\omega^2 g_{22} \qquad \text{(B.30)}$$

$$X_{32} = \rho\omega^2 g_{23} \qquad \text{(B.31)}$$

$$X_{33} = Dg_{22} + \frac{\partial B_2}{\partial u^2} - B^j \frac{\partial g_{2j}}{\partial u^2} \qquad \text{(B.32)}$$

$$X_{34} = Dg_{23} - B^j \frac{\partial g_{3j}}{\partial u^1} \qquad \text{(B.33)}$$

$$X_{41} = \rho\omega^2 g_{32} \qquad \text{(B.34)}$$

$$X_{42} = \rho\omega^2 g_{33} \qquad \text{(B.35)}$$

$$X_{43} = Dg_{32} \qquad \text{(B.36)}$$

$$X_{44} = Dg_{33} \qquad \text{(B.37)}$$

$$K_{11} = \frac{\partial B^2}{\partial u^1} + \frac{B^2}{B_*}\left[B^k B^m \frac{\partial g_{km}}{\partial u^1} - (DB_1) + B_1 D \right] \qquad \text{(B.38)}$$

$$K_{12} = -\frac{B^2}{B_*} \qquad \text{(B.39)}$$

$$K_{21} = \frac{\partial B^3}{\partial u^1} + \frac{B^3}{B_*}\left[B^k B^m \frac{\partial g_{km}}{\partial u^1} - (DB_1) + B_1 D \right] \qquad \text{(B.40)}$$

$$K_{22} = -\frac{B^3}{B_*} \qquad \text{(B.41)}$$

$$K_{31} = -\rho\omega^2 g_{21} - Dg_{21}D - \left[\frac{\partial B_2}{\partial u^1} - B^j\frac{\partial g_{1j}}{\partial u^2}\right] \tag{B.42}$$

$$K_{32} = \frac{\partial}{\partial u^2} \tag{B.43}$$

$$K_{41} = -\rho\omega^2 g_{31} - Dg_{31}D - \frac{\partial B_3}{\partial u^1}D \tag{B.44}$$

$$K_{42} = \frac{\partial}{\partial u^3} \tag{B.45}$$

The preceding system of equations may be written in a form more suitable to both analytical and numerical computations if Hamada coordinates are chosen and if b^2 and b^3 are eliminated from the equations for the vectors $\vec{X}$ and $\vec{Y}$. After some tedious but straightforward algebra, the linearized ideal MHD equations for an axisymmetric toroidal equilibrium described by the Hamada coordinates given in Appendix A are given below. Equations (B.46) to (B.49) are to be solved for v^1, p^*, v^2 and v^3.

$$\frac{\partial \vec{X}}{\partial \Phi} = \ddot{A}\cdot\vec{X} + \ddot{C}\cdot\vec{Y} \tag{B.46}$$

$$\ddot{\chi}\cdot\vec{Y} = \ddot{K}\cdot\vec{X} \tag{B.47}$$

$$\vec{X} = \begin{bmatrix} v^1 \\ i\omega p^* \end{bmatrix} \tag{B.48}$$

$$\vec{Y} = \begin{bmatrix} v^2 \\ v^3 \end{bmatrix} \tag{B.49}$$

The remaining perturbed quantites, b^1, b^2, b^3, are given explicitly in terms of v^1, p^*, v^2, v^3 by Eqs.(B.50)-(B.52) below:

$$i\omega b^1 = Dv^1 \tag{B.50}$$

$$i\omega b^2 = \chi_{31}v^2 + \chi_{32}v^3 - K_{31}v^1 - K_{32}(i\omega p^*) \tag{B.51}$$

$$i\omega b^3 = \chi_{41}v^2 + \chi_{42}v^3 - K_{41}v^1 - K_{42}(i\omega p^*) \quad . \tag{B.52}$$

The matrices $\ddot{A}$, $\ddot{C}$, $\ddot{\chi}$ and $\ddot{K}$ are defined as follows in Eqs.(B.53) to (B.68):

$$\chi_{11} = \rho\omega^2 g_{22} + \vec{B}\cdot\nabla\left(g_{22} - \frac{B_2 B_2}{B_*}\right)\vec{B}\cdot\nabla \tag{B.53}$$

$$\chi_{12} = \rho\omega^2 g_{23} + \vec{B}\cdot\nabla\left(g_{23} - \frac{B_2 B_3}{B_*} \right)\vec{B}\cdot\nabla = \chi_{21} \qquad \text{(B.54)}$$

$$\chi_{22} = \rho\omega^2 g_{33} + \vec{B}\cdot\nabla\left(g_{33} - \frac{B_3 B_3}{B_*} \right)\vec{B}\cdot\nabla \quad . \qquad \text{(B.55)}$$

The matrix operator, $\overleftrightarrow{\chi}$, can be shown to be self-adjoint under the assumption of periodic boundary conditions by writing it in the form used in Eq.(2.34), i.e.,

$$\overleftrightarrow{\chi} = \lambda\overleftrightarrow{M}(\theta) + \frac{\partial}{\partial\theta}\left| \overleftrightarrow{K}(\theta) \frac{\partial}{\partial\theta} \right| \quad ,$$

and considering vectors $\vec{Y}$ and $\vec{Z}$ which satisfy the boundary conditions of Eq.(2.36)-(2.37). The vectors $\vec{Y}$ and $\vec{Z}$ may be written in the form

$$\vec{Y}(\theta,\beta) = \vec{y}(\theta)e^{iN\beta} \quad ,$$

with the vector $\vec{y}(\theta)$ satisfying the boundary condition

$$\vec{y}(\theta + 2\pi) = \vec{y}(\theta)e^{i2\pi Nq} \quad .$$

By considering the integral, I, where

$$I = \oint d\theta d\beta\, \vec{Y}(\theta,\beta)^* \cdot \left[\overleftrightarrow{\chi}(\theta)\cdot\vec{Z}(\theta,\beta) \right]$$

and integrating by parts twice, one finds

$$I = \oint d\theta d\beta \left[\overleftrightarrow{\chi}(\theta)\cdot\vec{Y}(\theta,\beta)^* \right]\cdot\vec{Z}(\theta,\beta) \quad .$$

Hence, $\overleftrightarrow{\chi} = \overleftrightarrow{\chi}^+$ so $\overleftrightarrow{\chi}$ is self-adjoint.

The remaining matrices, $\overleftrightarrow{K}$, $\overleftrightarrow{C}$, and $\overleftrightarrow{A}$ are listed below:

$$K_{11} = -\rho\omega^2 g_{12} - Dg_{12}D + \left[\frac{\partial B_1}{\partial u^2} - \frac{\partial B_2}{\partial u^1}\right]D + Dg_{2j}\frac{\partial B^j}{\partial u^1}$$

$$+ D\frac{B_2}{B_*}\left[B^k B^m \frac{\partial g_{km}}{\partial u^1} - (DB_1) \right] + D\frac{B_1 B_2}{B_*}D \qquad \text{(B.56)}$$

$$K_{12} = \frac{\partial}{\partial u^2} - D\frac{B_2}{B_*} \qquad \text{(B.57)}$$

$$K_{21} = -\rho\omega^2 g_{13} - Dg_{13}D - \frac{\partial B_2}{\partial u^1}D + Dg_{3j}\frac{\partial B^j}{\partial u^1}$$

$$+ D\frac{B_3}{B_*}\left[B^k{}_{B^m}\frac{\partial g_{km}}{\partial u^1} - (DB_1)\right] + D\frac{B_1B_3}{B_*}D \tag{B.58}$$

$$K_{22} = \frac{\partial}{\partial u^3} - D\frac{B_3}{B_*} \tag{B.59}$$

$$C_{11} = K_{12}^{+} \tag{B.60}$$

$$C_{12} = K_{22}^{+} \tag{B.61}$$

$$C_{21} = -K_{11}^{+} \tag{B.62}$$

$$C_{22} = -K_{21}^{+} \tag{B.63}$$

K_{ij}^{+} denotes the adjoint operator to K_{ij}.

$$A_{11} = \frac{1}{B_*}\left[B^k{}_{B^m}\frac{\partial g_{km}}{\partial u^1} - (DB_1)\right] + B_1D - \frac{\partial \ln J}{\partial u^1} \tag{B.64}$$

$$A_{12} = -\frac{1}{B_*} \tag{B.65}$$

$$A_{21} = \rho\omega^2 g_{11} + Dg_{11}D + \frac{\partial B_1}{\partial u^2}D - B^j\frac{\partial g_{1j}}{\partial u^1}D - Dg_{1j}\frac{\partial B^j}{\partial u^1}$$

$$-D\frac{B_2}{B_*}\left[B^k{}_{B^m}\frac{\partial g_{km}}{\partial u^1} - (DB_1)\right] - D\frac{B_1B_2}{B_*}D \tag{B.66}$$

$$A_{22} = D\frac{B_1}{B_*} - \frac{1}{B_*}\left[B^k{}_{B^m}\frac{\partial g_{km}}{\partial u^1} - (DB_1)\right] \tag{B.67}$$

APPENDIX C

In this appendix, expressions for the derivatives of the unit vectors $\hat{\Phi}$, $\hat{\chi}$, and $\hat{\phi}$ with respect to ϕ, χ, ϕ, in an orthogonal flux coordinate system, are provided for the convenience of the reader.

$$\frac{\partial \hat{\Phi}}{\partial \phi} = \frac{-1}{RB_P} \frac{\partial \ell n(B_T/B_P)}{\partial \ell_P} \hat{\chi} \tag{C.1}$$

$$\frac{\partial \hat{\Phi}}{\partial \chi} = RB_P \frac{\partial}{\partial \Phi}\left(j_o B_P\right) \hat{\chi} \tag{C.2}$$

$$\frac{\partial \hat{\Phi}}{\partial \phi} = RB_P \frac{\partial R}{\partial \Phi} \hat{\phi} \tag{C.3}$$

$$\frac{\partial \hat{\chi}}{\partial \phi} = \frac{1}{RB_P} \frac{\partial \ell n(B_T/B_P)}{\partial \ell_P} \hat{\Phi} \tag{C.4}$$

$$\frac{\partial \hat{\chi}}{\partial \chi} = -RB_P \frac{\partial}{\partial \Phi}\left(j_o B_P\right) \hat{\Phi} \tag{C.5}$$

$$\frac{\partial \hat{\chi}}{\partial \phi} = -R \frac{\partial \ell n B_T}{\partial \ell_P} \hat{\phi} \tag{C.6}$$

$$\frac{\partial \hat{\phi}}{\partial \phi} = \frac{\partial \hat{\phi}}{\partial \chi} = 0 \tag{C.7}$$

$$\frac{\partial \hat{\phi}}{\partial \phi} = -RB_P \frac{\partial R}{\partial \Phi} \hat{\Phi} + R \frac{\partial \ell n B_T}{\partial \ell_P} \hat{\chi} \tag{C.8}$$

APPENDIX D

SHEAR ALFVEN WAVE CONTINUUM CODES

A series of three numerical codes are used to generate solutions for the shear Alfvén wave continuum of the Tokapole II device. All three codes run on the Cray-1 computers of the MFE network. Recent versions of each code are available from the author, user number 1457. With relatively minor modifications, the codes can be adapted for use with any other tokamak. The following codes were used to generate the numerical solutions presented in Chapter 3 of this thesis:

TEQCRAY This version of the MHD equilibrium code, TOPEC[25] was written originally by M. Phillips to solve the Grad-Shafranov equation for the Tokapole II device. The input to the code is specified in a file TOKIN, which allows the user to specify the magnetic field strength on axis, the total plasma current, and the positions of the four internal rings which are driven inductively to form the divertor region of the discharge. Output files from the code include TOKFLUX, BPFIELD, and BTFIELD, which specify the poloidal magnetic flux, and the poloidal and toroidal magnetic field strengths, respectively, on an (89,45) array covering the lower half of the Tokapole II cross section.

MATRIX This code generates the matrices $\vec{\vec{M}}$ and $\vec{\vec{N}}$

which are needed to solve the continuum equations, Eq. (2.33). Flux surface quantities are also calculated. Input to the code includes the files TOKFLUX, BPFIELD, and BTFIELD. Output files include:

EQUIM - contains elements of $\vec{\vec{M}}$

EQUIN - contains elements of $\vec{\vec{N}}$

BP - contains poloidal magnetic field values on a flux surface

FLUXES - contain the flux surface quantities

FREQ This code solves the continuum equations, Eq. (2.33), according to the methods outlined in Chapter 4. It uses the output files from the code MATRIX and the output file TOKFLUX from the code TEQCRAY. A model density profile for the Tokapole II discharge is incorporated into the code. The user interactively specifies the approximate poloidal and toroidal mode numbers desired and up to three different flux surfaces for which the poloidal structure of the wave will be supplied in the output file FUNC. Shear Alfvén eigenvalues and eigenfrequencies in Mhz are output in the files EIGEN and OMEGA, respectively. These files also contain the eigenvalues and eigenfrequencies corresponding to the approximate dispersion relation, Eq. (3.9), an estimate for the relative error in each eigenvalue, and the number of iterations required for convergence.

APPENDIX E

AN INVARIANT OF HAMILTONIAN SYSTEMS

In Chapter 5, the number of linearly independent periodic solutions to the continuum equations for a given eigenvalue was determined by transforming the continuum equations into an equivalent Hamiltonian form and using the results of Floquet theory. A particular invariant, Eq. (4.53) formed by solutions of the Hamiltonian system, Eq. (4.41), was used to derive Eq. (4.55). The existence of this particular invariant for any Hamiltonian system has been demonstrated by Courant and Snyder[38]. In this appendix, their proof for a second order system, is reproduced for the convenience of the reader.

The starting point is the Hamiltonian system

$$\frac{d\vec{v}}{d\theta} = \vec{S} \cdot \vec{H} \cdot \vec{v} \tag{E.1}$$

where θ varies from 0 to 2π, the matrix $\vec{S}$ is defined as

$$\vec{S} = \begin{bmatrix} 0 & 1 \\ 1 & 0 \end{bmatrix} \tag{E.2}$$

and the matrix $\vec{H}$ is real and symmetric, i.e.,

$$\vec{H}^T = \vec{H} \tag{E.3}$$

where $\vec{H}^T$ is the transpose of the matrix $\vec{H}$. From Eq. (E.2) it is easy to verify that

$$\vec{S} \cdot \vec{S} = -I \tag{E.4}$$

where I is the identity matrix, and that

$$\vec{S}^T \cdot \vec{S} = I \quad . \tag{E.5}$$

The inner product of any two solutions of Eq. (E.1) is defined as follows

$$\langle \vec{v}_i | \vec{v}_j \rangle = \oint d\theta \vec{v}_i^{\,+} \cdot \vec{v}_j \tag{E.6}$$

where + denotes the complex conjugate of the transpose. Using the

definition Eq. (E.6), the existence of the invariant can be readily verified.

Consider the derivative with respect to θ of the inner product of vector solution $\vec{V}_i$ with the product $\vec{\vec{S}}\cdot\vec{V}_j$, i.e.,

$$A \equiv \frac{d}{d\theta} \langle V_i | \vec{\vec{S}}\cdot\vec{V}_j \rangle \quad . \tag{E.7}$$

Using the distributional property of the derivative over the vector product in Eq. (E.7), one finds

$$A = \langle \frac{d\vec{V}_i}{d\theta} \mid \vec{\vec{S}}\cdot\vec{V}_j \rangle + \langle \vec{V}_i \mid \vec{\vec{S}} \cdot \frac{d\vec{V}_j}{d\theta} \rangle \tag{E.8}$$

Incorporating Eqs. (E.1) and (E.4) into (E.8) now yields

$$A = \langle \vec{\vec{S}}\cdot\vec{\vec{H}}\cdot\vec{V}_i | \vec{\vec{S}}\cdot\vec{V}_j \rangle - \langle \vec{V}_i | \vec{\vec{H}}\cdot\vec{V}_j \rangle \tag{E.9}$$

In fact, however, A = 0, since

$$\begin{aligned} \langle \vec{\vec{S}}\cdot\vec{\vec{H}}\cdot\vec{V}_i | \vec{\vec{S}}\cdot\vec{V}_j \rangle &= \langle \vec{V}_i | (\vec{\vec{S}}\cdot\vec{\vec{H}})^T\cdot\vec{\vec{S}}\cdot\vec{V}_j \rangle = \langle \vec{V}_i | \vec{\vec{H}}^T\cdot\vec{\vec{S}}^T\cdot\vec{\vec{S}}\cdot\vec{V}_j \rangle \\ &= \langle \vec{V}_i | \vec{\vec{H}}\cdot\vec{V}_j \rangle \quad , \end{aligned} \tag{E.10}$$

where Eqs. (E.3) and (E.5) have been used. Thus, any two solutions, $\vec{V}_i$ and $\vec{V}_j$, to the Hamiltonian system (E.1), may be used to construct an invariant of the system which satisfies

$$\frac{d}{d\theta} \langle \vec{V}_i | \vec{\vec{S}}_j\cdot V_j \rangle = 0 \quad . \tag{E.11}$$

This result is obviously generalizable to higher order Hamiltonian systems.

APPENDIX F

SUPPLEMENT TO CHAPTER 5

In Chapter 5, it is stated that the following expectation value,

$$\langle \vec{\xi}_o \cdot \vec{F} \cdot \vec{\xi}_o \rangle \equiv \langle \vec{g}_o | \vec{K}_o \cdot \vec{C}_o | \vec{g}_o \rangle \quad , \tag{F.1}$$

where $\vec{\xi}_o$ is defined in Eqs.(5.8) and (5.63), vanishes identically when the tokamak equilibrium possesses reflection symmetry about the midplane. That this is true will be demonstrated in this appendix, using parity arguments. For brevity's sake, only a few terms appearing in Eq.(F.1) will be treated explicitly. Similar considerations, however, apply in the evaluation of the remaining terms.

When the equilibrium is symmetric with respect to reflection about the midplane, equilibrium quantities such as $g_{ij}(\theta)$ are even in θ while derivatives of these quantities with respect to θ, i.e., $\partial g_{ij}/\partial\theta$, are odd in θ. In a similar fashion, the vector $\vec{g}(\theta)$ is characterized by certain parity properties. It was shown in Chapter 5 that in an up-down symmetric equilibrium, two real, periodic, linearly independent solutions for $\vec{g}_o$ – one even with respect to θ,β and one odd with respect to θ,β – can be found for a given eigenfrequency. These two solutions may be written as

$$\vec{Y}_1 = \vec{a}(\theta)\cos N\beta + \vec{c}(\theta)\sin N\beta \tag{F.2}$$

$$\vec{Y}_2 = \vec{c}(\theta)\cos N\beta - \vec{a}(\theta)\sin N\beta$$

where $\vec{a}(\theta)=\vec{a}(-\theta)$ and $\vec{c}(\theta)=-\vec{c}(-\theta)$. By taking linear combinations of these two solutions, the vector $\vec{g}_o$, as given in Eq.(5.63), may be written as

$$\vec{g}_o = \vec{A}(\theta)e^{iN\beta} = [\vec{a}(\theta) - i\vec{c}(\theta)]e^{iN\beta} \quad . \tag{F.3}$$

The parity properties of $\vec{g}_o$ are thus given in terms of the even and odd functions, $\vec{a}(\theta)$ and $\vec{c}(\theta)$, respectively.

The elements of the matrix, $\vec{F}$, are given below:

$$F_{11} = K_{11}K_{12}^{+} - K_{12}K_{11}^{+}$$

$$F_{12} = K_{11}K_{22}^{+} - K_{12}K_{21}^{+} = -F_{21}^{+} \tag{F.4}$$

$$F_{22} = K_{21}K_{22}^{+} - K_{22}K_{21}^{+} \quad ,$$

where the elements of $\vec{K}$ are given in Appendix B in Eqs.(B.56)-(B.59) and the superscripts "+" denotes the adjoint. In the remainder of

this appendix, only the following two terms, present in F_{11}, will be evaluated explicitly:

$$T = -(B^2)^2\left[\frac{\partial g_{12}}{\partial\theta}\frac{\partial}{\partial\theta}\right]\frac{\partial}{\partial\theta} + (B^2)^2\frac{\partial}{\partial\theta}\left[\frac{\partial}{\partial\theta}g_{12}\frac{\partial}{\partial\theta}\right] \qquad (F.5)$$

where $B^2 \equiv \vec{B}\cdot\nabla\theta$ is a flux function in Hamada coordinates. By expanding the differentials in Eq.(F.5), the expression for T reduces to the following:

$$T = (B^2)^2\left[\frac{\partial^2 g_{12}}{\partial\theta^2}\frac{\partial}{\partial\theta} + \frac{\partial g_{12}}{\partial\theta}\frac{\partial^2}{\partial\theta^2}\right] \qquad (F.6)$$

In an up-down symmetric equilibrium, $\partial^2 g_{12}/\partial\theta^2$ is an even function of θ while $\partial g_{12}/\partial\theta$ is an odd function of θ. Combining Eq.(F.4) with the form, Eq.(5.63), for $\hat{g}_o$ yields one term of the expectation value of Eq.(F.1), namely,

$$I = \oint d\theta\, A_1^*(\theta)\, T(\theta)\, A_1(\theta) \qquad (F.7)$$

where A_1 is the upper component of the vector $\hat{A}$, the asterick denotes the complex conjugate, and the integration over the angle β has already been performed. By integrating the second term in $T(\theta)$ by parts and using the periodicity condition,

$$\hat{A}(\theta+2\pi) = \hat{A}(\theta)e^{-i2\pi Nq} \qquad (F.8)$$

to cancel the surface term, the integral I reduces to:

$$I = \oint d\theta\, \frac{\partial A_1^*}{\partial\theta}\frac{\partial^2 g_{12}}{\partial\theta^2}\frac{\partial A_1}{\partial\theta} \qquad (F.9)$$

One can now easily show that this integral vanishes identically in an up-down symmetric tokamak by substituting Eq.(F.3) for A_1 and recognizing that the total integral of an even periodic function multiplied by an odd periodic function is equal to zero. In a similar fashion, the remaining terms in Eq.(F.1) can all be shown to vanish in a tokamak possessing reflection symmetry about the midplane.

BIBLIOGRAPHY

[1]David, S.L.;PPPL-1982 (1982).

[2]Plasma Physics and Nuclear Fusion Research, ed. Richard D. Gill, Academic Press, N.Y., N.Y. (1981).

[3]Tataronis, J. and Grossmann, W.; Z. Physik 261, 203 (1973).

[4]Grossmann, W. and Tataronis, J.; Z. Physik 261, 217 (1973).

[5]Golovato, S.N., Shohet, J.L., and Tataronis, J.A.; Phys. Rev. Lett. 37, 1272 (1976).

[6]Demirkanov, R.A., et al.; Plasma Physics and Controlled Nuclear Fusion Research, Symposium Proceedings, Berchtesgaden, Oct. 6-13, 1976; pg. 31-37, STI/PUB/439, Vol. 3, IAEA, Vienna (1977).

[7]Obiki, T., Mutoh, T., Kinoshita, S., Sato, M., Iiyoshi, A. and Uo, K., Heating in Toroidal Plasmas, Proceedings of the Joint Grenoble-Varenna International Symposium, Vol. 1, pg. 109, ed. Consoli, Pergamon Press (1979).

[8]Keller, R. and Pochelon, A.; Nucl. Fusion 18, 1051 (1978).

[9]Tataronis, J.A. and Grossmann, W.; Nucl. Fusion 16, 667 (1976).

[10]DeChambrier, A. et al., Plasma Physics 24, 893 (1982).

[11]Witherspoon, F.D., Kieras, C.E., Sprott, J.C., and Prager, S.C.; Proceedings of the Fourth Topical Conference on Radio Frequency Plasma Heating, Austin, TX, B15 (1981).

[12]Lin, S.H., Bengston, R.D., Michie, R., Oakes, M.E. and Watkins, J.G., Proceedings of the Fourth Topical Conference on Radio Frequency Plasma Heating, Austin, TX, B16 (1981).

[13]Tataronis, J.A.,; Courant Institute of Mathematical Sciences, NYU, Report MF-68, COO-3077-46 (1974).

[14]Tataronis, J.A. and Grossmann, W.; Courant Institute of Mathematical Sciences, NYU, Report MF-84, COO-3077-102 (1977).

[15]Hasegawa, A. and Uberoi, C.; The Alfvén Wave, Technical Information Center, USDOE (1982).

[16]Cumberbatch, E.; J. Aerospace Sci. 70, 3277 (1973).

[17]Friedman, B.; Principles and Techniques of Applied Mathematics, John Wiley & Sons, Inc., NY (1956).

[18]Tataronis, J.A., Talmadge, J.N., and Shohet, J.L.; Proceedings of the Third Topical Conference on Radio Frequency Plasma Heating, Pasadena, CA (1978); also Comments Plasma Phys. Controlled Fusion 7, 29 (1982).

[19]Hildebrand, F.B.; Advanced Calculus for Applications, 2nd ed., Prentice-Hall, NJ (1976).

[20]Pao, Y.P.; Nucl. Fusion 15, 631 (1975).

[21]Goedbloed, J.P.; Phys. Fluids 18, 1258 (1975).

[22]Tataronis, J.A. and Salat, A.; Proceedings of the Second Joint Grenoble-Varenna International Symposium on Heating in Toroidal Plasmas, Como, Italy (1980).

[23]Hameiri, E. and Hammer, J.H.; Phys. Fluids 22, 1700 (1979).

[24]Sprott, J.C.; UW-Madison Physics Dept. Report PLP 750, COO-2387-91 (1978).

[25]Phillips, M.W., UW-Madison Physics Dept. Report PLP 765 (1978).

[26]Schmidt, G.; Physics of High Temperature Plasmas, 2nd ed., Academic Press, NY (1979).

[27]Hildebrand, F.B.; Methods of Applied Mathematics, Prentice-Hall, NY (1952).

[28]Tataronis, J.A. private communication.

[29]Glasser, A.H.; Proceedings of the Finite Beta Workshop, Varenna, Italy, ed. B. Coppi and W. Sadowski (1977).

[30]Ware, A.A. and Haas, F.A.; Phys. Fluids 9, 956 (1966).

[31]Davydov, A.S.; Quantum Mechanics, 2nd ed., Pergamon Press (1965).

[32]Kieras, C.E. and Tataronis, J.A.; Bull. Am. Phys. Soc. 26, 1018 (1981).

[33]Kieras, C.E. and Tataronis, J.A.; Proceedings of the Third Joint Grenoble - Varenna International Symposium on Heating in Toroidal Plasmas, Grenoble, France (1982).

[34]Phillips, M.W.; private communication.

[35]Hameiri, E., Phys. Fluids 24, 562 (1981).

[36]Ince, E.L.; Ordinary Differential Equations, Longmans, Green and Co. Ltd., NY (1944).

[37]Eastham, M.S.P.; The Spectral Theory of Periodic Differential Equations, Academic Press, London (1973).

[38]Courant, E.D. and Snyder, H.S.; Annals of Physics 3, 1 (1958).

[39]Boyce, W.E. and DiPrima, R.C.; Elementary Differential Equations and Boundary Value Problems, 2nd ed., John Wiley & Sons, Inc., NY (1969).

[40]Schiff, L.; Quantum Mechanics, 3rd ed., McGraw-Hill, NY (1968).

[41]Kittel, C.; Introduction to Solid State Physics, 5th ed., John Wiley & Sons, Inc., NY (1976).

[42]Dewar, R.L., Greene, J.M., Grimm, R.C., and Johnson, J.L.; PPPL-MATT-1099, December (1974).

[43]Chance, M.S., Greene, J.M., Grimm, R.C. and Johnson, J.L.; Nucl. Fusion 17, 65 (1977).

[44]Pogutse, O.P. and Yurchenko, E.I.; Nucl. Fusion 18, 1629 (1978).

[45]D'Ippolito, D. and Goedbloed, J.P.; Plasma Physics 22, 1091 (1980).

[46]Hasegawa, A. and Chen, L.; Phys. Rev. Lett. 35, 370 (1975).

[47]Hasegawa, A. and Chen, L.; Phys. Fluids 19, 1924 (1976).

[48]Ross, D.W., Chen, G.L., Mahajan, S.M.; Phys. Fluids 25, 652 (1982).

[49]Tsang, K.T., Sigmar, D.J., Whitson, J.C.; Phys. Fluids 24, 1508 (1981).

[50]Hamada, S.; Nucl. Fusion 2, 23 (1962).

[51]Solov'ev, L.S. and Shafranov, V.D.; Rev. of Plasma Physics, Vol. 5, ed. A.M.A. Leontovitch, Consultants Bureau, NY (1970).

[52]Spies, G.O. and Nelson, D.B.; Phys. Fluids 17, 1879 (1974).

[53]Bateman, G.: MHD Instabilities, MIT Press, MA (1978).

[54]Greene, J.M. and Johnson, J.L.; Phys. Fluids 5, 510 (1962).

[55]VanDam, J.W.; UCLA Report PP6-415 (1979).

[56]Greene, J.M.; Ecole Polytechnique Federale de Lausanne, LRP114/76 (1976).

[57]Shafranov, V.D., Connor, J.W., and Watson, C.J.H.; Sov. J. Plasma Physics 2, 99 (1976).

[58]Symon, K.R. and Callen, J.D., lecture notes from course entitled Special Topics in Plasma Physics, Fall (1979).

[59]Zakharov, L.E. and Shafranov, V.D.; Oak Ridge National Lab. Report ORNL-TR-4467, trans. J.T. Hogan (1980).

[60]Budiansky, B.; in Handbook for Applied Mathematics; ed. C.E. Pearson, Von Nostrand Reinhold Co., NY (1974).

[61]Armentrout, C.J.; UW-Madison Physics Dept. Report PLP 667 (1967).

[62]Tataronis, J.A. private communication.

[63]Newcomb, W.A.; Phys. Fluids 2, 362 (1959).